

DESIGN AND PROCESS OPTIMIZATION OF INTEGRATED PHOTONIC CRYSTAL STRUCTURES

A THESIS

submitted by

RASHMI JOSHI

for the award of the degree

of

MASTER OF SCIENCE

(by Research)



**DEPARTMENT OF ELECTRICAL ENGINEERING
INDIAN INSTITUTE OF TECHNOLOGY MADRAS
CHENNAI-600036**

AUGUST 2014

THESIS CERTIFICATE

This is to certify that the thesis titled **DESIGN AND PROCESS OPTIMIZATION OF INTEGRATED PHOTONIC CRYSTAL STRUCTURES**, submitted by **Rashmi Joshi**, to the Indian Institute of Technology, Madras, for the award of the degree of **Master of Science**, is a bona fide record of the research work done by him under our supervision. The contents of this thesis, in full or in parts, have not been submitted to any other Institute or University for the award of any degree or diploma.

Prof. Nandita DasGupta
Research Guide
Professor
Dept. of Electrical Engineering
IIT-Madras,
Chennai-600036

Place: Chennai

Dr. Bijoy Krishna Das
Research Guide
Associate Professor
Dept. of Electrical Engineering
IIT-Madras
Chennai-600036

Date: 13th August 2014

ACKNOWLEDGEMENTS

This thesis acknowledgement gives me an opportunity to thank all those who supported me at various stages of my research work and my stay at IIT Madras. First I would like to thank my research guide Prof. Nandita DasGupta and Dr. Bijoy Krishna Das, for their guidance and giving me opportunity to work in exciting area of PhCW with excellent people. I would like to thank my GTC members Dr. Shanti Bhattacharya and Prof. MS Ramachandra Rao for their support and suggestions in my review meetings. I would like to thank Prof. Amitava DasGupta, Prof. Enakshi Bhattacharya, Prof. Sreepad Karmalkar, Dr. Nitin Chandrachoodan for teaching me courses. I would like to thank Dr. Manu Jaiswal and Dr. V. Pramitha for helping me in technical issues related to electron beam lithography. I am grateful to all my seniors for teaching basic fabrication and characterization methods. My special thanks to Sujith and Sakthivel for helping me in all the fabrication steps and optical characterization. I thank Seethalakshmi for helping me in optimization of fabrication process steps and making the project reports and presentations. I thank the support staff of microelectronics and MEMS lab Mr. Rajendran, Mr Praksh, Mr. Joseph, Mr. Sreedhar and all the technicians and project staffs for their help in various technical problems in fabrication and characterization equipment's. I thank all my lab mates from IOgroup Sidharth, Saket, Shantanu Sreevatsa, Parimal, Riddhi, Sumi, Meenatchi, Varun, Dadaveli, Ramesh for motivating me time to time and helping me in my research. I would like to acknowledge some of my friends who have graduated from IOgroup Gaurang, Harish, Karthick, Siresha, Vivek, and Mandar for their advise and suggestions. I thank all my friends from Microelectronics group Sreenidhi, Navin, Vamshi, Vikrant, Vishal, Gourab, Prashanth, Shelly, Priya, Ankit, Gaurav, Madhup, Mohan, Udit, Sarath for helping me whenever I was in need. My special thanks to Rahul and Shon for all their help and support. I am grateful to all my friends at IIT Madras for making my stay pleasant and cheerful.

Last but not the least, I am grateful to my mother, my Dadaji and all my family members for supporting me all the time. Finally I thank to all those who directly or indirectly have helped me in my research work.

ABSTRACT

The theoretical understanding of Photonic Crystal (PhC) structure and its potential application areas have been known for a long time. Its usage in developing functional photonic devices has been limited due to stringent fabrication requirements. However, with recent advancements in nano-scale technologies, two-dimensional (2D) PhC structures could be fabricated for compact waveguide devices, high Q resonance cavity, etc.

In this work, single-mode 2D air bridge photonic crystal waveguides (PhCWs) have been studied in both GaAs/AlGaAs and SOI platforms for planar lightwave circuit applications operating at communication band ($\sim 1.55 \mu\text{m}$). The design parameters of PhC were optimized to obtain sufficiently large photonic bandgap (PBG) of the order of 500 nm centering at third generation optical communication window ($\lambda \sim 1550 \text{ nm}$). In the optimized PhCs, a line defect was introduced to realize the waveguide. The optimized PhCW defect widths for single mode condition are 176 nm and 150 nm for GaAs and silicon, respectively. Design of SOI based PhCWs are further modified by introducing taper at both ends to improve coupling of light into PhCW from photonic wire waveguide. Using the designed taper, the throughput transmission has been improved from 14% to 33%. The extracted group velocity of a SOI based PhCW was found to be 3-10 times slower than that of a photonic wire waveguide operating at $1510 < \lambda < 1570 \text{ nm}$. Such structures can be useful for slow-light and non linear applications. All the design parameters have been optimized using commercial FDTD tool.

Since the design parameters of PhCW were in sub-micron dimensions, conventional UV photolithography techniques could not be used to realize the structure. Therefore, this work also extends into optimization of Electron-Beam Lithography parameters and etching recipe of silicon using Inductively Coupled Plasma Reactive Ion Etching (ICP RIE).

KEYWORDS: Photonic Crystal Waveguide, Planar Lightwave Circuit, Photonic Band Gap, Silicon On Insulator, Gallium Arsenide, Aluminum Gallium Arsenide

TABLE OF CONTENTS

| | |
|---|------------|
| ACKNOWLEDGEMENTS | i |
| ABSTRACT | ii |
| LIST OF TABLES | vi |
| LIST OF FIGURES | x |
| ABBREVIATIONS | xi |
| NOTATION | xiv |
| 1 INTRODUCTION | 1 |
| 1.1 Motivation | 1 |
| 1.2 Research Objective | 6 |
| 1.3 Thesis Outline | 6 |
| 2 Photonic Crystals : Theoretical Background | 8 |
| 2.1 1D PhC | 9 |
| 2.2 2D PhC | 13 |
| 2.3 3D PhC | 17 |
| 2.4 2D Photonic Crystal Slab | 18 |
| 2.5 Conclusions | 18 |
| 3 Device Design and Simulation | 19 |
| 3.1 Square Lattice Hole Slab PhC | 19 |
| 3.2 Triangular Lattice Hole Slab PhC | 24 |
| 3.3 Design of PhCW with Triangular Lattice Geometry | 25 |
| 3.4 Integrated PhCW | 29 |
| 3.4.1 Design of Single Mode PhW | 30 |
| 3.4.2 Taper Design | 31 |

| | | |
|----------|--|-----------|
| 3.5 | Group Velocity Dispersion | 34 |
| 3.6 | Conclusions | 34 |
| 4 | Fabrication | 36 |
| 4.1 | Fabrication of Micro-structures | 36 |
| 4.1.1 | Etching Studies on GaAs | 36 |
| 4.1.2 | Etching Studies of Silicon | 39 |
| 4.2 | Fabrication of Nano-structures : PhCs | 42 |
| 4.2.1 | PMMA as Hard Mask | 42 |
| 4.2.2 | Al as Hard Mask | 46 |
| 4.2.3 | HSQ as Hard Mask | 51 |
| 4.2.4 | Photonic Wire Waveguide (PhW) Fabrication | 57 |
| 4.3 | Conclusions | 58 |
| 5 | Conclusions | 59 |
| 5.1 | Summary | 59 |
| 5.2 | Scope for Future Work | 60 |
| A | Codes | 61 |
| A.1 | Matlab Code to Calculate Band Structure using Theoretical Analysis | 61 |
| A.1.1 | 1D PhC : Normal Incidence | 61 |
| A.1.2 | 1D PhC : Angular Incidence | 62 |
| A.1.3 | 2D PhC | 63 |
| A.2 | Script for Band Structure Calculation Using LUMERICAL | 65 |
| A.2.1 | Code for Band Structure Calculation of PhC | 65 |
| A.2.2 | Code for Band Structure Calculation of PhCW | 69 |
| B | Mask Generation | 72 |
| B.1 | Mask File Design | 72 |

LIST OF TABLES

| | | |
|-----|---|----|
| 3.1 | Optimized parameters for triangular lattice PhC Structures | 25 |
| 4.1 | Specifications of SOI and Silicon wafer used for fabrication process. | 42 |
| 4.2 | Spin coating parameters for PMMA. | 44 |
| 4.3 | Recipe used for RIE to realize PhC on silicon. | 46 |
| 4.4 | Fabrication process flow for getting Al hard mask using wet Al etching. | 48 |
| 4.5 | Fabrication process flow for getting Al hard mask using lift-off. | 50 |
| 4.6 | Spin coating parameters for ≈ 180 nm thick HSQ. | 52 |
| 4.7 | Spin coating parameters for ≈ 130 nm thick HSQ. | 53 |
| 4.8 | Optimized development parameters for HSQ. | 55 |
| 4.9 | Recipe used for ICPRIE to realize PhC on silicon. | 56 |

LIST OF FIGURES

| | | |
|-----|--|----|
| 1.1 | Photonic Crystal schemes : (a) 1D periodic structure, (b) 2D periodic hole slab structure, (c) 3D PhC. | 2 |
| 1.2 | Different types of defects in 2D PhC : (a) Point defect, (b) Line defect. | 2 |
| 1.3 | Components using 2D PhC : (a) Waveguide, (b) 60° bend, and (c) Y-splitter. | 3 |
| 1.4 | Schematic of PhC nano cavity (Akahane <i>et al.</i> , 2003). | 4 |
| 1.5 | (a) SEM image of PhC nano cavity. (b) Schematic of PhC nano cavity (Notomi <i>et al.</i> , 2005). | 4 |
| 1.6 | Schematic of MZI using PhCW (Jiang <i>et al.</i> , 2007). | 5 |
| | | |
| 2.1 | Schematic of a 1D periodic medium consisting of two alternating material layers of refractive indices n_1 and n_2 ; thickness d_1 and d_2 , respectively. | 9 |
| 2.2 | Photonic band structure of a 1D periodic medium at normal incidence. The red curves near vertical axis is the imaginary part of the Bloch wave number. The periodic medium is a quarter-wave stack formed with GaAs-air for 1500 nm wavelength. | 11 |
| 2.3 | Photonic band structure at normal incidence for three different multilayer films (quarter wave stack layer with 1500 nm wavelength) : (a) GaAs bulk, (b) GaAs/AlGaAs multilayer, (c) GaAs/air multilayer. | 12 |
| 2.4 | Photonic band structure of a wave in a periodic medium (GaAs-air quarter wave stack layer with 1550 nm) for : (a) TE wave, (b) TM wave. The green colored zones are allowed photonic bands in which $ \cos Ka < 1$. While the red colored zones are forbidden bands that are called PBGs | 13 |
| 2.5 | Schematic drawing of some 2D PhC structures : (a) Dielectric vein, (b) high index material rods, (c) Square lattice air holes in high index material slab, (d) Triangular lattice hole slab. | 14 |
| 2.6 | (a) 2D periodic structure, (b) First Brillouin zone of square lattice 2D PhC in K space. The shaded triangle region along Γ , X and M is the irreducible Brillouin zone. | 14 |
| 2.7 | Equipfrequency contours in K_x, K_y plane of a 2D PhC structures at different normalized frequencies: $\frac{\omega}{\lambda} = 0.1, 0.2, 0.23, 0.258, 0.283, 0.29, 0.31, 0.33$. The normalized surfaces are plotted in the Brillouin zone. The parameters used for calculation are $n_1^2 = 0.5, n_2^2 = 8.2, d_1 = 0.8a$, and $d_2 = 0.2a$ | 16 |

| | | |
|------|--|----|
| 2.8 | Band structure of a 2D periodic medium. The vertical axis is the normalized frequency in units of $\frac{a}{\lambda}$ and horizontal axis is normalized wavevector in different direction along the irreducible Brillouin zone. The parameters used for calculation are $n_1^2 = 0.5$, $n_2^2 = 8.2$, $d_1 = 0.8a$, and $d_2 = 0.2a$ | 16 |
| 2.9 | Example of 3D PhC structures. | 17 |
| 2.10 | Some examples of 2D PhC structures : (a) Square lattice high index rods in air, (b) Triangular lattice air holes etched in high index slab. | 18 |
| 3.1 | Scheme of square lattice PhC : (a) Real space lattice structure and the unit cell used for calculation is shown within the black color boundary, here n_1 and n_2 are refractive indices of air holes of radius (r) and slab respectively. (b) Reciprocal space lattice structure with first Brillouin zone of square lattice PhC. The shaded triangle region within Γ , X and M is irreducible Brillouin zone. | 20 |
| 3.2 | (a) Dispersion curve for square lattice 2DPhC on GaAs (extending uniformly in third direction) for both TE and TM polarization, here A_1 and A_2 are maxima and minima of lower and upper band respectively for TE case, similarly B_1 and B_2 are maxima and minima of lower and upper band for TM case. (b) PBG variation with r/a ratio for both TE and TM polarization. | 21 |
| 3.3 | (a) Square lattice PhC slab. (b) 3D view of unit cell of square lattice geometry hole slab PhC with Bloch Boundary (BB) on all four sides, PML and Symmetry boundary on top and middle of the slab, respectively. | 22 |
| 3.4 | (a) Dispersion curve of 2DPhC on GaAs slab of thickness $h = 220$ nm, radius $r = 217$ nm and period $a = 495$ nm. The curve with circular dot is the dispersion of air cladding (light line). (b) Dispersion curve of 2DPhC on silicon. The parameters taken from [(Loncar <i>et al.</i> , 2000)] to validate our simulation result are : $h = 272$ nm, $r = 198$ nm and $a = 496$ nm. | 23 |
| 3.5 | Triangular lattice PhC (a) Real space lattice structure and the unit cell used for calculation is shown within the black color boundary. (b) Reciprocal space lattice structure with first Brillouin zone of triangular lattice PhC, here the shaded region along Γ , J and M is irreducible Brillouin zone. | 24 |
| 3.6 | (a) 3D view of unit cell of triangular lattice geometry hole slab PhC with Bloch Boundary (BB) on all four sides, PML and Symmetry boundary on top and middle of the slab, respectively. | 24 |
| 3.7 | Dispersion curve of triangular lattice PhC for the designed parameters on (a) GaAs/AlGaAs and (b) SOI. | 25 |
| 3.8 | (a) Schematic of 2D air bridge PhCW. (b) Unit cell of PhCW with boundary condition used for band structure calculation. | 26 |

| | | |
|------|--|----|
| 3.9 | (a) Brillouin zone of PhCW and reduced Brillouin zone of waveguide is shown from Γ - J' . (b) Dispersion curve of GaAs/AlGaAs single defect width PhCW along Γ -J direction. | 28 |
| 3.10 | Dispersion curve of GaAs/AlGaAs PhCW along Γ -J direction. It explicitly shows single guided mode lying in PBG below light line. Practically mode above light line is leaked out in cladding. Here x axis is normalized wavevector and vertical axis is (a) Frequency in THz. (b) Normalized frequency in units of $\frac{a}{\lambda}$ | 28 |
| 3.11 | Dispersion curve of SOI PhCW along Γ -J direction. Here x axis is normalized wavevector and vertical axis is Frequency in THz. (a) Single defect PhCW (b) Single mode PhCW. | 29 |
| 3.12 | Effective index variation with change in width of PhW for TE ₀ , TM ₀ , TE ₁ , TM ₁ , SiO ₂ | 31 |
| 3.13 | Mode intensity profile of PhW of dimensions height H = 250 nm and width W = 540 nm : (a) TE ₀ , (b) TM ₀ | 31 |
| 3.14 | (a) Schematic of integrated PhCW and PhW using the taper. (b) Transmission at the output PhW for single defect PhCW on SOI. | 32 |
| 3.15 | Transmission spectrum at the output PhW for single mode PhCW on SOI. | 33 |
| 3.16 | Electric field distribution obtained from FDTD simulation in integrated PhCW-PhW structure in SOI. | 33 |
| 3.17 | Variation of group velocity as a function of wavelength for 476 nm width PhW and single mode PhCW structure. | 34 |
| 4.1 | Effect of (a) ICP Power, (b) Pressure, (c) BCl ₃ : Cl ₂ ratio, (d) N ₂ : Ar ratio, while keeping all other parameters constant | 37 |
| 4.2 | SEM image of square pattern (250 × 250 μm ²) etched using high pressure of 5 mTorr pressure during ICPRIE. (RF Power - 80 Watts, ICP Power - 200 Watts, BCl ₃ /Cl ₂ /Ar flow rate - 3/4/12 sccm). | 38 |
| 4.3 | SEM Image showing smooth and vertical side-wall of square pattern etched using BCl ₃ /Cl ₂ /Ar flow rate of 6/1/12 sccm during ICPRIE (RF Power - 80 Watts, ICP Power - 200 Watts, Pressure - 2 mTorr). | 39 |
| 4.4 | (a) Confocal microscope image of a square lattice circular hole (r = 2 μm) pattern with a defect line. (RF Power - 80 Watts, ICP Power - 200 Watts, Pressure - 3 mTorr, BCl ₃ /Cl ₂ /Ar/N ₂ flow rate - 6/1/11/1 sccm). (b) SEM Image of square lattice circular hole (r = 2 μm) pattern. (RF Power - 80 Watts, ICP Power - 200 Watts, Pressure - 3 mTorr, BCl ₃ /Cl ₂ /Ar/N ₂ flow rate - 6/1/11/1 sccm). | 39 |
| 4.5 | Confocal microscope image of a square lattice circular hole (r = 4 μm) pattern with a defect line. (RF Power - 80 Watts, ICP Power - 400 Watts, Pressure - 40 mTorr, SF ₆ /Ar flow rate - 20/20 sccm). | 41 |

| | | |
|------|---|----|
| 4.6 | Confocal microscope image of closer view of square lattice circular hole ($r = 4 \mu\text{m}$) pattern with a defect line. (RF Power - 80 Watts, ICP Power - 400 Watts, Pressure - 40 mTorr, SF_6/Ar flow rate - 20/20 sccm). | 41 |
| 4.7 | Fabrication process flow of PhC patterning using PMMA resist. . . | 43 |
| 4.8 | Figure shows (a) Screen shot of mask file, here dark region will be exposed to e-beam and (b) SEM image of PhC after development on PMMA. | 45 |
| 4.9 | Fabrication process flow of PhC patterning on Al using wet etching method. | 47 |
| 4.10 | Confocal microscopic image of PhC after development on PMMA for wet Al etching method. | 47 |
| 4.11 | Confocal microscopic image of etched Al using PMMA mask. . . . | 48 |
| 4.12 | Fabrication process flow of PhC patterning on Al using Lift-off. . . | 49 |
| 4.13 | SEM image of PhC pattern on (a) PMMA with inverted mask and (b) After lift-off | 50 |
| 4.14 | Fabrication process flow of PhC patterning using HSQ resist. | 52 |
| 4.15 | SEM image of developed silicon (a) with TMAH and (b) with MF-319. | 54 |
| 4.16 | Figure shows (a) Screen shot of mask file and (b) SEM image of PhC after development with MF-319 on SOI. | 54 |
| 4.17 | SEM image of etched silicon (a) with SF_6/Ar and (b) with Cl_2 plasma. | 55 |
| 4.18 | Tilted SEM images of etched silicon with Cl_2 plasma. | 56 |
| 4.19 | SEM image of PhC after etching on SOI with Cl_2 plasma. | 56 |
| 4.20 | SEM image of PhW after development. | 57 |
| 4.21 | SEM image of PhW after etching : (a) Top view, (b) End facet. . . . | 58 |
| B.1 | Screen shot of mask files of PhCs (a) For positive resist. (b) For negative resist (Inverted mask) | 73 |
| B.2 | By subtracting the a and b we should get c | 73 |
| B.3 | Lines in the mask. | 73 |
| B.4 | (a) Unit cell. (b) Array of patterns made using the unit cell in raith layout editor. | 74 |
| B.5 | SEM image of patterned HSQ using the mask file made in raith layout editor. | 74 |

ABBREVIATIONS

| | |
|---------------|--|
| PhC | Photonic Crystal |
| PhCW | Photonic Crystal Waveguide |
| 1D | One Dimensional |
| 2D | Two Dimensional |
| 3D | Three Dimensional |
| PBG | Photonic Band Gap |
| TIR | Total Internal Reflection |
| EBL | Electron Beam Lithography |
| PhW | Photonic wire Waveguide |
| SOI | Silicon On Insulator |
| Band C | Conventional wavelength band ($\lambda \sim 1527$ to 1567 nm) |
| Band L | Long wavelength band ($\lambda \sim 1567$ to 1607 nm) |
| BOX | Buried Oxide |
| CMOS | Complementary Metal Oxide Semiconductor |
| DI | De-ionized (water) |
| FDTD | Finite Difference Time Domain |
| ICP | Inductively Coupled Plasma |
| MZI | Mach Zehnder Interferometer |
| PML | Perfectly Matched Layer |
| RIE | Reactive Ion Etching |
| PMMA | Poly Methyl Metha Acrylate |
| HSQ | Hydrogen Silsesquioxane |
| MIBK | Methyl Isobutyl Ketone |
| IPA | Iso Propyl Alcohol |
| TMAH | Tetra Methyl Ammonium Hydroxide |
| FBMS | Fixed Beam Moving Stage |
| CAD | Computer Aided Design |
| PPR | Positive Photo Resist |

| | |
|------------|------------------------------------|
| SEM | Scanning Electron Microscope |
| SOI | Silicon-On-Insulator |
| TE | Transverse Electric (polarization) |
| TM | Transverse Magnetic (polarization) |
| BZ | Brillouin Zone |
| IG | Index Guided |
| GG | Gap Guided |
| UV | Ultra-Violet |

Chemical Names

| | |
|-----------------------------------|---------------------------|
| Al | Aluminum |
| AlGaAs | Aluminum Gallium Arsenide |
| Ar | Argon |
| Cl₂ | Chlorine |
| GaAs | Gallium Arsenide |
| HF | Hydro Fluoric Acid |
| HNO₃ | Nitric Acid |
| H₂O | Water |
| H₂O₂ | Hydrogen Peroxide |
| NaOH | Sodium Hydroxide |
| SF₆ | Sulfur Hexafluoride |
| Si | Silicon |
| SiO₂ | Silicon dioxide |
| TCE | Tri-chloro Ethylene |

Units

| | |
|------------|---------------------|
| dB | Decibel |
| dBm | Decibel milli-Watts |
| mW | milli Watts |
| THz | Tera Hertz |
| nm | Nanometer |
| μm | Micrometer |

| | |
|---|--------------------------------------|
| $\mu\text{C}/\text{cm}^2$ | Micro coulomb per centi meter square |
| mm | mili meter |
| ps | Pico Second |
| pA | Pico Ampere |
| μs | Micro Second |
| sccm | standard cubic centimeter per minute |
| mTorr | milli-Torr (of pressure) |
| ml | milli-liter (of fluid) |
| rpm | revolution per minute |

NOTATION

| | |
|--------------|--|
| r | Radius |
| \mathbf{a} | Lattice period |
| h | Slab thickness |
| c | Speed of light |
| λ | Wavelength |
| n | Refractive index |
| K | Bloch wavevector |
| ϵ | Permittivity |
| ϵ_0 | Permittivity in free space |
| ϵ_r | Permittivity in medium |
| μ | Permeability |
| μ_0 | Permeability in free space |
| β | Arbitrary constant |
| T | Transmission coefficient |
| E | Electric field |
| H | Magnetic induction field |
| D | Electric displacement field |
| B | Magnetic field |
| ρ | Charge density |
| J | Current density |
| ω | Angular frequency |
| L_π | Length required to get π phase shift |
| v_g | Group velocity |
| n_{eff} | Effective index |

CHAPTER 1

INTRODUCTION

Within the scope of this thesis, we have investigated Photonic Crystal (PhC) structures in both SOI and GaAs/AlGaAs for planar light-wave circuit applications operating at communication band ($\sim 1.55 \mu\text{m}$). In this chapter we will discuss the motivation of this thesis work, and then research objective followed by thesis outline.

1.1 Motivation

Telecommunications and optical computing applications require efficient control and guiding of light on a single photonic chip. Traditionally, it is accomplished by using properly designed dielectric waveguide structures which guide the light efficiently. Besides, generation, detection, and active control of light paths, tightly confined guided mode is essential for sharper bending and smaller footprints of integrated optical circuits. PhCs have been proposed as a potential solution to many of the above mentioned applications. PhCs are periodically varying (1D, 2D and 3D) dielectric structures that exhibit a special property called photonic bandgap (PBG) analogous to energy bandgap of a crystalline atomic lattice (Joannopoulos *et al.*, 2007). To observe the PBG, periodicity of the structure should be of the order of wavelength of the light used. Electromagnetic radiation with frequencies within the PBG cannot propagate through the PhC structure. This provides exciting ways of light confinement and propagation for functional devices. Initially, PhCs were proposed as materials useful for light localization (John, 1987) and the way for controlling the spontaneous emission of photon within the PBG (Yablonovitch, 1987).

A 1D periodic structure is the simplest PhC and it was first introduced by Lord Rayleigh in 1887 (Rayleigh, 1887). A one dimensional PhC as shown in Fig.1.1a is an alternating multilayer structure that can be used as a Bragg mirror. It can be fabricated easily by depositing epitaxial layers of material with varying refractive indices. Two dimensional (2D) PhCs shown in Fig.1.1b have attracted significant research attention

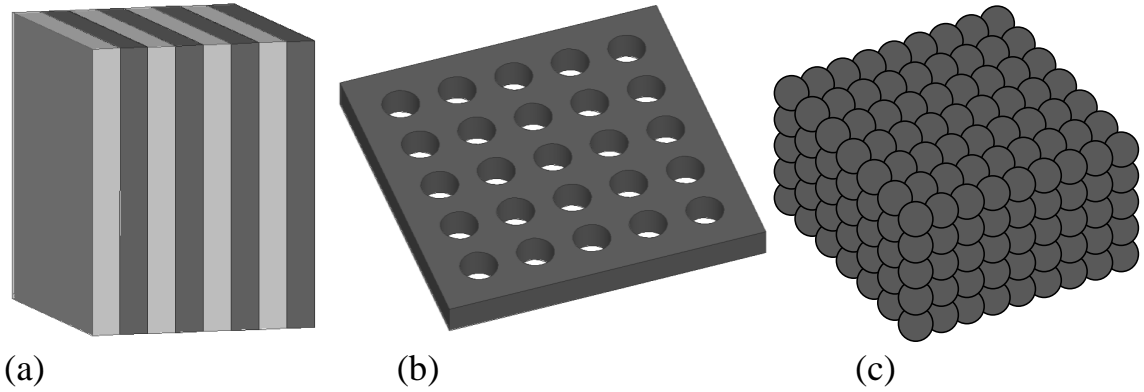


Figure 1.1: Photonic Crystal schemes : (a) 1D periodic structure, (b) 2D periodic hole slab structure, (c) 3D PhC.

in the last two decades due to their potential application in ultra-small miniaturized devices and large-scale photonic integrated circuits. As a 2D PhC hole slab structure provides control of light in lateral as well as vertical directions, it can be used as a waveguide or a cavity by introducing a line or point defect, respectively. Introduction of defect destroys periodicity of PhCs and the defect region opens a way to confine light laterally by means of PBG and vertically by total internal reflection (Notomi *et al.*, 2001). The scheme of point defect and line defect in 2D triangular lattice PhC are shown in Fig.1.2. Creating defects in PhC is analogous to doping in semiconductors, it pulls the state in the bandgap from air band or from dielectric band depending upon the type of impurity or defects (Notomi, 2010). Since, the light in the defect region is surrounded by PhC it will be reflected back and forth and confined there. The point defects are used in high Q cavity resonator. In the line defect the light is reflected from the PBG mirrors adjacent to the defect and it propagates in the direction of defect. Schemes of waveguide components using PhC defects is shown in Fig.1.3. The first line

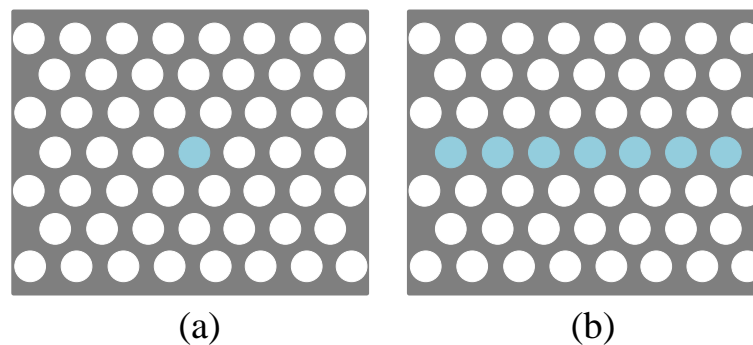


Figure 1.2: Different types of defects in 2D PhC : (a) Point defect, (b) Line defect.

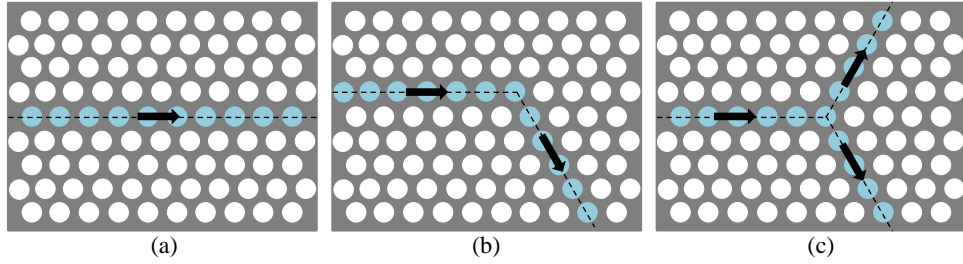


Figure 1.3: Components using 2D PhC : (a) Waveguide, (b) 60° bend, and (c) Y-splitter.

defect waveguide was discussed by Meade et al. (Meade *et al.*, 1994). The bends and junction PhC waveguide structures were subsequently proposed in 1996 (Mekis *et al.*, 1996). However, in these works the 2D PhC considered was rod slab structure. The 2D PhC rod slab structure provides wide PBG and introduction of defect line in such structures opens a wide transmission band. However, for practical applications, some way of optical confinement is required in the third direction also. On the other hand hole slab Photonic Crystal Waveguide (PhCW) provides confinement in both the directions (El-Kady *et al.*, 1999). Using point defects in 2D PhC slabs high Q cavity resonators ($Q = 45000$) (Akhane *et al.*, 2003) and highly efficient light emitting diodes (LED) (Meier *et al.*, 1999) have been demonstrated. With introduction of line defects compact single mode waveguide (Loncar *et al.*, 2000), sharp bends (Baba *et al.*, 1999), branches with low insertion loss (0.5-1 dB for 1640-1680 nm) (Lin *et al.*, 2002), add drop filters (Noda *et al.*, 2000), all optical switches (Notomi *et al.*, 2005), phase shifter for slow-light applications (Jiang *et al.*, 2007) and other components have been demonstrated which are useful for constructing large scale integrated photonic chips. Moreover, the planar 2D PhCW can easily be fabricated with conventional CMOS technology unlike the 3D PhC structure shown in Fig.1.1c, which is very difficult to fabricate, though it offers a more complete PBG (Noda *et al.*, 1999).

Using the slab PhCW many functional devices have been demonstrated for integrated optical circuit applications. In PhC high Q-value nano cavity resonator is an attractive example (see Fig.1.4), in which light is confined in the point defect. Since the mode is lying in PBG it is prohibited to propagate in all the directions. By optimizing the shift of air holes close to cavity shown in Fig.1.4c, the Q value reported was 45000 with the large free spectral region of 100 nm for the ultra small L3 cavity of Volume : $7 * 10^{-14} \text{cm}^{-3}$ (Akhane *et al.*, 2003).

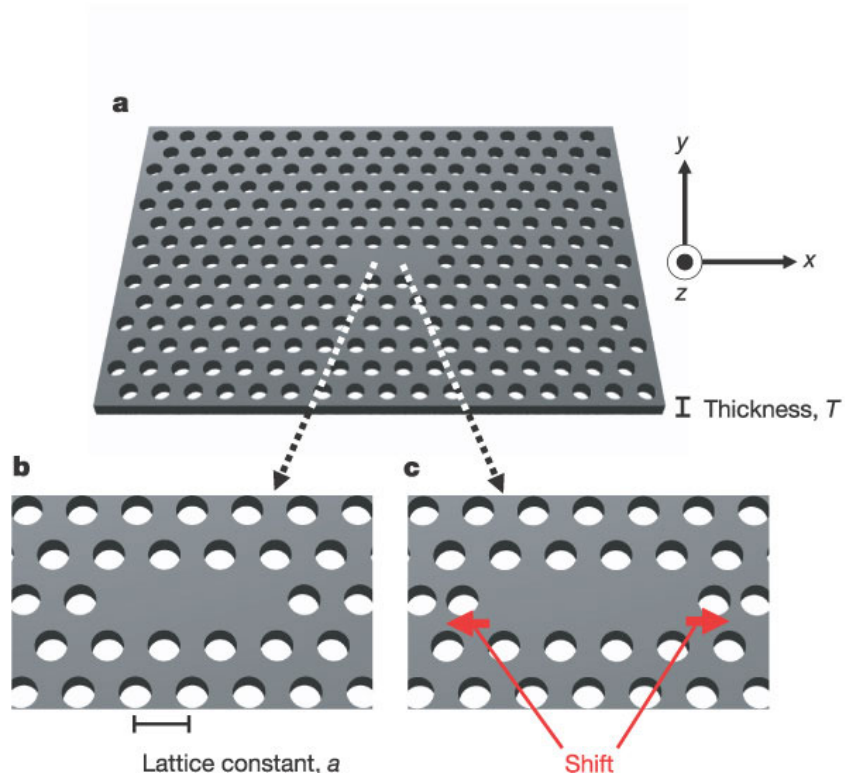


Figure 1.4: Schematic of PhC nano cavity (Akaahane *et al.*, 2003).

Planar high Q nano cavity optical bi-stable switch has also been demonstrated on silicon by Notomi *et al.* (Notomi *et al.*, 2005). The SEM image of fabricated nano cavity and the schematic of the structure are shown in Fig.1.5a and Fig.1.5b, respectively. Its a two mode resonant tunneling device. Using the optical non-linearity of the PhC, this four defect ultra cavity resonator can be used as an optical bi-stable switch that

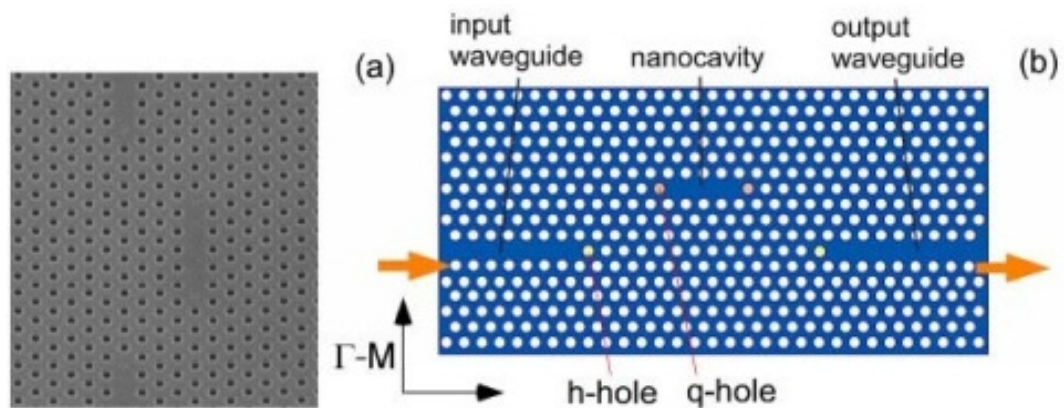


Figure 1.5: (a) SEM image of PhC nano cavity. (b) Schematic of PhC nano cavity (Notomi *et al.*, 2005).

can be operated with much lower switching energy. With the high Q value of 33400 and 7350 at resonant wavelength 1535 nm and 1568.7 nm respectively, two resonant

modes bi-stable switching was demonstrated with switching energy of the order of pJ. Conventional nonlinear Fabry-Parot etalons require much higher switching energy of the order of μJ . The high $\frac{Q}{V}$ of the PhC cavity, provides a way for switching at much lower energy.

Another promising application of PhCW is slow-light, using which the first electro-optic high speed compact modulator was demonstrated with carrier injection into $80\ \mu\text{m}$ long PhCW based phase shifter on silicon. The driving voltage to get π phase shift was reported as low as $v_\pi = 7.5\ \text{mV}$ (Jiang *et al.*, 2005). The schematic of MZI modulator structure based on PhCW is shown in Fig.1.6. Generally using conventional dielectric (rib) waveguide, the length required to get the π phase shift in MZI is one half to several millimeters due to small effective change in refractive index. However, PhCW offers extraordinary dispersion behavior and this opens opportunity to develop ultra-compact modulators.

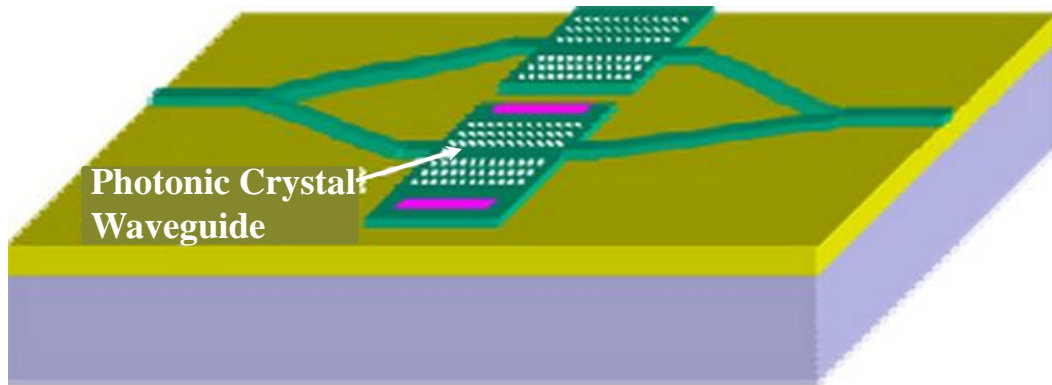


Figure 1.6: Schematic of MZI using PhCW (Jiang *et al.*, 2007).

The 2D PhCW that has been demonstrated so far is classified into three categories. Conventional Semiconductor Cladding (SC), Air Bridge or membrane type (AB) and Oxide Cladding (OC) PhCW (Sugimoto *et al.*, 2002). Among these categories, the air bridge structure provides the highest dielectric contrast, and therefore greatest degree of confinement can be achieved without any cross talk in TE and TM modes. It is realized through etching of holes in slab and subsequent etching of cladding layer through the etched holes in slab. While in the semiconductor cladding and oxide cladding PhCWs, index contrast is relatively low and the light confinement is poor with cross coupling in TE and TM modes. The problem with air bridge structure is, however, its poor mechanical strength.

Silicon on Insulator (SOI) and GaAs on AlGaAs (GaAs/AlGaAs) are two promising platforms for PhCW devices as both the materials are transparent for telecommunication bands ($\sim 1.3 \mu\text{m}$ and $\sim 1.5 \mu\text{m}$) and provide large refractive index contrast for compact device designs.

The 2D Planar slab PhCW have been used to demonstrate many functional devices. However, they suffer from some limitations like inefficient coupling of light into the PhCW. Coupling of light from index guided waveguide to PhCW poses a challenge because of significant difference in mode profile and guiding principle (Mittal and Sabarinathan, 2005). Though PhC based structures have attractive properties, to our knowledge it has not been exploited much for commercial planar photonic circuit applications due to stringent fabrication requirements to make such fine structures.

1.2 Research Objective

Though many groups have demonstrated air bridge PhCW, to our knowledge the minimum loss reported so far is 5 dB/cm (Kuramochi *et al.*, 2005). Losses in PhCW are mainly due to the discrepancies in dimensions of periodic structure after fabrication. Due to small fabrication imperfection, the PhC does not act as a perfect mirror thereby increasing the possibility of light being coupled to some non guided modes. Coupling of light is another major issue that give rise to insertion loss in to PhCW. Here arises the need to design a taper to improve the coupling efficiency. Most research groups are focusing on taper design to improve the coupling efficiency into PhCW for single defect waveguide. The Objective of this work is designing of single mode air bridge 2D PhCW on GaAs/AlGaAs and SOI platforms for telecommunication band ($\sim 1.55 \mu\text{m}$). Design of a taper to improve the coupling efficiency from photonic wire waveguide (PhW) to single mode PhCW and optimization of unit process steps have also been carried out

1.3 Thesis Outline

This chapter gave a brief overview of PhC and motivation of this work.

Chapter 2 presents classification of PhC structures continued with the theoretical

study of 1D and 2D periodic structures using semi-analytical model.

Chapter 3 focuses on the design and simulation methodology of 2D square lattice and triangular lattice PhC hole slab with GaAs/AlGaAs and SOI. Design of single mode 2D air bridge PhCW with triangular lattice PhCs on both the platforms is described in this chapter. Design of taper to improve the coupling efficiency for single mode PhCW on SOI and dispersion characteristics of SOI based single mode PhCW is also covered in this chapter.

Chapter 4 presents etching optimization of GaAs and silicon using UV photolithography. Fabrication of nano structures : electron beam lithography and inductively coupled plasma reactive ion etching process optimization of PhC on SOI using two e-beam resists viz. PMMA and HSQ are also discussed.

Chapter 5 This chapter presents the summary and outlook of the research work.

CHAPTER 2

Photonic Crystals : Theoretical Background

As mentioned in previous chapter, one can construct 1D, 2D, and 3D photonic crystal structures by engineering the dielectric constant of the medium periodically. In this chapter dispersion characteristics and PBG property of 1D and 2D structures will be discussed using theoretical approach.

The propagation of a electromagnetic wave in a medium is governed by Maxwell's equations.

$$\begin{aligned}\nabla \cdot \mathbf{D} &= \rho \\ \nabla \cdot \mathbf{B} &= 0 \\ \nabla \times \mathbf{E} &= -\frac{\partial \mathbf{B}}{\partial t} \\ \nabla \times \mathbf{H} &= \mathbf{J} + \frac{\partial \mathbf{D}}{\partial t},\end{aligned}\tag{2.1}$$

where \mathbf{E} and \mathbf{H} are macroscopic electric and magnetic fields, \mathbf{D} and \mathbf{B} are electric displacement and magnetic induction fields, ρ and \mathbf{J} are charge and current densities respectively. Considering all the charges and currents to be zero ($\rho = 0$ and $\mathbf{J} = 0$), we have

$$\begin{aligned}\mathbf{D} &= \epsilon \mathbf{E} = \epsilon_0 \epsilon_r(\mathbf{r}) \mathbf{E} \\ \mathbf{B} &= \mu \mathbf{H} = \mu_0 \mu_r \mathbf{H}.\end{aligned}\tag{2.2}$$

After substituting the equations (2.2) in to Maxwells equations (2.1), we get wave equation as follows :

$$\frac{c^2}{n^2(\mathbf{r})} \nabla^2 \mathbf{E}(\mathbf{r}, t) - \frac{\partial^2 \mathbf{E}(\mathbf{r}, t)}{\partial t^2} = 0,\tag{2.3}$$

where n is the refractive index of the medium. In case of homogeneous isotropic

medium the solution of this wave equation will be a plane wave given as,

$$\mathbf{E}(\mathbf{r}, t) = \text{Re}[\mathbf{E}_0 e^{j\mathbf{k}\mathbf{r}} e^{-j\omega t}], \quad (2.4)$$

where \mathbf{E}_0 describes both amplitude and phase of the plane wave.

However, for a periodic structure $n(\mathbf{r})$ will be modulated periodically and therefore the solution of wave equation given in equation (2.4) will no more be valid. The following section describes the theoretical background of PhC : its working principle and Photonic Band Gap (PBG) properties will be discussed .

2.1 1D PhC

Schematic of a 1D periodic medium with periodic variation along z direction is shown in Fig.2.1. For a periodic medium electromagnetic wave propagation can be explained by the four macroscopic Maxwells equations (2.1). Now the wave equation (2.3) can be modified as

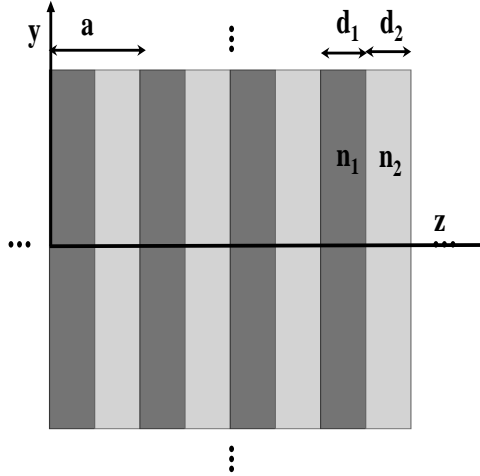


Figure 2.1: Schematic of a 1D periodic medium consisting of two alternating material layers of refractive indices n_1 and n_2 ; thickness d_1 and d_2 , respectively.

$$\frac{c^2}{n^2(z)} \frac{\partial^2}{\partial z^2} \mathbf{E}(z, t) - \frac{\partial^2}{\partial t^2} \mathbf{E}(z, t) = 0. \quad (2.5)$$

Since, the structure is periodic along z direction with period a , we can write

$$n(z) = n(z + a), \quad (2.6)$$

where $\mathbf{a} = d_1 + d_2$

Bloch theorem has been widely used in solid state physics to study the wave propagation in periodic media. The same concept can be used to study the electromagnetic wave propagation in a periodic dielectric medium.

According to the Bloch theorem, the electric field vector of a normal mode of propagation in periodic medium can be given as

$$\mathbf{E} = \mathbf{E}_K(z) e^{j(\omega t - k_y y)} e^{-jKz}, \quad (2.7)$$

where optical wave propagation is considered in yz plane, \mathbf{E}_K is a periodic function with period a , the constant K is the Bloch wave number, k_y is a wavevector component along y direction and ω is angular frequency. Since, \mathbf{E}_K is a periodic function in the z direction, it can be written as,

$$\mathbf{E}_K(z) = \mathbf{E}_K(z + \mathbf{a}). \quad (2.8)$$

Now, to study the PBG we have to find out the dispersion relation i.e. relation between ω and K . By using the Bloch wave theorem and matrix method approach given in (Yariv and Yeh, 2006), the analytical equation (dispersion relation) for normal incidence i.e. ($k_y = 0$) can be expressed as

$$\cos K\mathbf{a} = \cos k_1 d_1 \cos k_2 d_2 - \frac{1}{2} \left(\frac{n_2}{n_1} + \frac{n_1}{n_2} \right) \sin k_1 d_1 \sin k_2 d_2, \quad (2.9)$$

where

$$k_1 = \frac{\omega n_1}{c},$$

$$k_2 = \frac{\omega n_2}{c}.$$

k_1 and k_2 are propagation constant in medium n_1 and n_2 , respectively. We have chosen GaAs/air quarter wave stack multilayer structure ($d_1 = 375$ nm, $d_2 = 110.95$ nm and $a = 485.95$ nm) to study PBG for 1D PhC. By considering n_1 and n_2 to be 3.38 (GaAs) and 1 (air), the ω - K curve have been plotted for normal incidence as shown in Fig.2.2. Since, the Bloch waves are periodic with period $\frac{2\pi}{a}$, the ω - K curve have been plotted for the

irreducible Brillouin zone from $K = 0$ to $\frac{\pi}{a}$. Real K values are plotted with blue color and imaginary K values are plotted with red color. It can be seen from Fig.2.2 that for certain range of frequencies only real K values have solutions while the imaginary part of K is zero, waves with these frequencies are allowed in the crystal. However, when K has imaginary part the Bloch wave becomes evanescent and it is not allowed to propagate in the periodic structure. Hence, in the spectral regime $| \cos Ka | < 1$ correspond to real K values with allowed solutions in the periodic medium and $| \cos Ka | > 1$ with imaginary K values correspond to PBG. The fundamental PBG centered around $\omega_0 a / 2\pi c$ is shown in the Fig.2.2 with $\frac{\Delta\omega a}{2\pi c}$ for $0.21 \leq \omega a / 2\pi c \leq 0.44$. As we go further for higher frequencies we can see higher order stop bands for $0.86 \leq \omega a / 2\pi c \leq 1.09$ and $1.51 \leq \omega a / 2\pi c \leq 1.75$.

To study the stop band variation with change in index contrast, the dispersion curves are plotted for three different multilayer structures as shown in Fig.2.3. The dispersion curves were calculated for the first Brillouin zone from $K = -\frac{\pi}{a}$ to $\frac{\pi}{a}$. For the homogeneous medium as shown in Fig.2.3a stop band does not exist. With the introduction of perturbation PBG starts opening as shown in Fig.2.3b for GaAs/AlGaAs multilayer structure. GaAs/AlGaAs multilayer structures can be used in laser applications. With further increase in index contrast, PBG becomes wide as shown in Fig.2.3c for GaAs/air

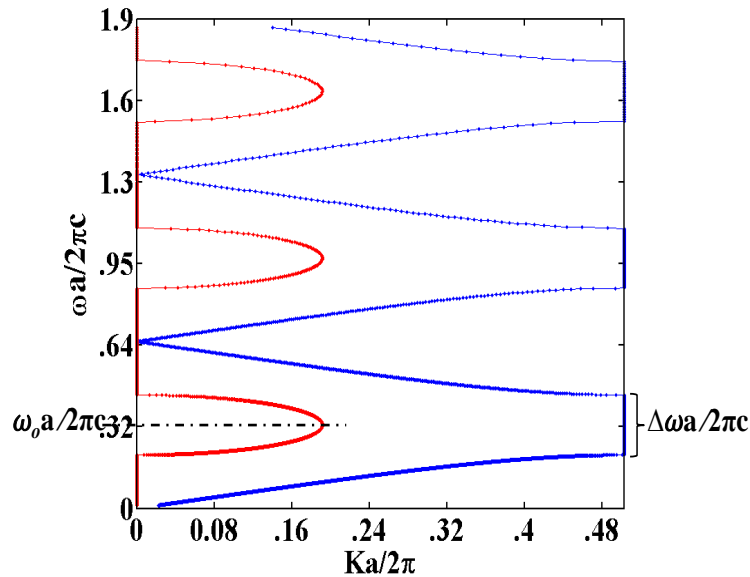


Figure 2.2: Photonic band structure of a 1D periodic medium at normal incidence. The red curves near vertical axis is the imaginary part of the Bloch wave number. The periodic medium is a quarter-wave stack formed with GaAs-air for 1500 nm wavelength.

multilayer structure. Large PBG of GaAs/air multilayer structure can be exploited to design passive devices.

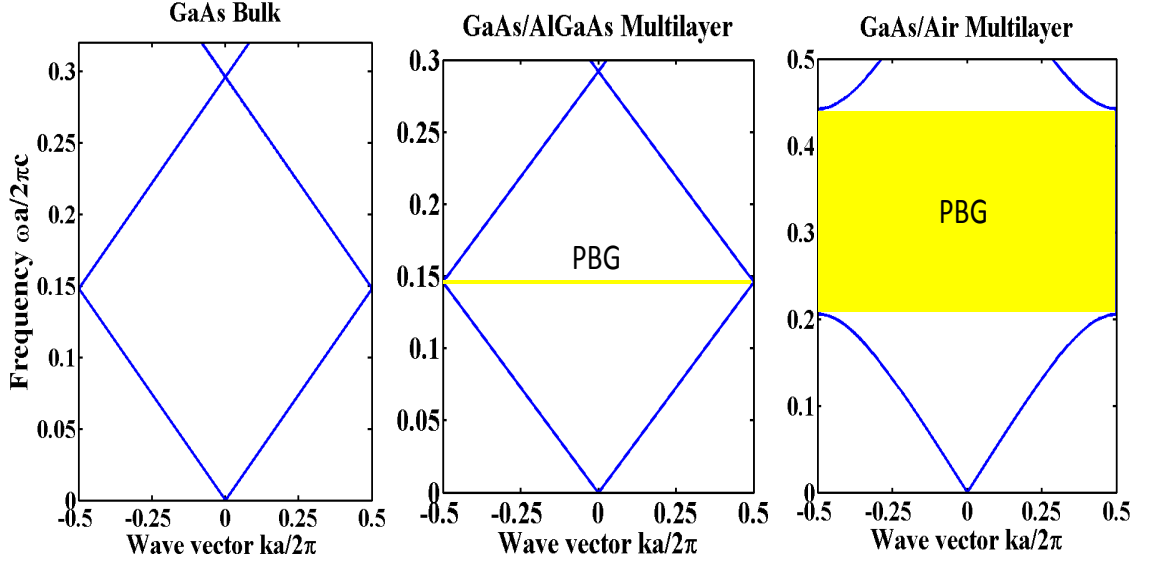


Figure 2.3: Photonic band structure at normal incidence for three different multilayer films (quarter wave stack layer with 1500 nm wavelength) : (a) GaAs bulk, (b) GaAs/AlGaAs multilayer, (c) GaAs/air multilayer.

In case of off-axis propagation, where $k_y \neq 0$ the dispersion relation will be polarization dependent. The analytical equations for TE (\mathbf{E} vector polarized perpendicular to the yz plane, the plane of propagation) and TM (\mathbf{E} vector polarized parallel to the yz plane) polarizations are given in equation (2.10) and (2.11), respectively from (Yariv and Yeh, 2006).

$$\cos K\mathbf{a} = \cos k_{1z}d_1 \cos k_{2z}d_2 - \frac{1}{2} \left(\frac{k_{2z}}{k_{1z}} + \frac{k_{1z}}{k_{2z}} \right) \sin k_{1z}d_1 \sin k_{2z}d_2 \quad (2.10)$$

$$\cos K\mathbf{a} = \cos k_{1z}d_1 \cos k_{2z}d_2 - \frac{1}{2} \left(\frac{n_{1z}^2 k_{2z}}{n_{2z}^2 k_{1z}} + \frac{n_{2z}^2 k_{1z}}{n_{1z}^2 k_{2z}} \right) \sin k_{1z}d_1 \sin k_{2z}d_2, \quad (2.11)$$

where

$$k_{1z} = \sqrt{\left(\frac{n_1 \omega}{c} \right)^2 - k_y^2}, \quad (2.12)$$

$$k_{2z} = \sqrt{\left(\frac{n_2 \omega}{c} \right)^2 - k_y^2}. \quad (2.13)$$

Dispersion curve for TE and TM polarization are shown in Fig.2.4a and Fig.2.4b, respectively. In the dispersion curve the red zones are the region where $|\cos K a| > 1$ i.e. PBG and green zones are where $|\cos K a| < 1$ i.e. allowed solution. It can be seen from the Fig.2.4a and Fig.2.4b that for normal incidence ($k_y = 0$) the dispersion is polarization independent. However, for angular incidence the dispersion curve is different for both the polarization and since the frequency range of stop band for different directions of propagation is different, there is no PBG when all the possible k_y are included.

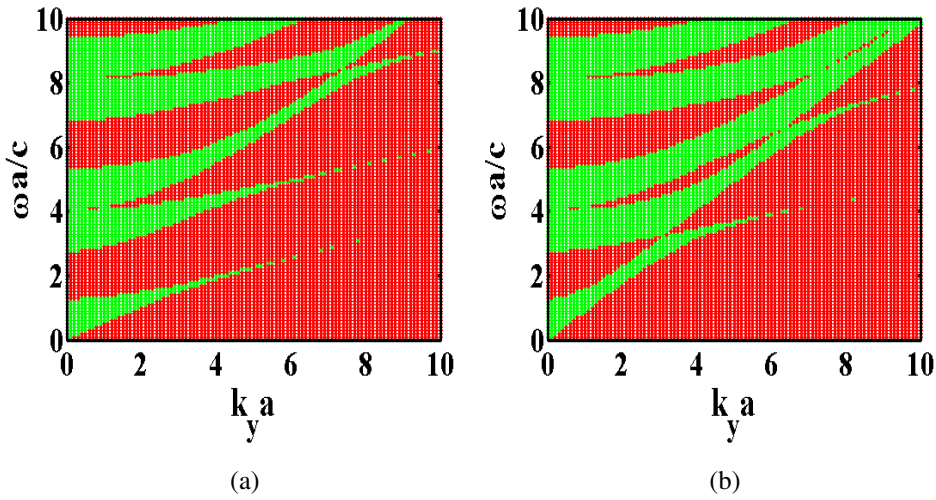


Figure 2.4: Photonic band structure of a wave in a periodic medium (GaAs-air quarter wave stack layer with 1550 nm) for : (a) TE wave, (b) TM wave. The green colored zones are allowed photonic bands in which $|\cos K a| < 1$. While the red colored zones are forbidden bands that are called PBGs

2.2 2D PhC

Since 1D periodic structure offers stop band over a frequency band only for a fixed direction of propagation, a 2D or 3D periodic medium is required to stop the propagation of a given frequency in all the directions. Fig.2.5 shows scheme of some 2D periodic structures. However, the solution of Bloch waves in 2D or 3D periodic media requires numerical analysis and computational methods. To study the band structure of 2D periodic medium using theoretical analysis a simple structure whose dielectric constant is separable can be considered as shown in Fig.2.6a (Yariv and Yeh, 2006). Schematic of reduced Brillouin zone of square lattice 2D PhC is shown in Fig.2.6b, where Γ , X and M points are high symmetry points.

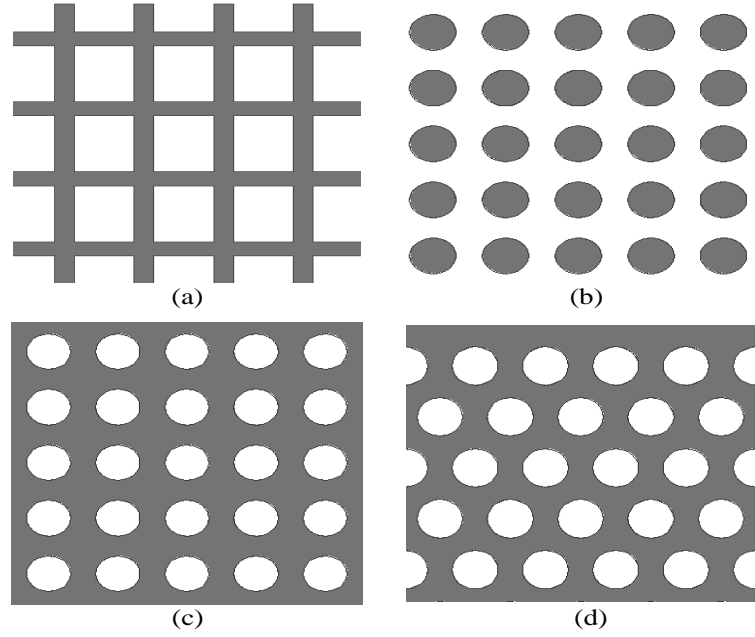


Figure 2.5: Schematic drawing of some 2D PhC structures : (a) Dielectric vein, (b) high index material rods, (c) Square lattice air holes in high index material slab, (d) Triangular lattice hole slab.

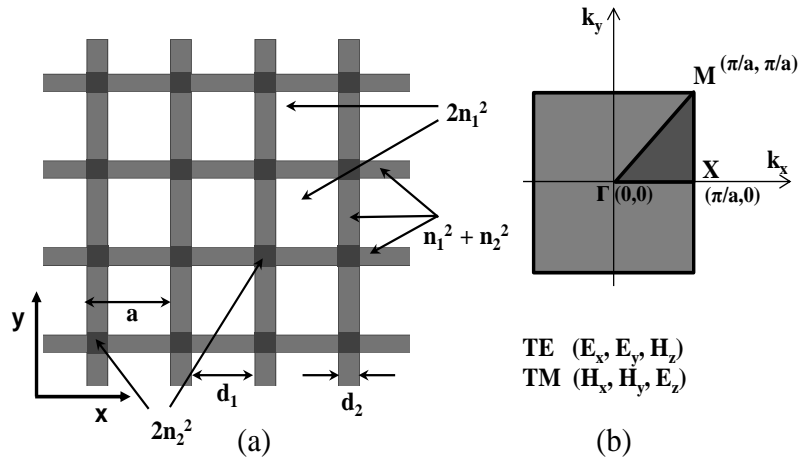


Figure 2.6: (a) 2D periodic structure, (b) First Brillouin zone of square lattice 2D PhC in K space. The shaded triangle region along Γ , X and M is the irreducible Brillouin zone.

The dielectric constant of such 2D periodic structure can be written as,

$$\epsilon(x, y) = \epsilon_H(x) + \epsilon_V(y) = \epsilon_0 n_H(x)^2 + \epsilon_0 n_V(y)^2, \quad (2.14)$$

where $n_H(x)$ and $n_V(y)$ are 1D periodic functions. The index profile of a 2D periodic structure whose dielectric constants are separable can be separated into sum of two

periodic layered media with index profile given by

$$n_H(x)^2 = \begin{cases} n_1^2, & 0 < x < d_1 \\ n_2^2, & d_1 < x < d_1 + d_2 = \mathbf{a} \end{cases}$$

$$n_V(y)^2 = \begin{cases} n_1^2, & 0 < y < d_1 \\ n_2^2, & d_1 < y < d_1 + d_2 = \mathbf{a} \end{cases}$$

The dispersion (ω - \mathbf{K}) relation for this kind of structure can be given by equation (2.15) and equation (2.16) from (Yariv and Yeh, 2006).

$$\cos K_x \mathbf{a} = \cos k_{1x} d_1 \cos k_{2x} d_2 - \frac{1}{2} \left(\frac{k_{2x}}{k_{1x}} + \frac{k_{1x}}{k_{2x}} \right) \sin k_{1x} d_1 \sin k_{2x} d_2 \quad (2.15)$$

$$\cos K_y \mathbf{a} = \cos k_{1y} d_1 \cos k_{2y} d_2 - \frac{1}{2} \left(\frac{k_{2y}}{k_{1y}} + \frac{k_{1y}}{k_{2y}} \right) \sin k_{1y} d_1 \sin k_{2y} d_2, \quad (2.16)$$

where K_x and K_y are components of Bloch wavevector and k_{1x} , k_{2x} , k_{1y} and k_{2y} are given by

$$k_{1x} = \sqrt{\left(\frac{n_1 \omega}{c} \right)^2 - \beta^2},$$

$$k_{2x} = \sqrt{\left(\frac{n_2 \omega}{c} \right)^2 - \beta^2},$$

$$k_{1y} = \sqrt{\left(\frac{n_1 \omega}{c} \right)^2 - \beta^2},$$

$$k_{2y} = \sqrt{\left(\frac{n_2 \omega}{c} \right)^2 - \beta^2},$$

where β is an arbitrary constant. The value of period \mathbf{a} was considered to be 155 nm. Using the equation (2.15) and (2.16), we can obtain relationship between ω and (K_x , K_y) and the photonic band structure. To obtain the dispersion relationship $\omega = \omega(K_x, K_y)$, normal surfaces for different normalized frequencies ($\frac{\omega \mathbf{a}}{2\pi c} = \frac{\mathbf{a}}{\lambda}$) have been plotted within the reduced Brillouin zone ($-1 < \frac{k_x \mathbf{a}}{\pi} < 1$, $-1 < \frac{k_y \mathbf{a}}{\pi} < 1$) as shown in Fig.2.7. To plot the band structure, the irreducible Brillouin zone along the Γ , X and M points was considered. To plot the band structure along ΓX direction, K_y was set to be 0, and the

normalized frequencies were plotted with K_x from 0 to $\frac{\pi}{a}$. Similarly to plot the band structure along XM direction, K_x was set to be $\frac{\pi}{a}$ and normalized frequencies were plotted with K_y from 0 to $\frac{\pi}{a}$ and for $M\Gamma$ direction normalized frequencies were plotted with both K_x and K_y from $\frac{\pi}{a}$ to 0. The band structure along the irreducible Brillouin zone boundary is shown in Fig.2.8.

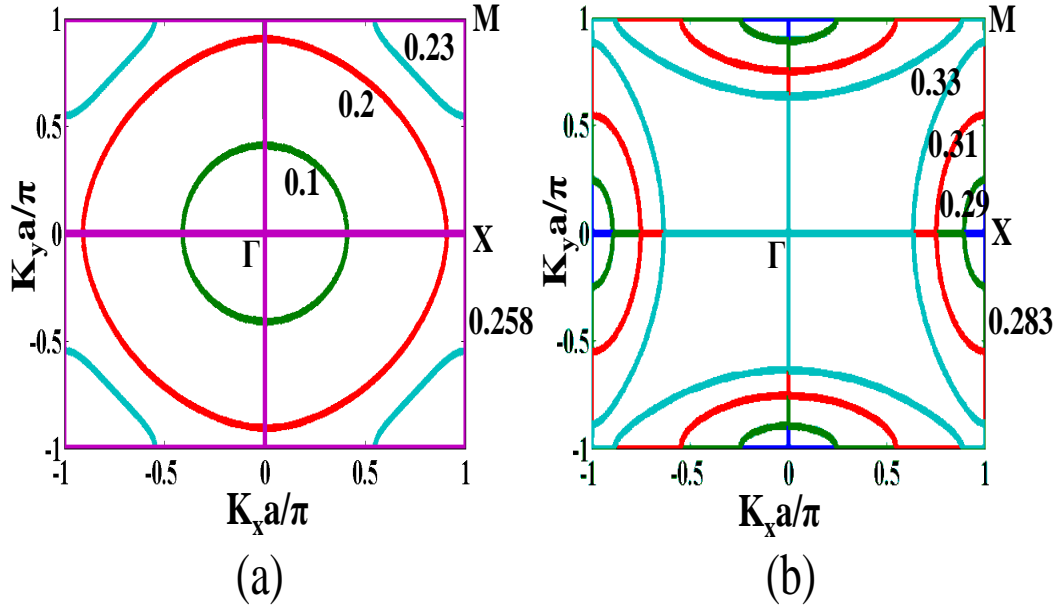


Figure 2.7: Equifrequency contours in K_x, K_y plane of a 2D PhC structures at different normalized frequencies: $\frac{a}{\lambda} = 0.1, 0.2, 0.23, 0.258, 0.283, 0.29, 0.31, 0.33$. The normalized surfaces are plotted in the Brillouin zone. The parameters used for calculation are $n_1^2 = 0.5, n_2^2 = 8.2, d_1 = 0.8a$, and $d_2 = 0.2a$

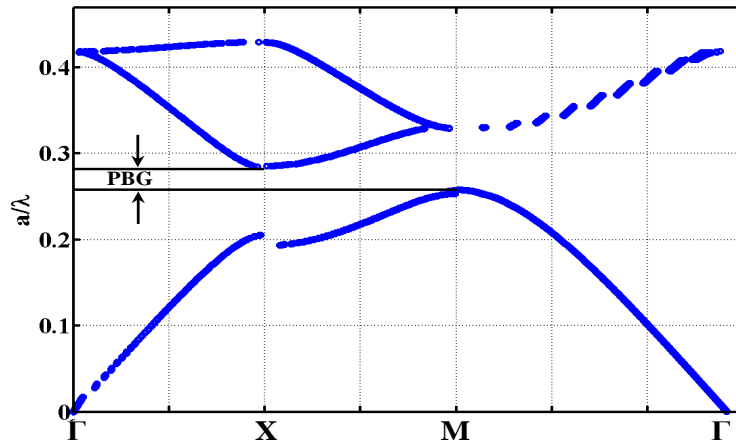


Figure 2.8: Band structure of a 2D periodic medium. The vertical axis is the normalized frequency in units of $\frac{a}{\lambda}$ and horizontal axis is normalized wavevector in different direction along the irreducible Brillouin zone. The parameters used for calculation are $n_1^2 = 0.5, n_2^2 = 8.2, d_1 = 0.8a$, and $d_2 = 0.2a$

The fundamental PBG exists between maxima of lower band and minima of upper band (0.258, 0.283) (see Fig.2.8). The value of fundamental PBG was around 53.07 nm.

The theoretical analysis was done for a periodic structure which has three different regions with unique refractive indices. However, practically it is not possible to fabricate such structures.

2.3 3D PhC

3D periodic structures contain periodic dielectric variation in all the three directions. The 3D PhC structures can offer complete bandgap similar to electronic energy bandgap in crystals having 3D periodic potentials. 3D PhCs have the best properties to control the light in all the three directions due to their omnidirectional PBG. However, it is difficult to fabricate the 3D PhC structure using the current planar fabrication technology. Some of the examples of 3D periodic structures are synthetic opal, inverted opal, Yablonovite and woodpile structure. The schematic of woodpile structure is shown in Fig.2.9 which is fabricated by the layer by layer fabrication approach. Since 3D PhC structures are generally not utilized in planar circuits as well as its very difficult to fabricate such structures, they have not been studied in the present work.

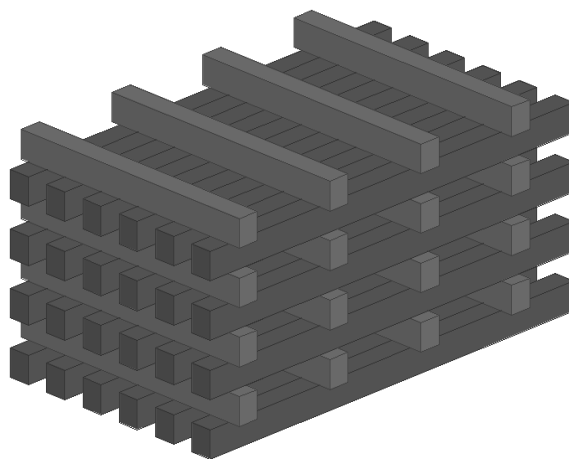


Figure 2.9: Example of 3D PhC structures.

2.4 2D Photonic Crystal Slab

Generally 2D PhCs are much easier to fabricate as compared to 3D PhCs. However, the 2D PhC structure which is homogeneous in the third direction cause radiation of the light. Therefore, to bound the light in the plane of 2D photonic crystals, the 2D PhC structures can be combined with the slab waveguide in the third direction. When 2D PhC structures are combined with slab it is called as 2D photonic crystal slab. In PhC slab light is confined in the plane due to high refractive index of the slab.

2.5 Conclusions

Dispersion curve and PBG property of 1D and 2D periodic structures have been theoretically studied using semi-analytical method. However, a 2D periodic structure with unique refractive indices in three different regions is practically impossible to fabricate. The two main configurations of 2D PhCs that can be fabricated and are being widely used in PhC based research areas are shown in Fig.2.10. To calculate PBG for these structures, computational method or numerical analysis is required. The first structure, called as rod slab structure is composed of high index material rods as shown in Fig.2.10a. This structure gives rise to PBG for TM polarized waves, where electric field is polarized normal to the plane of periodicity. The second type of 2D PhC as shown in Fig.2.10b is called as hole slab, it consists of periodic circular air holes etched in high index material slab. This structure gives rise to PBG for TE polarized waves, where electric field is polarized along the plane of periodicity. The hole slab structures is mostly used in experimental studies due to their ease of fabrication.

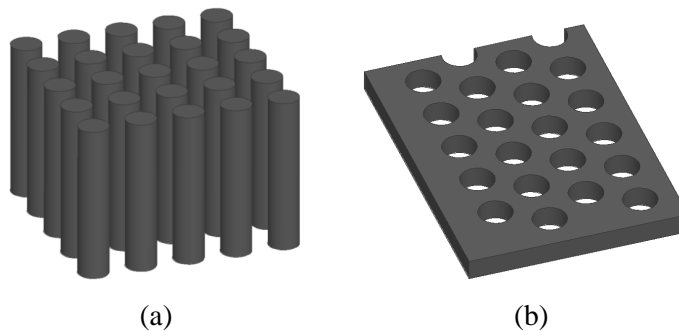


Figure 2.10: Some examples of 2D PhC structures : (a) Square lattice high index rods in air, (b) Triangular lattice air holes etched in high index slab.

CHAPTER 3

Device Design and Simulation

In this chapter, simulation methodology used in designing of air bridge 2D PhCW with GaAs/AlGaAs and SOI substrate for telecommunication wavelength will be discussed. The design parameters of PhC were optimized to obtain sufficiently large PBG centering at third generation optical communication window ($\lambda \sim 1550 \text{ nm}$) for optoelectronic and optical interconnect applications.

Square lattice and triangular lattice geometry PhCs are two well known structures. We have theoretically studied and analyzed PhC hole slab structure (high index material slab containing periodic circular air holes of radius r) with both the geometries. In the following sections we will be discussing design and simulation results of square and triangular lattice hole slab PhC and PhCW.

3.1 Square Lattice Hole Slab PhC

The dispersion and PBG variation with change in air filling factor for square lattice geometry PhC hole slab were studied using commercial FDTD based solver (LUMERICAL FDTD Solutions). In 2D Finite Difference Time Domain (FDTD) simulations, the structure is considered to be infinite in the third direction. The structure of interest is shown in Fig.3.1a, where $\vec{a}_1 = (a, 0)$ and $\vec{a}_2 = (0, a)$ are real space lattice vectors in x and y directions respectively. Its reciprocal lattice is shown in Fig.3.1b, where $\vec{b}_1 = (\frac{2\pi}{a}, 0)$ and $\vec{b}_2 = (0, \frac{2\pi}{a})$ are reciprocal space lattice vectors. Square region in Fig.3.1b shows the first Brillouin zone or unit cell in reciprocal space. $\Gamma = (0, 0)$, $X = (\frac{\pi}{a}, 0)$ and $M = (\frac{\pi}{a}, \frac{\pi}{a})$ are high symmetry points. The dispersion curve was calculated along all the edges of irreducible Brillouin zone (highlighted right angled triangle within the reduced Brillouin zone). Maxima and minima of the bands occur at high symmetry points. Therefore, band structure was calculated along these points.

To study the polarization effects on band structure, initially 2D simulations were carried out on a GaAs PhC hole slab for both TE and TM polarization with square

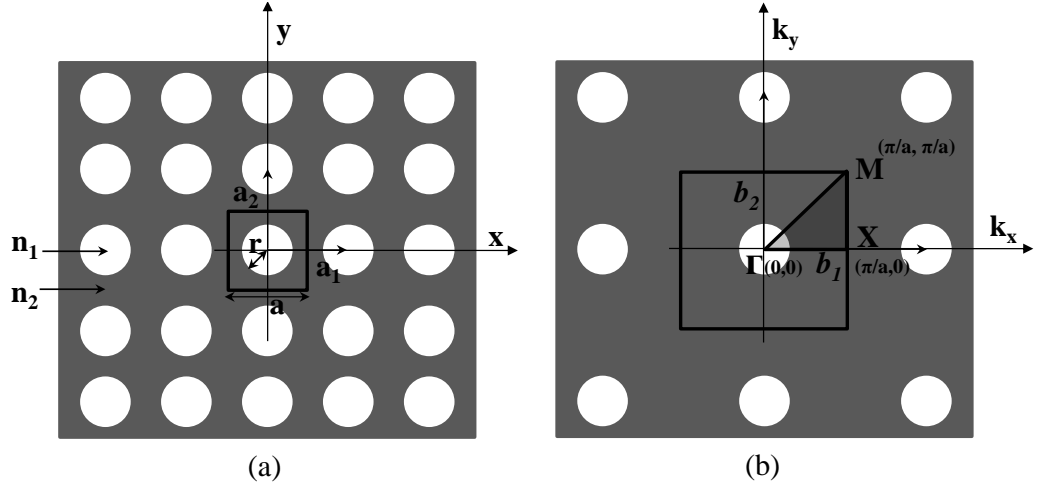


Figure 3.1: Scheme of square lattice PhC : (a) Real space lattice structure and the unit cell used for calculation is shown within the black color boundary, here n_1 and n_2 are refractive indices of air holes of radius (r) and slab respectively. (b) Reciprocal space lattice structure with first Brillouin zone of square lattice PhC. The shaded triangle region within Γ , X and M is irreducible Brillouin zone.

lattice geometry. In TE polarization electric field was polarized in the plane of periodicity with major field components (E_x, E_y, H_z) . In TM polarization electric field was polarized in perpendicular direction to the plane of periodicity with major field components (H_x, H_y, E_z) . The refractive index of GaAs was considered to be 3.38. For FDTD simulations, the fundamental unit cell has been considered as shown in Fig.3.1a. The infinitely extended 2D PhC has been accounted by Bloch boundary condition. Randomly located broadband dipole sources were used to excite the resonant modes within the unit cell. Electromagnetic (EM) field at every time step was calculated using time monitors within the unit cell. The calculated EM field was Fourier transformed to obtain the frequency spectrum. Resonant frequencies were calculated by sweeping wave-vectors from Γ to X, X to M and M to Γ along irreducible Brillouin zone. The wavevector k_x was scanned from 0 to $\frac{\pi}{a}$ by keeping $k_y = 0$ for Γ to X, similarly for X to M k_y was scanned from 0 to $\frac{\pi}{a}$ by keeping $k_x = \frac{\pi}{a}$ and for M to Γ both k_x and k_y were scanned from $\frac{\pi}{a}$ to 0 and resonant frequencies for all the wavevectors were calculated. The calculated band structure for the design parameters corresponding to maximum PBG (for TE polarization) centered around 1550 nm is shown in Fig.3.2a with red color. In the plot x axis represents wavevector in different directions in reciprocal space and y axis represents normalized frequency in units of $\frac{a}{\lambda}$ where a is period of the PhC and λ is free space wavelength. A_1 and A_2 are maxima of lower band and minima of upper band,

respectively. The gap between the maxima and minima point is called as PBG. For TE polarization maximum PBG comes around 170 nm for $r = 217$ nm and $a = 495$ nm. Using the design parameters of TE polarization, calculated band structure for TM polarization is shown in the Fig.3.2a with blue color. B_1 and B_2 are maxima of lower band and minima of upper band respectively. The maximum PBG in case of TM polarization comes around 509 nm for $r = 264$ and $a = 495$ nm. However, for these design parameters hole starts merging with their neighbor. Since, in the band structure vertical axis is the normalized frequency $\frac{a}{\lambda}$, from the mid point of PBG the period can be calculated corresponding to 1550 nm center wavelength.

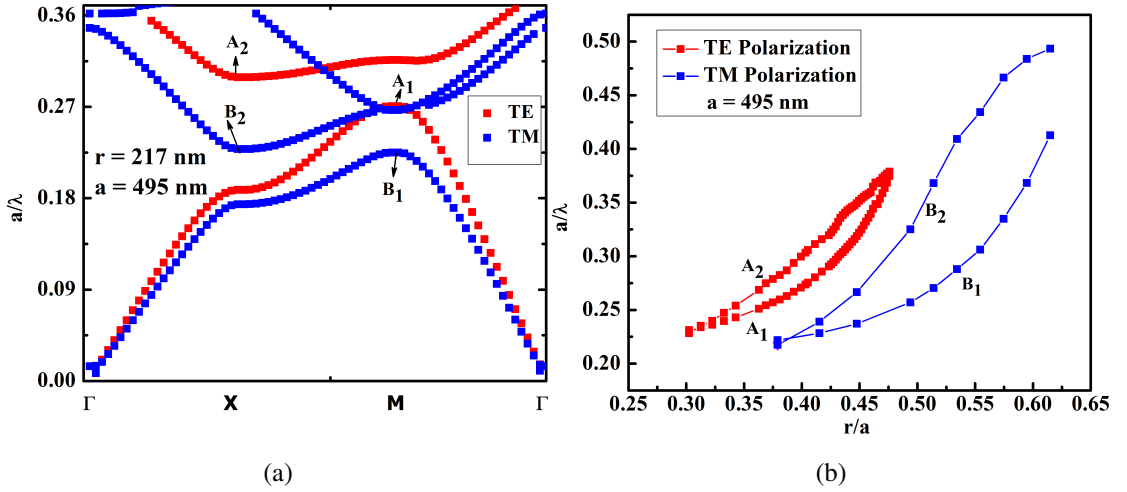


Figure 3.2: (a) Dispersion curve for square lattice 2DPhC on GaAs (extending uniformly in third direction) for both TE and TM polarization, here A_1 and A_2 are maxima and minima of lower and upper band respectively for TE case, similarly B_1 and B_2 are maxima and minima of lower and upper band for TM case. (b) PBG variation with r/a ratio for both TE and TM polarization.

The variation of PBG with change in radius (r)/period (a) ratio was analyzed using 2D FDTD method. Simulations were carried out for fixed value of lattice period ($a = 495$ nm) with variation in radius (r) for both TE and TM polarization. The bandgap variation with change in r/a ratio were calculated for both TE and TM polarization as shown in Fig.3.2b, where in the plot for a particular polarization the lower edge corresponds to the maxima of first band and the upper edge corresponds to the minima of second band. It was found that the hole slab supports PBG only for TE polarization. In case of TE polarization PBG increases with increase in radius and it starts reducing when holes start merging as shown in Fig.3.2b. In the case of TM polarization, PBG starts opening around $r = 220$ nm ($r/a = 0.45$) but holes merge with their neighbors as

r/a exceeds 0.5. One need to visualize the structure by considering the fact that the circular holes disappear (as we go beyond 0.5) by leaving isolated high dielectric pillar structure that causes to open PBG for TM polarization and as we go beyond 0.5, we can still observe increase in bandgap for TM polarization. It was found that the hole-slab structure supports PBG only for TE polarization. Therefore, further study and simulations were carried out only for TE polarization.

For practical applications, finite slab thickness is required. The thickness of the slab was considered to be 220 nm (250 nm) for GaAs (silicon). 3D FDTD simulations were carried out for the square lattice geometry PhC hole slab shown in Fig.3.3a to incorporate the finite slab thickness. The unit cell for the simulation is shown in Fig.3.3b with Bloch boundary condition on all the four sides perpendicular to the PhC slab, perfectly matched layer (PML) on the top and symmetry boundary condition at the middle of the slab. Since, air bridge PhCW structure has mirror symmetry along the middle of the slab, symmetry BC were used here. In case of symmetry boundary condition it calculates only even (TE like) eigenmodes of PhC structure and computation time can be reduced by half.

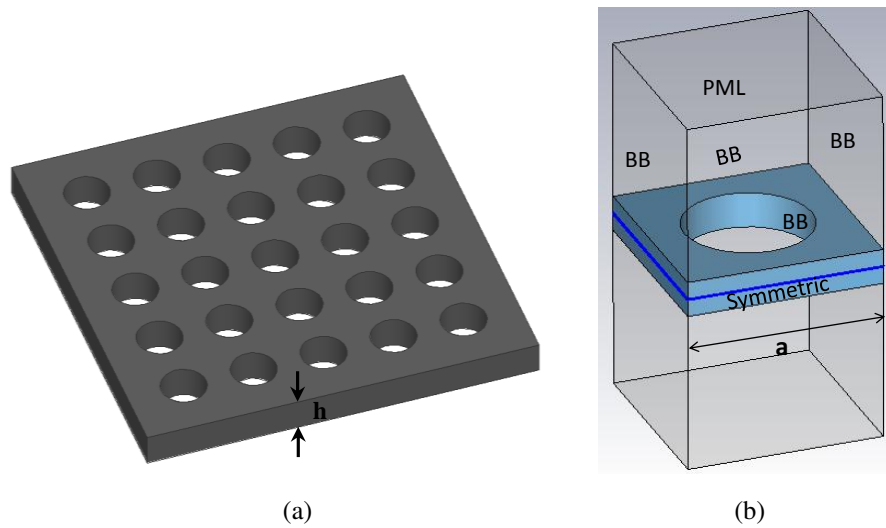


Figure 3.3: (a) Square lattice PhC slab. (b) 3D view of unit cell of square lattice geometry hole slab PhC with Bloch Boundary (BB) on all four sides, PML and Symmetry boundary on top and middle of the slab, respectively.

The calculated dispersion curve for optimized designed parameters period $a = 570$ nm and radius $r = 227$ nm corresponding to 1550 nm central wavelength and maximum PBG of the order of ~ 100 nm is shown in Fig.3.4a. In the plot x axis represents

wavevector in different directions in reciprocal space and y axis represents normalized frequency in units of $\frac{a}{\lambda}$, where a is period of the PhC and λ is free space wavelength. The curve with circular dots shown in the Fig.3.4a is the dispersion curve of cladding (in air bridge structure both the bottom and top cladding are air). It is also called as light line. Modes with frequencies above the light line will radiate its energy to the air cladding. In the vertical direction in slab the confinement will be due to total internal reflection and the modes above light line will be coupled to the continuum of radiation modes and therefore a PBG must lie below light line.

In order to validate our simulation methodology, we have reproduced the results given in literature (Loncar *et al.*, 2000) for SOI system with square lattice hole slab PhC having dimensions (272 nm slab thickness, 496 nm lattice period and 198 nm radius) and the dispersion curve for the same is shown in Fig.3.4b.

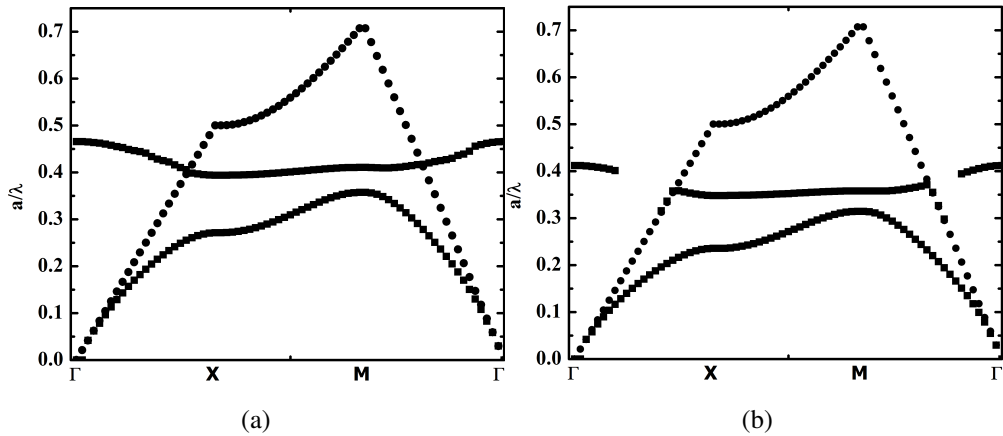


Figure 3.4: (a) Dispersion curve of 2DPhC on GaAs slab of thickness $h = 220$ nm, radius $r = 217$ nm and period $a = 495$ nm. The curve with circular dot is the dispersion of air cladding (light line). (b) Dispersion curve of 2DPhC on silicon. The parameters taken from [(Loncar *et al.*, 2000)] to validate our simulation result are : $h = 272$ nm, $r = 198$ nm and $a = 496$ nm.

The PBG in case of square lattice geometry hole slab PhC comes around 100 nm which might get closed due to low fabrication tolerance. For further investigation triangular lattice geometry hole slab PhC have been studied and simulated.

3.2 Triangular Lattice Hole Slab PhC

Triangular lattice PhC structure in real space is shown in Fig.3.5a, where $\vec{a}_1 = a \cdot \left(\frac{\sqrt{3}}{2}, \frac{1}{2}, 0\right)$ and $\vec{a}_2 = a \cdot \left(-\frac{\sqrt{3}}{2}, \frac{1}{2}, 0\right)$ are real space lattice vectors and its reciprocal lattice is shown in Fig.3.5b, where $\vec{b}_1 = \frac{4\pi}{a\sqrt{3}} \cdot \left(\frac{1}{2}, \frac{\sqrt{3}}{2}, 0\right)$ and $\vec{b}_2 = \frac{4\pi}{a\sqrt{3}} \cdot \left(\frac{1}{2}, -\frac{\sqrt{3}}{2}, 0\right)$ are reciprocal space lattice vectors. The hexagon region shown in Fig.3.5b is the first Brillouin zone and $\Gamma = (0, 0, 0)$, $M = \frac{2\pi}{a\sqrt{3}} \cdot \left(\frac{1}{2}, -\frac{\sqrt{3}}{2}, 0\right)$ and $J = \frac{4\pi}{3a} \cdot (0, 1, 0)$ are high symmetry points. 3D FDTD simulations were carried for calculating dispersion curve for GaAs ($n = 3.38$)

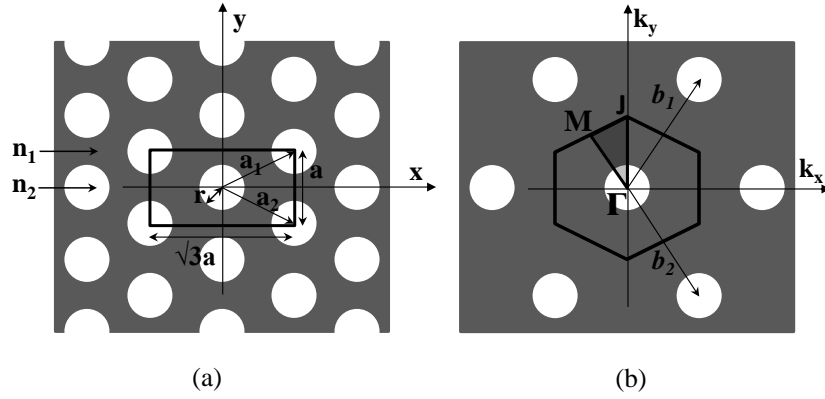


Figure 3.5: Triangular lattice PhC (a) Real space lattice structure and the unit cell used for calculation is shown within the black color boundary. (b) Reciprocal space lattice structure with first Brillouin zone of triangular lattice PhC, here the shaded region along Γ , J and M is irreducible Brillouin zone.

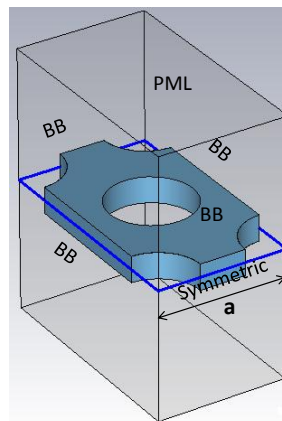


Figure 3.6: (a) 3D view of unit cell of triangular lattice geometry hole slab PhC with Bloch Boundary (BB) on all four sides, PML and Symmetry boundary on top and middle of the slab, respectively.

and silicon ($n = 3.4777$) based PhC. The thickness of the slab for GaAs (Si) was considered 220 nm (250 nm) to ensure single mode guiding. The effect of complete PhC was

studied by truncating it to a 3D single unit cell, the unit cell of the triangular lattice PhC is shown in Fig.3.6, with Bloch boundary condition on all the four sides perpendicular to the PhC slab, PML on the top and symmetry boundary condition at the middle of the slab. Resonant frequencies were calculated by sweeping wavevectors from Γ to J, J to M and M to Γ along irreducible Brillouin zone. The calculated band structures for the optimized design parameters are shown in Fig.3.7a and Fig.3.7b for GaAs and silicon, respectively and the design parameters are given in table 3.1.

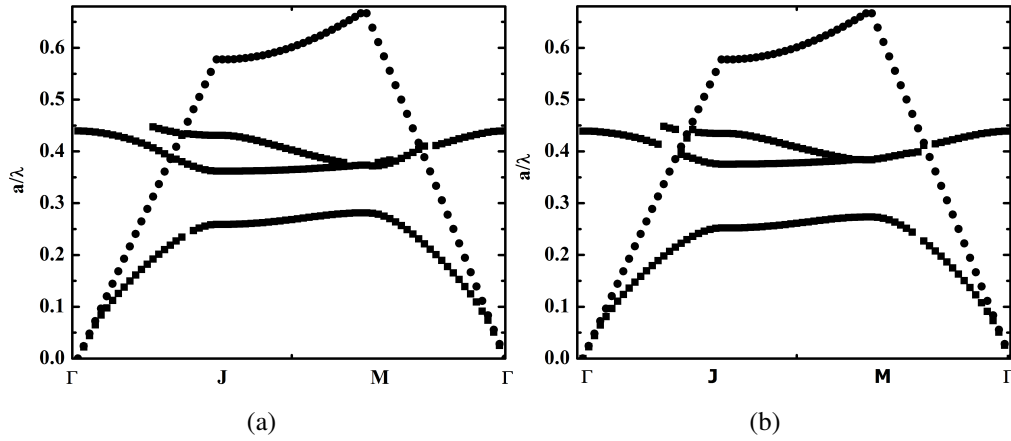


Figure 3.7: Dispersion curve of triangular lattice PhC for the designed parameters on (a) GaAs/AlGaAs and (b) SOI.

Table 3.1: Optimized parameters for triangular lattice PhC Structures

| Material | Slab thickness (nm) | Hole radius (nm) | Period (nm) | PBG (nm) |
|-------------|---------------------|------------------|-------------|----------|
| GaAs/AlGaAs | 220 | 150 | 500 | 396 |
| SOI | 250 | 163 | 500 | 497 |

The bandgap in triangular lattice PhC is much larger than the PBG in case of square lattice PhC due to its more symmetric Brillouin zone. Here again the PBG must lie below the light line. The designed triangular lattice PhC hole slab have been further used for designing of single mode PhCW.

3.3 Design of PhCW with Triangular Lattice Geometry

The simplest PhCW can be formed by removing a row of holes from the PhC structure and it is called as single defect PhCW. Introduction of defect destroys periodicity

of photonic crystals and the defect region opens a way to confine light by means of photonic bandgap. Adding a defect line in PhC is analogous to adding impurity in semiconductor crystal. When we remove a single row of holes it is similar to adding a donor impurity and with introduction of this impurity the modes from the air bands are pulled down into the PBG. In this work single mode triangular lattice based air bridge PhCW have been designed on GaAs/AlGaAs and SOI. The schematic of the air bridge PhCW structure is shown in Fig.3.8a. With the introduction of defect line in PhC it forms PhCW, PhC cladding beside the defect line act as PBG mirrors and light is not allowed to propagate in lateral direction. Propagation in vertical direction is prevented since the mode lies below light line. Light is only allowed to propagate along defect line and thereby enabling the guiding of lightwaves. The guiding of light in lateral direction happens due to PBG, while in the vertical direction it is due to high refractive index contrast (total internal reflection).

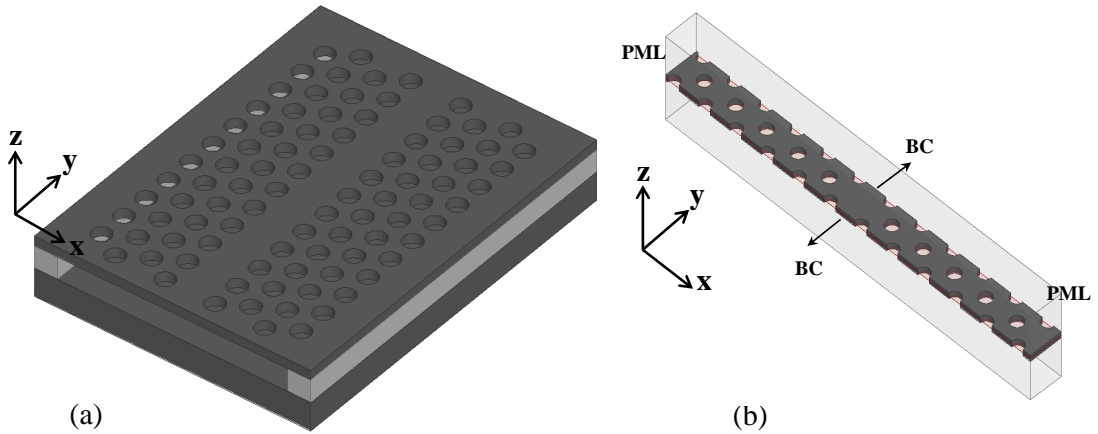


Figure 3.8: (a) Schematic of 2D air bridge PhCW. (b) Unit cell of PhCW with boundary condition used for band structure calculation.

3D FDTD simulation was carried out for the single defect width PhCW on GaAs/AlGaAs. A row of air holes were removed from the designed triangular lattice PhC along Γ -J direction. With the introduction of defect line translation symmetry is broken in x direction. However, the structure is still periodic along y direction. Unit cell of PhCW is shown in Fig.3.8b. Bloch boundary condition was used on both sides in y direction while symmetry boundary condition was used on middle of the slab and PML was used on top and in x direction after 5 layers of PhC.

The optimized design parameters of PhC; period, radius and slab thickness which are given in table 3.1 for GaAs/AlGaAs and SOI were used for the waveguide simula-

tions. Since, the guided mode should lie in the range where no PhC cladding modes exist, the bands of PhC from all the directions have to be projected on to Γ -J direction. For calculating the band structure, broadband dipole sources were located randomly to excite the resonant modes within the unit cell and time monitors were used to calculate the EM field at every time step. The calculated EM field were Fourier transformed to obtain the frequency spectrum. The wavevector k_y was scanned for Γ to J' along the reduced Brillouin zone as shown in Fig.3.9a from 0 to $\frac{\pi}{a}$ and resonant frequencies were calculated. The dispersion curve for single defect line on GaAs is shown in Fig.3.9b, where x axis is the normalized wavevector $\frac{k_y a}{2\pi}$ and y axis is frequency in Hz. In case of single defect line three modes (A, B and C) are lying in PBG. These modes are called as PBG Guided mode. However, the mode which exists below continuum of PhC cladding modes are also guided but the guiding principle here is total internal reflection in both lateral and vertical directions. This mode is called as Index Guided (IG) mode, it does not see perforated slab as a PBG material but see it as a low index material which has effective refractive index which is lower than refractive index of GaAs (3.38) slab. To obtain a single mode waveguide, the width of the waveguide was reduced to $0.55W$, where W is the width (from center to center of the circles adjacent to the defect line) of single defect waveguide. The dispersion curve for single mode waveguide on GaAs/AlGaAs is shown in Fig.3.10, here x axis is normalized wavevector while y axis in Fig.3.10a is frequency in Hz and in Fig.3.10b normalized frequency of unit $\frac{a}{\lambda}$. The guided mode below light line covers the range of $\frac{a}{\lambda}$ from 0.31604 to 0.3316 of bandwidth ~ 74 nm.

Dispersion curve for single defect and single mode waveguide on SOI is shown in Fig.3.11a and Fig.3.11b respectively. Here the guided mode below light line covers the range of $\frac{a}{\lambda}$ from 0.31914 to 0.33238 of bandwidth ~ 62 nm.

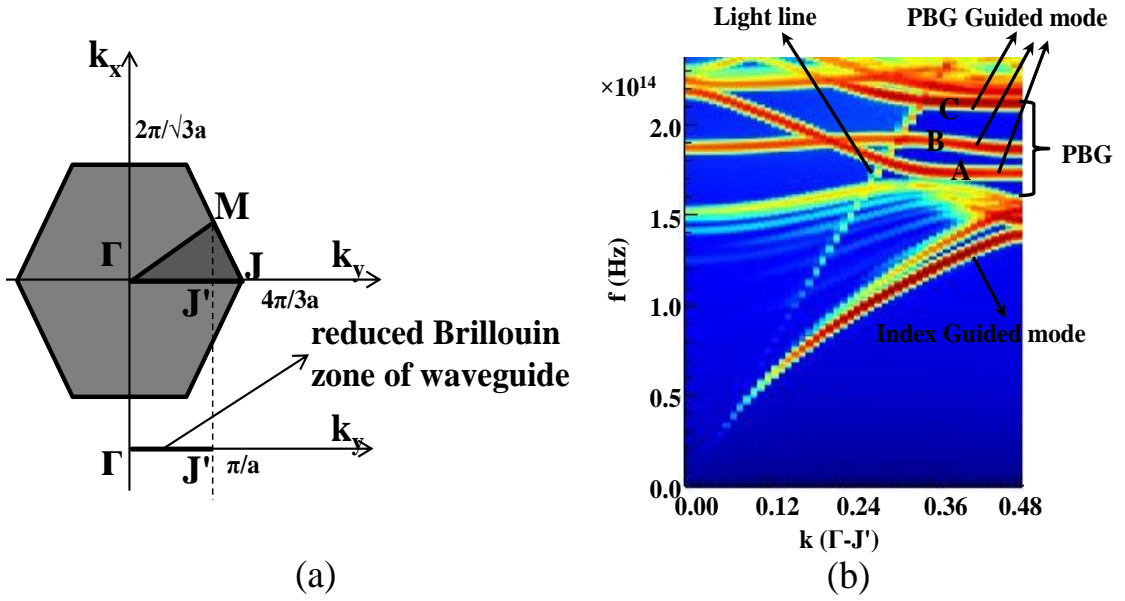


Figure 3.9: (a) Brillouin zone of PhCW and reduced Brillouin zone of waveguide is shown from Γ - J' . (b) Dispersion curve of GaAs/AlGaAs single defect width PhCW along Γ - J' direction.

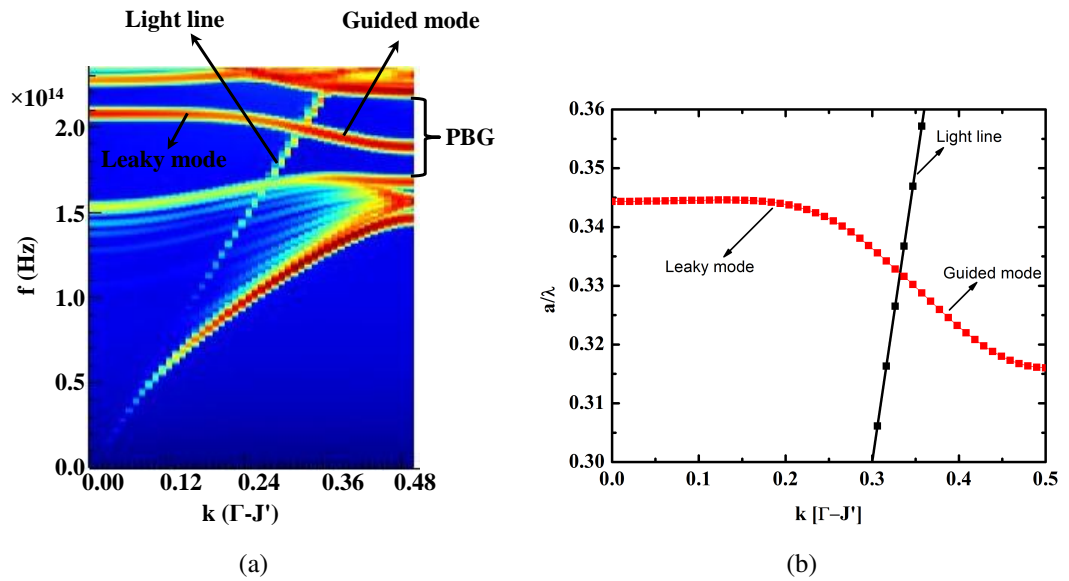


Figure 3.10: Dispersion curve of GaAs/AlGaAs PhCW along Γ - J' direction. It explicitly shows single guided mode lying in PBG below light line. Practically mode above light line is leaked out in cladding. Here x axis is normalized wavevector and vertical axis is (a) Frequency in THz. (b) Normalized frequency in units of $\frac{a}{\lambda}$.

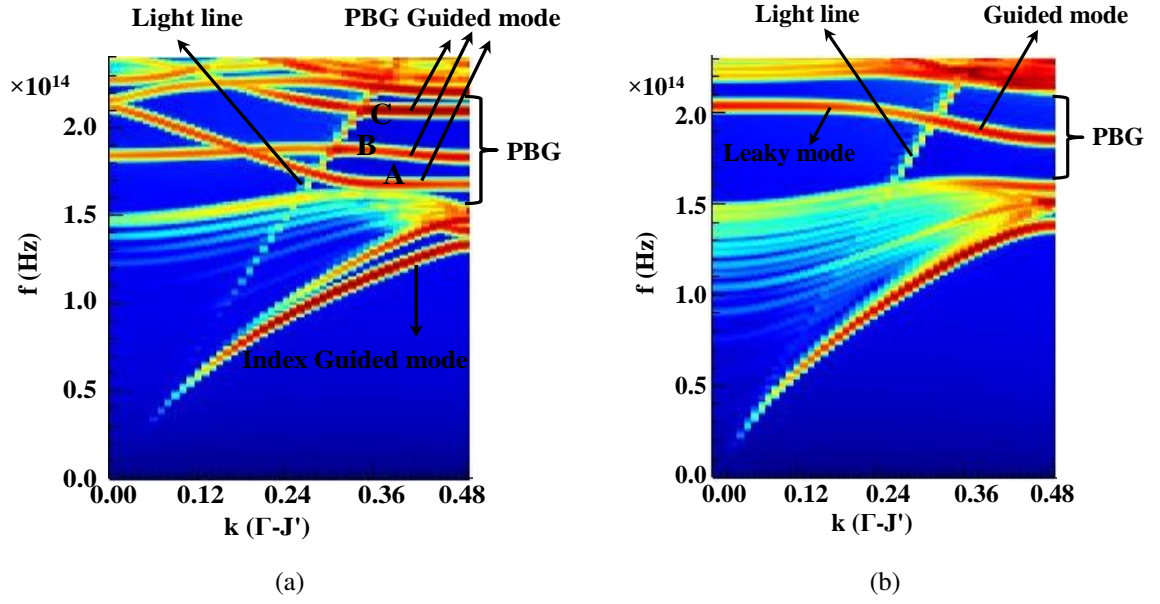


Figure 3.11: Dispersion curve of SOI PhCW along Γ -J direction. Here x axis is normalized wavevector and vertical axis is Frequency in THz. (a) Single defect PhCW (b) Single mode PhCW.

Triangular lattice hole slab PhC have been designed to obtain sufficiently large PBG centering at 1550 nm on GaAs and silicon slab. The designed parameters of PhC were used to design single mode PhCW. Triangular lattice PhC are much more fabrication tolerant than square lattice PhC due to its large PBG. The designed triangular lattice based PhCW on SOI has been further investigated for tapered structure to couple light into PhCW and for slow-light application. The designed PhCW on SOI was further considered for fabrication.

3.4 Integrated PhCW

To use the PhCW in practical applications in integrated photonic circuits, light has to be efficiently coupled into PhCW from fiber or dielectric waveguide. Coupling of light into PhCW from photonic wire waveguide is a critical issue. The mode behavior in a PhCW is different from the PhW in terms of mode size (Haxha *et al.*, 2009), group velocity (Lin *et al.*, 2011) and guiding principle. Large mode size and the slow group velocity of PhCW are the two major issues which cause mode mismatch at the interface of the two waveguides. In PhCW modes size becomes large due to the interaction with adjacent crystal structure and because of the mode size mismatch at the interface light

starts scattering and small part of it will be coupled to the PhCW. Another issue is slow-light, PhCW slows down the light near the Brillouin zone edge because of high dispersion. Slowing of light can even happen away from the Brillouin zone edge due to flat anti crossing mode and group velocity reduction. Solution to these problems is the use of taper to change the mode size and group velocity gradually.

In order to reduce the impedance mismatch at the junction, a taper can be designed either in PhW or PhCW. In case of PhCW taper it can be made in many ways :

- 1) By changing period with fixed radius (Martijn de Sterke *et al.*, 2009).
- 2) By gradually changing the radius with fixed period (Lin *et al.*, 2011).
- 3) By removing some holes of PhCW at the interface to make a gradual change of mode size and velocity (Sanchis *et al.*, 2004).
- 4) By shifting the lattice structure gradually away from the waveguide (Pottier *et al.*, 2007).
- 5) By gradually changing the size of holes adjacent to defect line only (Ngo *et al.*, 2012).

In the next two sections we will be discussing the design of a single mode PhW and taper for the integrated PhW-PhCW structure.

3.4.1 Design of Single Mode PhW

Single mode PhW have been designed using commercially available mode solver "Lumerical MODE Solutions" on SOI. By keeping the height of PhW fixed (250 nm), width was varied from 260 nm to 1000 nm and effective index n_{eff} was calculated for modes TE_0 , TE_1 , TM_0 and TM_1 . The n_{eff} for all the modes is shown in Fig.3.12. Since in the width range of 260 nm to 576 nm, only fundamental TE and TM modes have effective index more than index of SiO_2 , only these two modes will be guided and other higher order modes will be leaked in oxide cladding. However, for width greater than 576 nm, n_{eff} of TE_1 mode exceeds index of oxide, the region becomes multimoded at this point. Single mode region, multi mode region and single mode cutoff region are shown in Fig.3.12. We have chosen the PhW width to be 540 nm (476 nm) for single defect (single mode) PhCW for integrated structures. Mode profile for the fundamental mode TE_0 and TM_0 are shown in Fig.3.13a and Fig.3.13b, respectively.

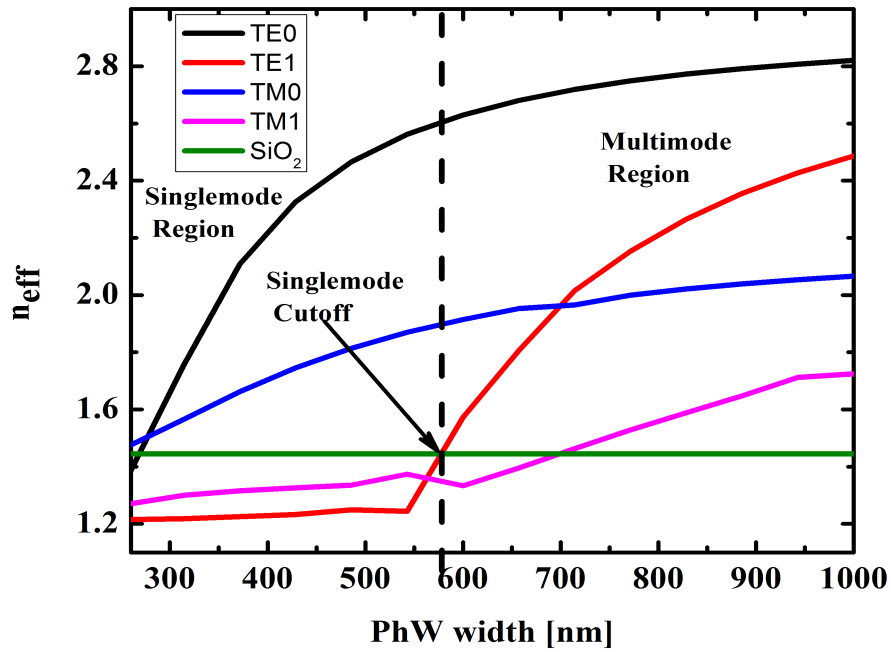


Figure 3.12: Effective index variation with change in width of PhW for TE_0 , TM_0 , TE_1 , TM_1 , SiO_2 .

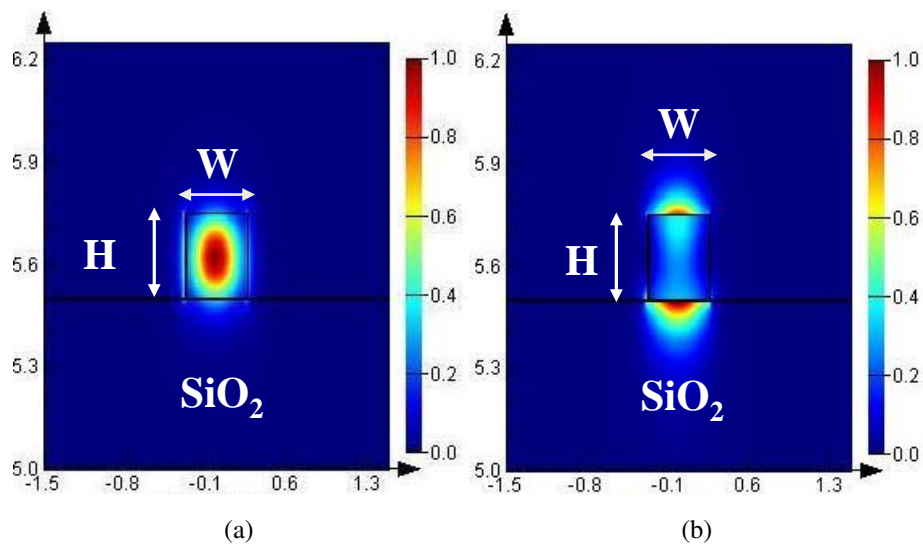


Figure 3.13: Mode intensity profile of PhW of dimensions height $H = 250$ nm and width $W = 540$ nm : (a) TE_0 , (b) TM_0 .

3.4.2 Taper Design

In the designed single defect PhCW on SOI, the waveguide width (from center to center of the circles adjacent to the defect line) was 866 nm. In the integrated structure single

mode PhW of width 540 nm and height 250 nm was used at the input and output ends of PhCW. For the integrated structure without any taper the calculated throughput transmission for fundamental mode wavelength 1740 - 1800 nm was around 56%. In order to improve the coupling efficiency, a taper was designed in PhCW by changing radius from 163 nm to 145 nm in 9 steps. By using the designed taper the throughput transmission was improved from 56% to 80%. Using the tapered structure for single defect PhCW, transmission spectrum was calculated for two different lengths of single defect PhCW as shown in Fig.3.14b. In transmission spectra, the peak A for wavelength range of 1740 - 1800 nm correspond to the fundamental (TE like) even PBG guided mode of PhCW, the peak C in wavelength range of 1427 - 1442 nm correspond to higher order PBG guided even mode. Since mode B as shown in Fig.3.11a is a (TM like) odd mode, it was not excited in the waveguide. However, we do not see complete dip in the frequency range where we have mode B, because the fundamental mode (A) above light line has not been completely leaked in air cladding due to small length of PhCW. For the 15 μm long PhCW, the mode frequencies above light line has not leaked in air cladding and a flat response is observed with a small dip in between but as we increase the length of PhCW to 58 μm , the radiation of mode above light line has increased and the transmission efficiency of higher order even mode has reduced to 40%. So, with even further increase in length the power of mode above light line can be completely leaked in cladding.

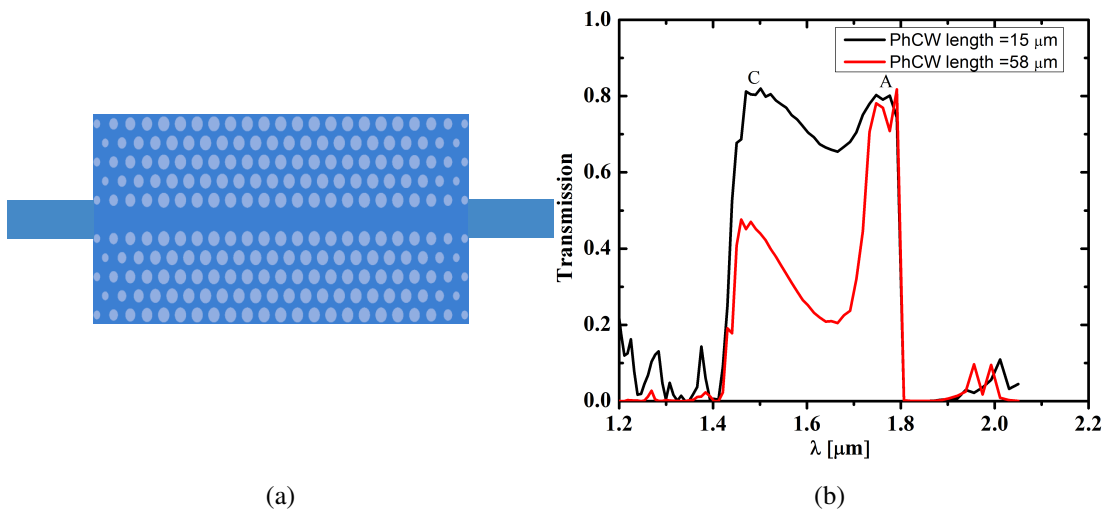


Figure 3.14: (a) Schematic of integrated PhCW and PhW using the taper. (b) Transmission at the output PhW for single defect PhCW on SOI.

In the designed single mode PhCW on SOI, the waveguide width (from center to

center of the circles adjacent to the defect line) was 476 nm. In the integrated structure, single mode PhW of width 476 nm and height 250 nm was used at the input and output ends of PhCW. For the integrated structure without any taper the calculated throughput

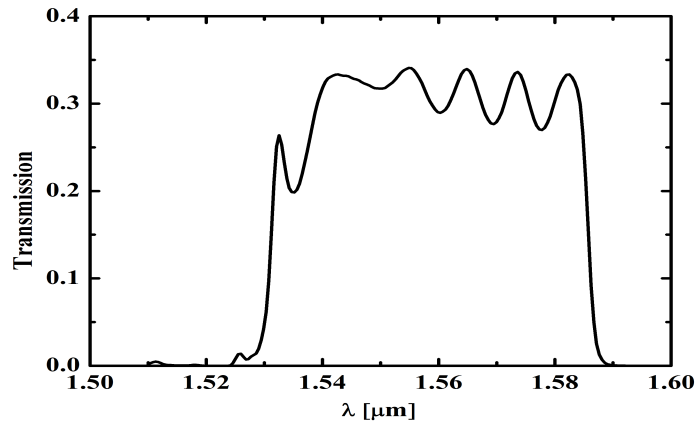


Figure 3.15: Transmission spectrum at the output PhW for single mode PhCW on SOI.

transmission for wavelength 1550 nm was around 14%. In order to improve the coupling efficiency, a similar taper was designed in PhCW by changing radius from 163 nm to 145 nm in 9 steps. The hole size could not be reduced further as the wavelength of interest moved above light line and it could couple with the radiation modes. By using the designed taper the throughput transmission was improved from 14% to 33%. Using the tapered structure for single mode PhCW, the calculated transmission at the output end is shown in Fig.3.15, where the ripples in transmission could be because of the computational error. Electric field distribution of the integrated structure with taper is shown in Fig.3.16.

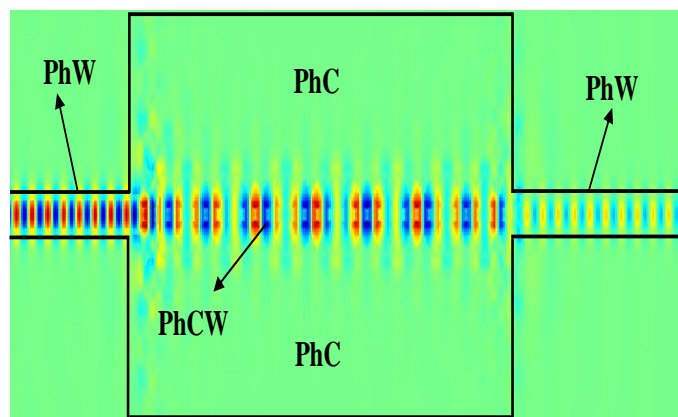


Figure 3.16: Electric field distribution obtained from FDTD simulation in integrated PhCW-PhW structure in SOI.

3.5 Group Velocity Dispersion

One of the unique features of PhCW is its low group velocity in the bandgap region. PhCW slows down the light near the Brillouin zone boundary because of the high dispersion. The group velocity (v_g) for the designed single mode PhCW on SOI was calculated and it was compared with single mode PhW (width : 476 nm, height : 250 nm). It was found that PhCW slows down the light by 3 to 10 times than that of PhW. The reduction in v_g is shown in Fig.3.17. Further this slow-light can be used for non linear applications, in delay lines and in compact MZI modulators.

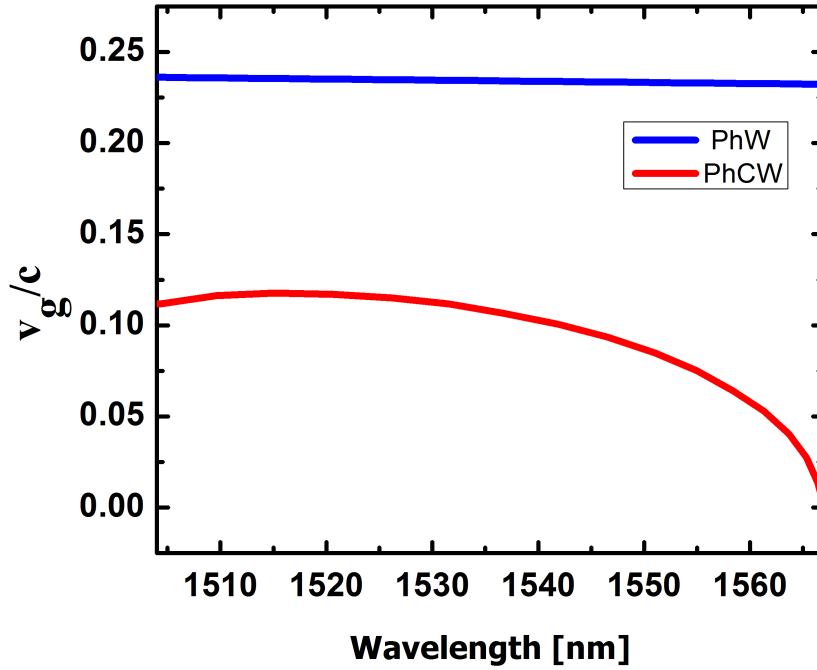


Figure 3.17: Variation of group velocity as a function of wavelength for 476 nm width PhW and single mode PhCW structure.

3.6 Conclusions

2D PhCs hole slab structures have been designed on GaAs/AlGaAs and SOI with square and triangular lattice geometry for sufficiently large PBG centered at 1550 nm. It was found that PBG was much smaller for square lattice geometry compared to triangular lattice geometry. By availing the large PBG of triangular lattice PhC, a single mode air bridge PhCW have been designed on both the platforms. The defect width for the designed single mode PhCW turned out to be 176 nm (150 nm) for GaAs/AlGaAs (SOI).

The bandwidth of guided mode below light line was 74 nm (62 nm) for GaAs/AlGaAs (SOI). A taper has been designed to improve the coupling efficiency of integrated (PhW-PhCW) structure. Finally, group velocity dispersion was calculated for single mode PhCW on SOI and it was compared with single mode PhW.

CHAPTER 4

Fabrication

In this chapter first we will be discussing fabrication of micro-structures with the available micro-fabrication facilities in microelectronics lab for doing the etching studies of GaAs and silicon. Further we will be discussing the fabrication of nano-structures (PhCs) using electron beam lithography on SOI with the optimized etch recipes of silicon.

4.1 Fabrication of Micro-structures

4.1.1 Etching Studies on GaAs

In order to fabricate PhCs on GaAs, circular air holes have to be etched in GaAs slab. Initially, using the fabrication facilities available in microelectronics lab, GaAs etching studies were carried out for large dimension structures. In this work, chlorine based etch chemistries were used to etch GaAs. It was found that $\text{BCl}_3/\text{Cl}_2/\text{Ar}$ recipe gives smoother surface and vertical sidewalls. The etch recipe has been optimized by varying various etch parameters i.e., pressure, ICP Power, RF Power and gas ratio. By changing the gas ratio, significant increase in anisotropy was observed. N_2 was introduced in the optimized recipe to improve the sidewall angle. GaAs substrate of orientation $\langle 100 \rangle$ was cleaned by boiling the samples in trichloroethylene (TCE) solution for 3 minutes. TCE cleaning was followed by immersing the wafer in boiling Acetone for 3 minutes. The sample was then rinsed in DI water followed by a 5 minutes HCl dip. HCl: DI water ratio was kept as 40:60. Finally the wafer was rinsed in DI water. In order to remove moisture content the cleaned sample was baked at 120°C for 5 minutes. Positive photoresist (PPR) was spin coated on the cleaned sample and pre-baking of the sample was carried out at 80°C for 25 minutes. Photo-lithography was carried out using mask with square patterns of $250 \times 250 \mu\text{m}^2$ dimension. 6 pellets of NaOH dissolved in 250 ml of DI water was used as the developer solution. Post-baking of the

developed sample was carried out at 120 °C for 35 minutes. ICPRIE was carried out on the patterned sample. Etching temperature, argon flow rate and total flow rate of gasses were kept constant at 25 °C, 12 sccm and 19 sccm respectively. However, ICP power, RF power, pressure and BCl_3/Cl_2 ratio were varied and their effects were studied. Later, N_2 was introduced to the recipe while keeping the BCl_3/Cl_2 ratio constant to improve sidewall angle. However, total flow rate was still maintained constant. After etching, PPR was removed from the sample by ashing the resist in oxygen plasma. Using this optimized recipe circular patterns of 4 μm diameter with 8 μm period and 3 μm diameter with 6 μm period were etched.

Results and discussion

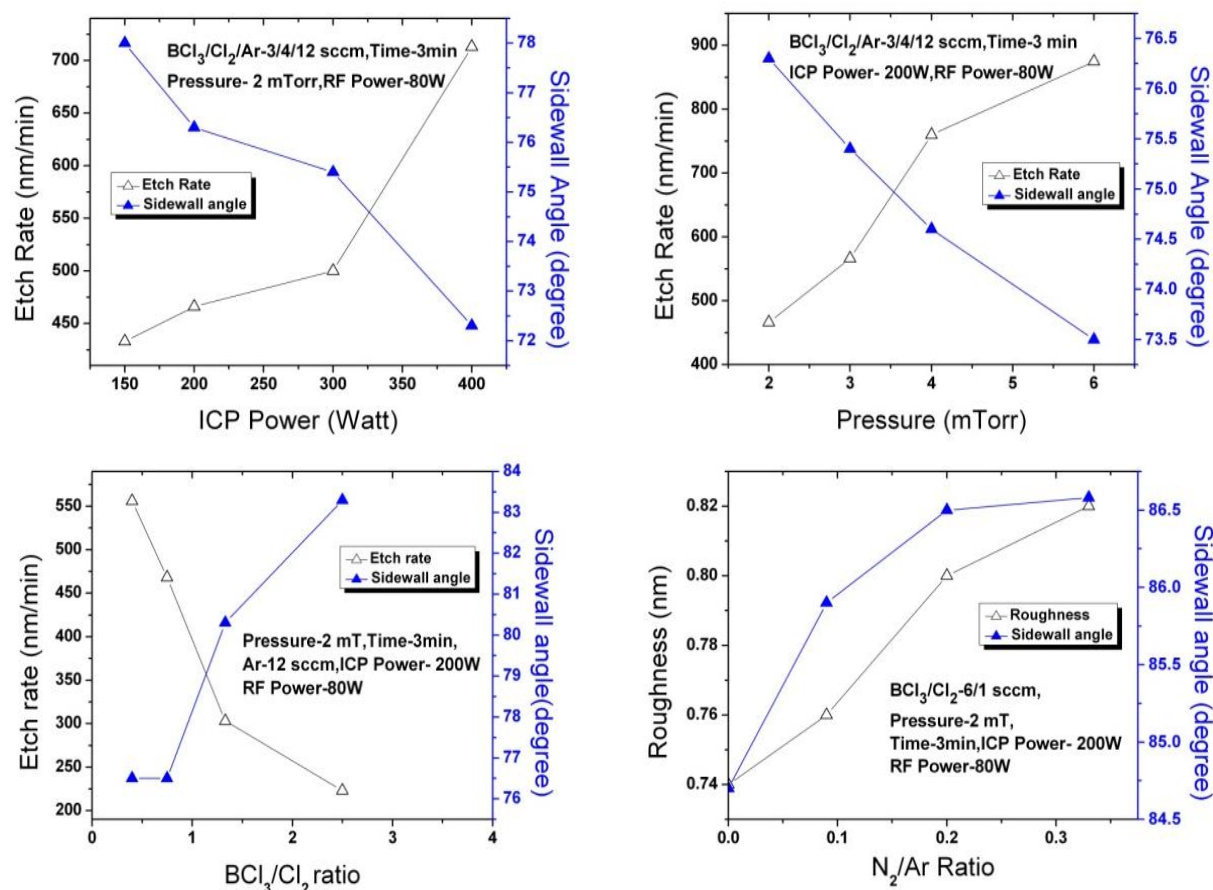


Figure 4.1: Effect of (a) ICP Power, (b) Pressure, (c) $\text{BCl}_3 : \text{Cl}_2$ ratio, (d) $\text{N}_2 : \text{Ar}$ ratio, while keeping all other parameters constant

Etch rate and verticality are shown as a function of ICP power, RF power, pressure and BCl_3/Cl_2 ratio in Fig.4.1. From Fig.4.1a and Fig.4.1b it can be observed that with increase in ICP power and pressure, etch rate increases but the anisotropy of etching

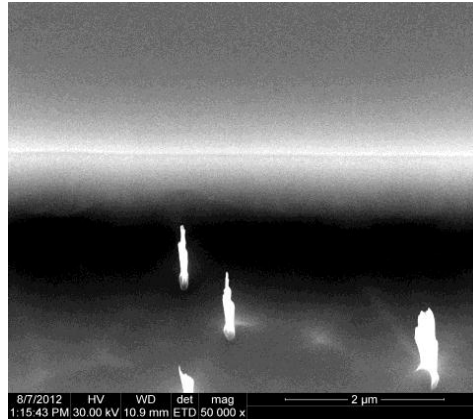


Figure 4.2: SEM image of square pattern ($250 \times 250 \mu m^2$) etched using high pressure of 5 mTorr pressure during ICPRIE. (RF Power - 80 Watts, ICP Power - 200 Watts, $BCl_3/Cl_2/Ar$ flow rate - 3/4/12 sccm).

decreases. It was also observed that with increase in pressure, roughness of the etched surface increase sharply due to particulate formation. SEM image of sample etched with high pressure of the order 5 mTorr is shown in Fig.4.2. This shows that chemical etching is more pronounced than physical etching. It was found that variation in RF Power does not affect the etch rate but the verticality reduces considerably with an increase in the RF power. Fig.4.1c indicates that with increase in BCl_3/Cl_2 ratio, etch rate decreases and there is also a significant increase in the sidewall angle. This result can be justified as it has been shown already that BCl_3 passivates the sidewalls through the formation of diboron tetrachloride (B_2Cl_4), a thin polymer layer (Volatier *et al.*, 2010). SEM image showing sidewalls of the square pattern etched using 6/1/12 sccm of $BCl_3/Cl_2/Ar$ recipe is given in Fig.4.3. It can be observed that the recipe gives highly anisotropic sidewalls and very smooth surface. Fig.4.1d shows the effect of adding N_2 to the recipe. Increase in sidewall angle is due to the fact that N_2 passivates the sidewalls further. However, once N_2 is increased beyond a threshold level (1 sccm in this case), enhanced passivation effect causes micro-masking there by increasing the roughness. Hence, the etch chemistry was optimized as 6/1/11/1 sccm ($BCl_3/Cl_2/Ar/N_2$). Other important etch parameters are: ICP power-200 W, RF power-80 W, pressure-3 mTorr, time-3 minutes and temperature- $25^\circ C$. For periodic holes with $4 \mu m$ diameter, etch rate of ≈ 556 nm/min along with a sidewall angle of 86° and surface roughness around 1 nm were obtained. Fig.4.4a shows the measurement of etch profile carried out using confocal microscope. It can be observed that the sidewall angle and smoothness of the etch profile are independent of etch surface dimensions. Moreover etch rate was found

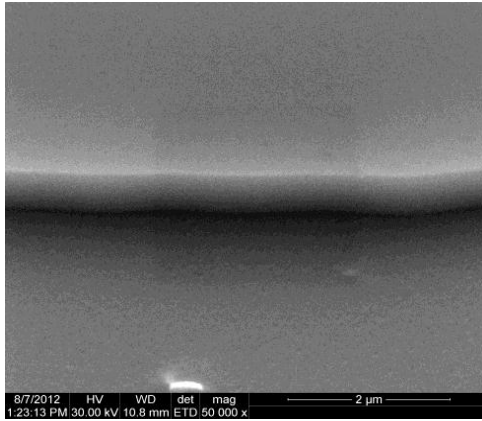


Figure 4.3: SEM Image showing smooth and vertical side-wall of square pattern etched using $\text{BCl}_3/\text{Cl}_2/\text{Ar}$ flow rate of 6/1/12 sccm during ICPRIE (RF Power - 80 Watts, ICP Power - 200 Watts, Pressure - 2 mTorr).

to decrease gradually with decrease in diameter of the circular patterns. The etch rate decreases from 540 nm to 450 nm as the hole diameters changes from $4\ \mu\text{m}$ to $3\ \mu\text{m}$. SEM image of the circular pattern is given in Fig.4.4b.

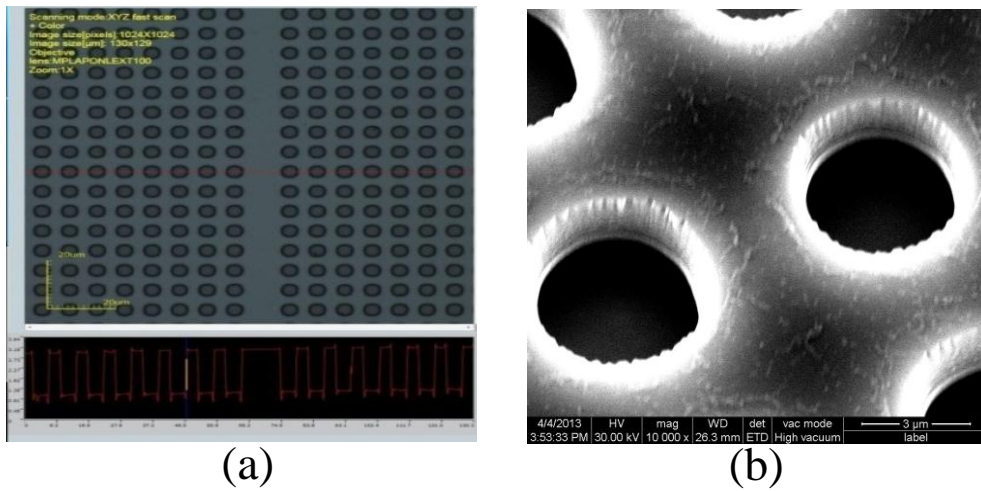


Figure 4.4: (a) Confocal microscope image of a square lattice circular hole ($r = 2\ \mu\text{m}$) pattern with a defect line. (RF Power - 80 Watts, ICP Power - 200 Watts, Pressure - 3 mTorr, $\text{BCl}_3/\text{Cl}_2/\text{Ar}/\text{N}_2$ flow rate - 6/1/11/1 sccm). (b) SEM Image of square lattice circular hole ($r = 2\ \mu\text{m}$) pattern. (RF Power - 80 Watts, ICP Power - 200 Watts, Pressure - 3 mTorr, $\text{BCl}_3/\text{Cl}_2/\text{Ar}/\text{N}_2$ flow rate - 6/1/11/1 sccm).

4.1.2 Etching Studies of Silicon

Etching studies of silicon have been carried out using $\text{SF}_6 : \text{Ar}$ plasma for large dimension structures. In this work, fluorine based etch chemistries were used to etch si. It

was found that SF₆/Ar recipe gives smoother surface and vertical sidewalls. The etch recipe has been optimized by varying various etch parameters i.e., pressure, ICP Power, RF Power and gas ratio. Silicon substrate of orientation <100> was cleaned by boiling the sample in trichloroethylene (TCE) solution for 3 minutes. TCE cleaning was followed by immersing the wafer in boiling Acetone for 3 minutes. The sample was then rinsed in DI water followed by boiling it in HNO₃ for 5 minutes. Then the sample was dipped in dilute HF for 30 seconds. Finally the sample was rinsed in DI water. In order to remove moisture the cleaned sample was baked at 120 °C for 5 minutes. Positive photoresist (PPR) was spin coated on the cleaned sample and pre-baking of the sample was done at 80 °C for 25 minutes. Photo-lithography was carried out using mask with periodic circular patterns of 4 μm diameter circles with 8 μm period. 6 pellets of NaOH dissolved in 250 ml of DI water was used as the developer solution. Post-baking of the developed samples was carried out at 120 °C for 35 minutes. ICPRIE was carried out on the patterned sample. Etching temperature and total flow rate of gasses were kept constant at 25 °C, 40 sccm respectively. However, ICP power, RF power, pressure and SF₆/Ar ratio were varied and the etch recipe was optimized to get anisotropic etching with low roughness. After etching, PPR was removed from the sample by ashing the resist in oxygen plasma.

Results and discussion

It was found that SF₆/Ar recipe gives smoother surface and vertical sidewalls. The etch recipe have been optimized by varying various etch parameters i.e., pressure, ICP Power, RF Power and gas ratio. The optimized parameters are ICP power 400 W, RF power 80 W, pressure 40 mTorr, gas ratio 20/20 (SF₆/Ar). For periodic holes with 4 μm diameter, etch rate of ≈ 540 nm/min along with a sidewall angle of 86 ° and surface roughness around 4 nm were obtained and the confocal images of etched silicon are shown in Fig.4.5 and Fig.4.6. However, this recipe resulted in large undercut as can be seen from Fig.4.6, the holes diameter have increased from 4 μm to 5.55 μm. Further etching optimization of silicon was carried out for sub-micron dimensions to fabricate the designed PhC in SOI.

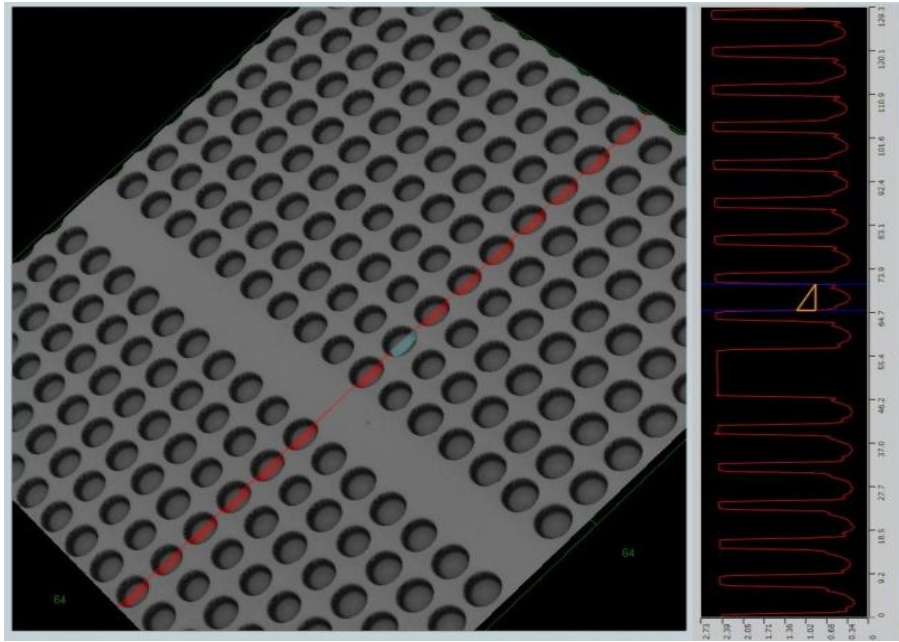


Figure 4.5: Confocal microscope image of a square lattice circular hole ($r = 4 \mu\text{m}$) pattern with a defect line. (RF Power - 80 Watts, ICP Power - 400 Watts, Pressure - 40 mTorr, SF_6/Ar flow rate - 20/20 sccm).

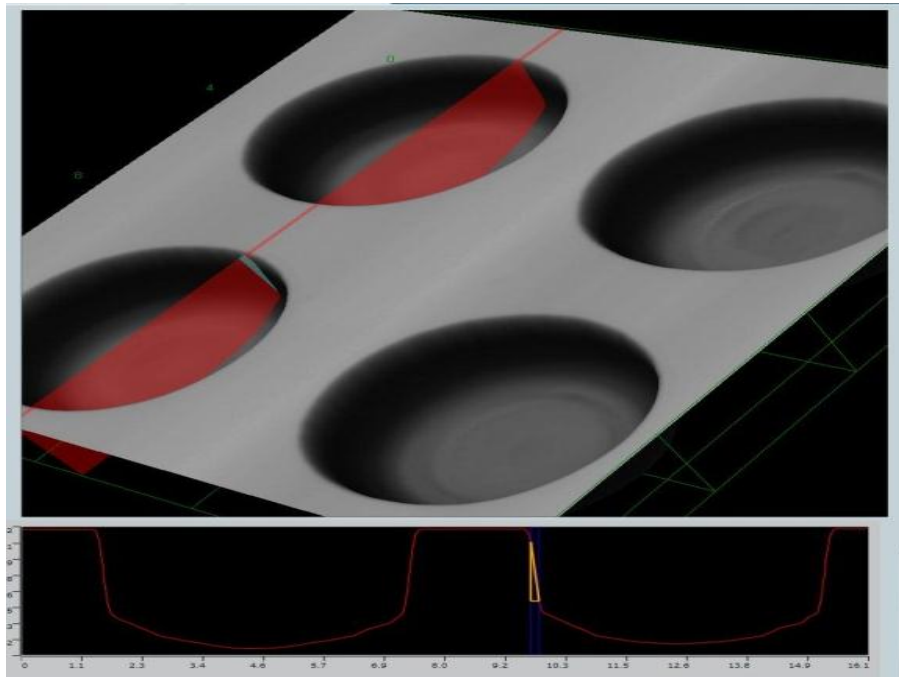


Figure 4.6: Confocal microscope image of closer view of square lattice circular hole ($r = 4 \mu\text{m}$) pattern with a defect line. (RF Power - 80 Watts, ICP Power - 400 Watts, Pressure - 40 mTorr, SF_6/Ar flow rate - 20/20 sccm).

4.2 Fabrication of Nano-structures : PhCs

In this section we will be discussing about fabrication steps of PhCW. The Fabrication of air bridge PhCW consist of three critical processes:

- 1) **Electron Beam Lithography (EBL)**: It is used to transfer PhC patterns on resist. Since, the designed dimensions are in sub-micron range, conventional UV photo lithography can not be used to realize these patterns due to diffraction limitation.
- 2) **Inductively Coupled Plasma Reactive Ion Etching (ICPRIE)**: It is used for dry etching of substrate. As etching recipes are materials selective, proper masking layer (known as hard mask) has to be used to prevent etching of unwanted area.
- 3) **Sacrificial layer etching**: It is used for making air bridge PhCW. In SOI, 3 μm buried silicon dioxide will act as sacrificial layer.

The following three sections of this chapter covers detailed fabrication steps of three different hard masks tried for silicon etching, in chronological order. The reasons for switching from one to another hard mask will also be discussed .

Optimization of a fabrication process requires multiple runs, so the EBL and ICPRIE process optimization has been done on silicon before trying them in SOI (SOI wafers are costlier than silicon). The specifications of SOI and silicon wafers are given in table 4.1.

Table 4.1: Specifications of SOI and Silicon wafer used for fabrication process.

| | SOI | Silicon |
|------------------------|----------------------------|-------------------------|
| Doping | P-type | P-type |
| Resistivity | 13-22.5 $\Omega\text{-cm}$ | 1-10 $\Omega\text{-cm}$ |
| Crystal Orientation | <100> | <100> |
| Wafer thickness | - | 500 μm |
| Device layer thickness | 250 nm | - |
| BOX thickness | 3 μm | - |
| Handle layer thickness | 500 μm | - |

4.2.1 PMMA as Hard Mask

The schematic of fabrication process flow is given in Fig.4.7 and corresponding details are given in following subsections.

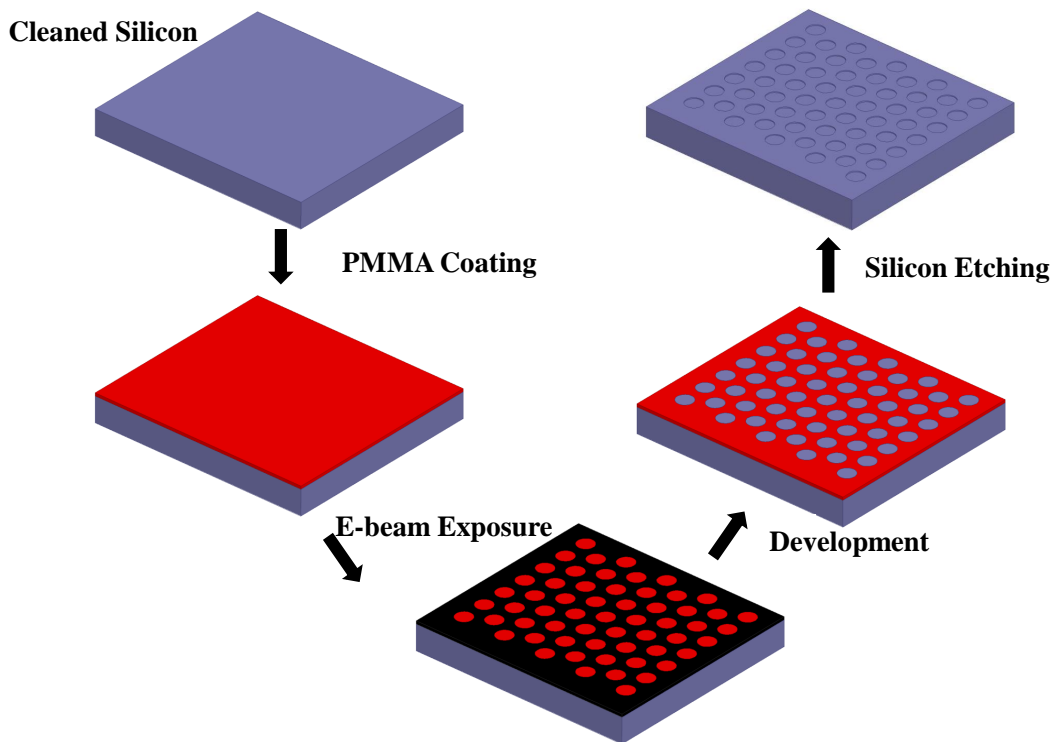


Figure 4.7: Fabrication process flow of PhC patterning using PMMA resist.

Wafer Cleaning

The first step in fabricating a device is to clean the wafer to remove all the surface contaminants. The sample of desired dimension was cleaved from wafer and cleaned using Trichloroethylene (TCE), Acetone, Nitric acid (HNO_3) or Piranha, Hydrofluoric acid (HF) and DI water. Silicon sample was boiled in trichloroethylene (TCE) solution for 3 minutes to remove grease and organic contamination. This was followed by immersing the sample in boiling Acetone for 3 minutes to remove TCE stains. The sample was then rinsed in DI water followed by drying with N_2 air gun. The metallic impurity was removed by boiling the sample in HNO_3 for 5 minutes followed by DI water rinse. This process grows a thin layer of oxide on silicon sample. The sample was dipped in dilute HF for 30 seconds to get fresh silicon surface by etching grown oxide. Finally the sample was rinsed in DI water and dried with N_2 air gun. The sample was heated on hot plate at 180°C for 5 minutes for removing moisture.

EBL

EBL is a direct writing procedure i.e. no physical mask is required. Here, high energy focused electron beam scans across the electron beam resist coated sample, selectively exposing the area defined by the pattern fed in to the system. Electron beam exposure changes the solubility of the resist in developer solution depending on the type of resist used. In positive e-beam resist, exposed area will become soluble in developer solution where as in negative e-beam resist, exposed area will become insoluble. Thus, on immersing the exposed sample in developer solution, patterns can be transferred on the resist.

1. E-beam Resist coating :

Initially, PMMA 950PMMA A4 (MICRO-CHEM) was used as e-beam resist. It is a positive e-beam resist i.e. e-beam exposed area will become soluble in developer solution. Optimized spin coating parameters are given in table 4.2. On measuring with ellipsometer, the thickness of PMMA for these spin parameters was ≈ 240 nm. Pre-baking was done on hot plate at 170°C for 3 minutes to harden the coated PMMA.

Table 4.2: Spin coating parameters for PMMA.

| | | |
|--------------|---|--------------|
| Speed | : | 4000 rpm. |
| Acceleration | : | 300 rpm/sec. |
| Time | : | 30 sec. |

2. MASK Designing :

EBL systems support mask in GDS format. Mask corresponding to desired dimensions, can be designed in any CAD (Computer Aided Drawing) tools like R-SOFT, CleWin, L-Edit, Raith layout editor and exported in GDS format. For current method, mask was designed in R-SOFT. Screen shot of mask is shown in Fig.4.8a.

3. E-beam exposure :

E-beam exposure was then performed on RAITH 150^{TWO} system, having resolution of 2 nm. The e-beam exposure for given write field depends on several parameters like accelerating voltage, aperture, working distance, step size and dose value. In our case, after several runs, dimensions of PhC near to designed values for 100 μm write field were obtained for accelerating voltage : 20 KV, aperture : 10 μm , working distance : 10 mm. The current for this aperture was around 40 pA. The step size used was 6 nm and the dose value was $\approx 150\text{-}155 \mu\text{C}/\text{cm}^2$.

4. E-beam Development :

After e-beam exposure sample was developed in 1/3 mixture of methyl-isobutyle-Ketone (MIBK) and Iso-propanol (IPA) for 30 second. This dissolved exposed PMMA, leaving behind unexposed area. This process was followed by 10 second dip in IPA and DI water rinse, in same order. The development time was optimized to get perfect side wall. However, the PMMA from the unexposed region was also slightly got etched during development and the thickness of the unexposed PMMA was reduced from $\approx 240 \text{ nm}$ to $\approx 100 \text{ nm}$. The sample after development was imaged using Raith SEM to check the dimensions and shape of the patterns. The SEM image of the patterned PhC on PMMA with optimized dose and development time is shown in Fig.4.8b.

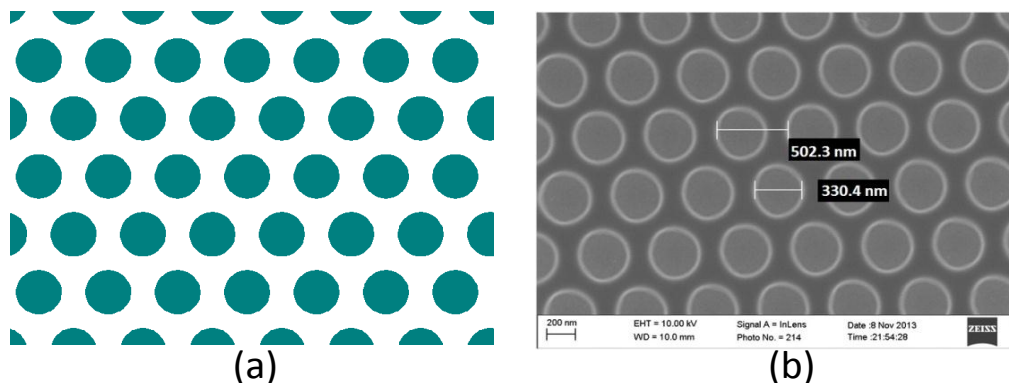


Figure 4.8: Figure shows (a) Screen shot of mask file, here dark region will be exposed to e-beam and (b) SEM image of PhC after development on PMMA.

Etching of Silicon

Reactive Ion Etching (RIE) (OXFORD) was carried out with SF₆/Ar plasma recipe to etch the exposed silicon. The complete recipe is given in table 4.3. The etch rate of a material highly depends on the dimension of the patterns and for the given recipe the etch rate of silicon for the designed dimensions (radius of air hole-163 nm and period-500 nm) was \simeq 90 nm/min. However, the etch rate of PMMA with SF₆/Ar plasma was also found to be same as silicon i.e. 90 nm/min. So, PMMA having thickness of 100 nm couldn't be used as a mask to selectively etch 250 nm of silicon device layer.

Table 4.3: Recipe used for RIE to realize PhC on silicon.

| | |
|---------------|--------------------------------------|
| Gas flow rate | : SF ₆ : Ar :: 20:20 sccm |
| Temperature | : 25 °C |
| Pressure | : 200 mTorr |
| RF Power | : 150 W |
| DC Bias | : 35 V |
| Etch rate | : 90 nm/min |

Conclusion

Due to PMMA's poor dry etching resistance, etching of 250 nm deep holes in silicon device layer was not possible. So, Al was used as hard mask.

4.2.2 Al as Hard Mask

In order to use Al as hard mask, patterns from resist have to be transferred on it. Two methods were tried to transfer PhC pattern on Al. 1)Wet Al etching. 2)Lift-off. These processes will be discussed in details in following subsections.

Wet Etching of Al to obtain desired pattern

The schematic of the wet etching of Al to transfer PhC pattern on Al is shown in Fig.4.9 and corresponding fabrication details are given in table 4.4.

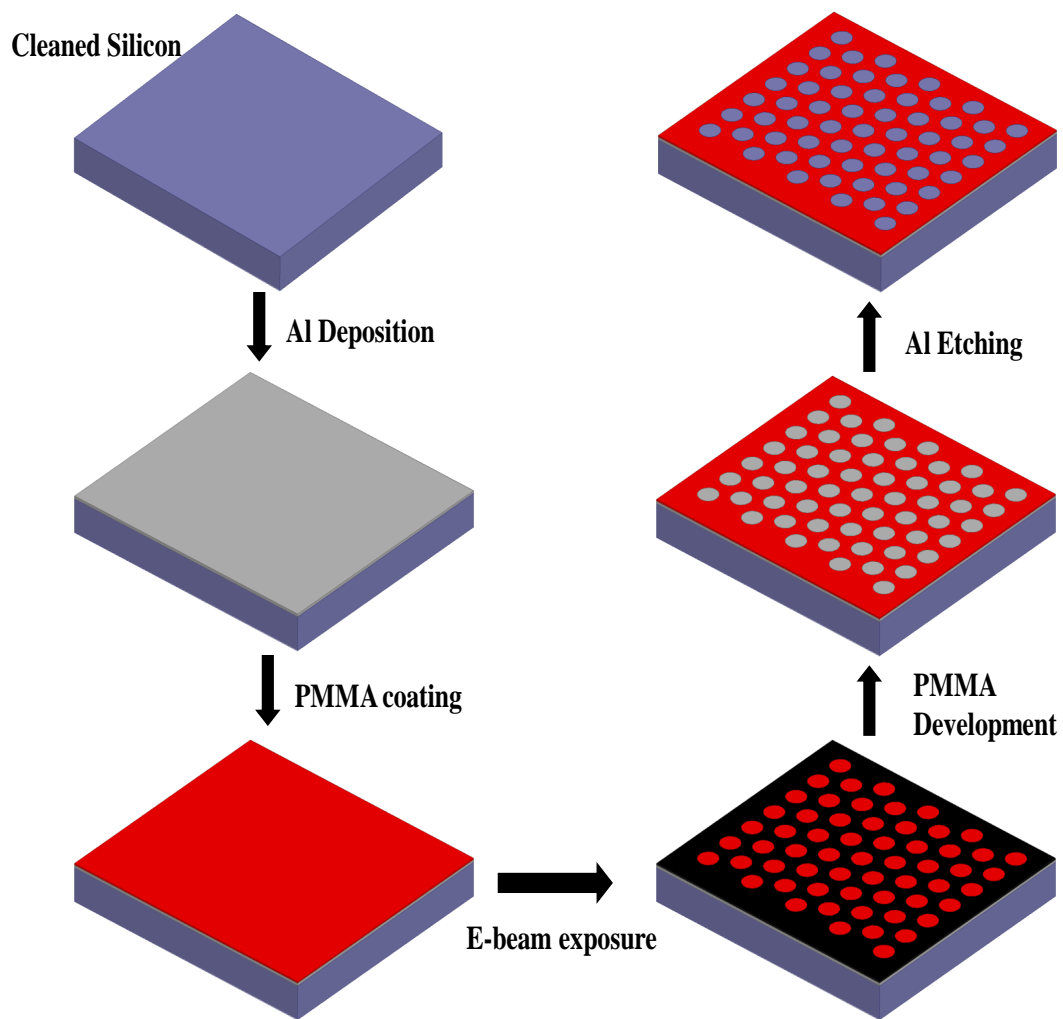


Figure 4.9: Fabrication process flow of PhC patterning on Al using wet etching method.

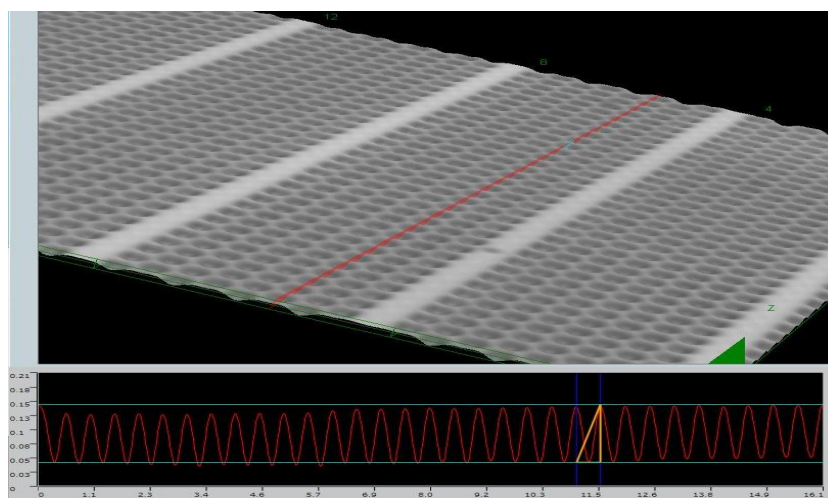


Figure 4.10: Confocal microscopic image of PhC after development on PMMA for wet Al etching method.

Table 4.4: Fabrication process flow for getting Al hard mask using wet Al etching.

| Process | Parameters / *remarks |
|--------------------|--|
| Wafer cleaning | Cleaned with the procedure given in section 4.2.1. |
| Metallization | 80 nm thick Aluminum was deposited on silicon by thermal evaporation. *PMMA cannot be used as a hard mask for (ICPRIE) dry etching of silicon so Al was deposited on silicon to use it as hard mask. |
| PMMA-950k coating | Spin parameters - 4000 rpm., 300 rpm/sec., 30 sec. *Thickness of PMMA \approx 240 nm. |
| Prebaking | 3 minute at 170 °C (Hot plate). |
| E-beam lithography | Triangular PhC Patterns corresponding to designed dimensions was transferred on PMMA using RAITH 150 ^{TWO} EBL system. Optimized dose \simeq 150-155 μ C/cm ² and the aperture used was 20 KV, 10 μ m, 10 mm. |
| Development | 30 sec. dip in MIBK/IPA - 1/3. 10 sec. dip in IPA. Rinse in DI water. *Confocal microscopic image of developed patterns is shown in Fig.4.10. |
| Al etching | Wet etching of Al was done through the patterns in PMMA using dilute HF 100:1 (DI Water : HF). Confocal microscopic image of etched Al is shown in Fig.4.11. *Al was completely etched under PMMA because of low tolerance in gap between two circles and less control on wet etching. HF was used to etch Al instead of Al etchant (H_3PO_4 : 77%, CH_3COOH : 15%, HNO_3 : 3%, and DI water : 5%) because etch rate of PMMA in later case was very high. |

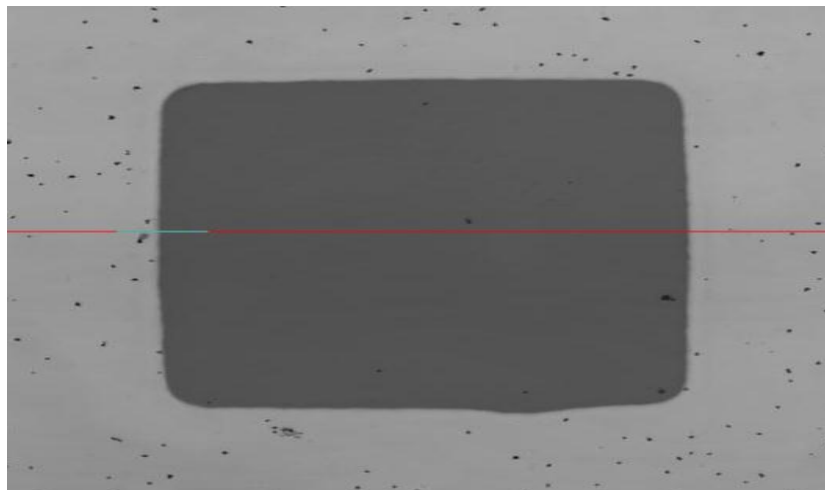


Figure 4.11: Confocal microscopic image of etched Al using PMMA mask.

Conclusion

Al wet etching method was not successful because of low tolerance in gap between two circles and less control on wet etching. Therefore, lift-off was tried to transfer the patterns on Al.

Lift off Al to obtain desired pattern

In case of lift-off, contrary to previous case metallization is done after making the inverted pattern of resist on the wafer. So, on removing the resist metal present on top of it will go leaving behind the rest. The schematic of fabrication process flow of lift-off process is shown in Fig.4.12 and the corresponding fabrication details are given in table 4.5.

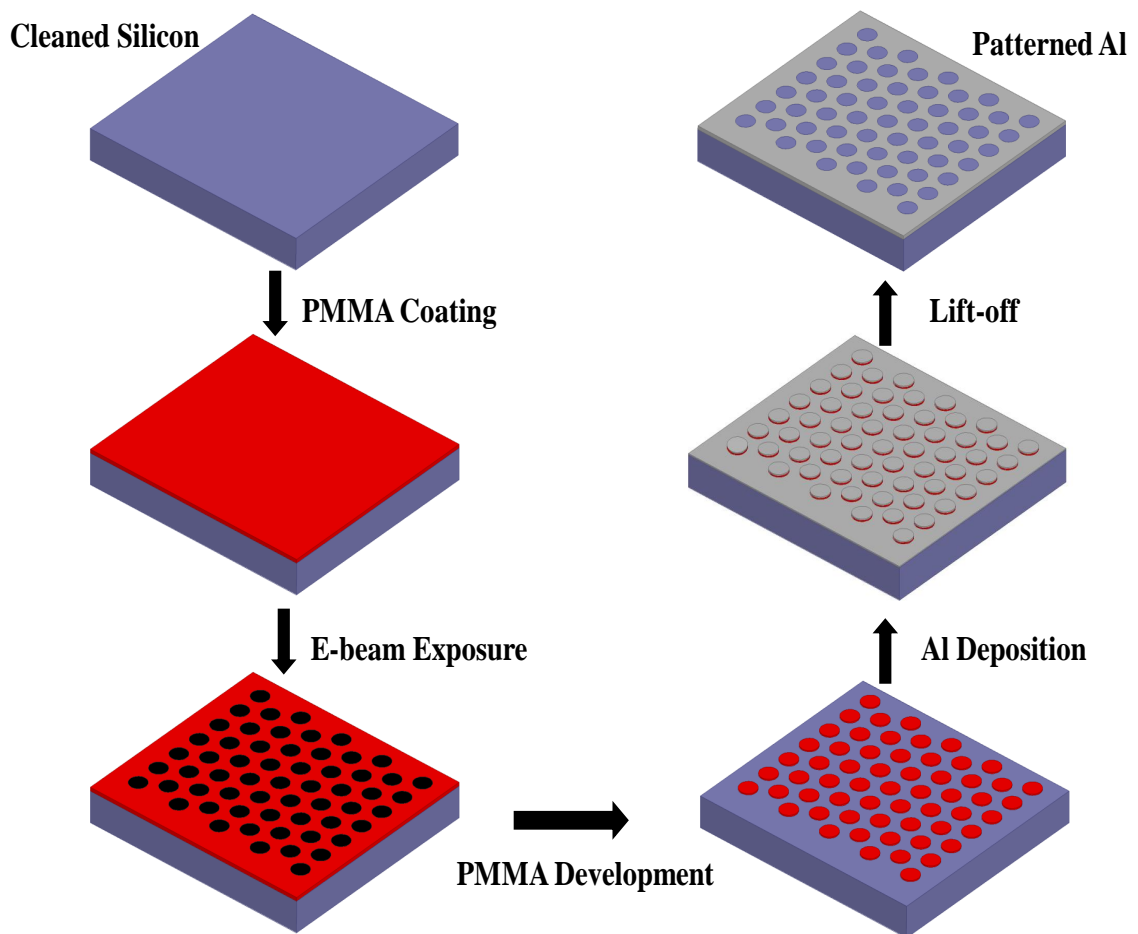


Figure 4.12: Fabrication process flow of PhC patterning on Al using Lift-off.

Table 4.5: Fabrication process flow for getting Al hard mask using lift-off.

| Process | Parameters / *remarks |
|--------------------|--|
| Wafer cleaning | Cleaned with the procedure given in section 4.2.1. |
| PMMA-950k coating | Spin parameters - 4000 rpm., 300 rpm/sec., 30 sec. *Thickness of PMMA \approx 240 nm. |
| Prebaking | 3 minute at 170 °C (Hot plate). |
| E-beam lithography | Triangular PhC Patterns corresponding to the designed dimensions was transferred on PMMA using RAITH 150 ^{TWO} EBL system using inverted mask. |
| Development | 30 sec dip in MIBK/IPA - 1/3. 10 sec dip in IPA. Rinse in DI water. *Fig.4.13a SEM image of patterned PMMA. After development thickness of PMMA got reduced to \approx 100 nm. |
| Metallization | 40 nm thick Aluminum was deposited on silicon by thermal evaporation. *Thickness of Al should be less than 1/2 of the thickness of PMMA for doing lift-off. |
| Lift-off | Sample was dipped in acetone. |
| Imaging | Fig.4.13b SEM image after lift-off. |

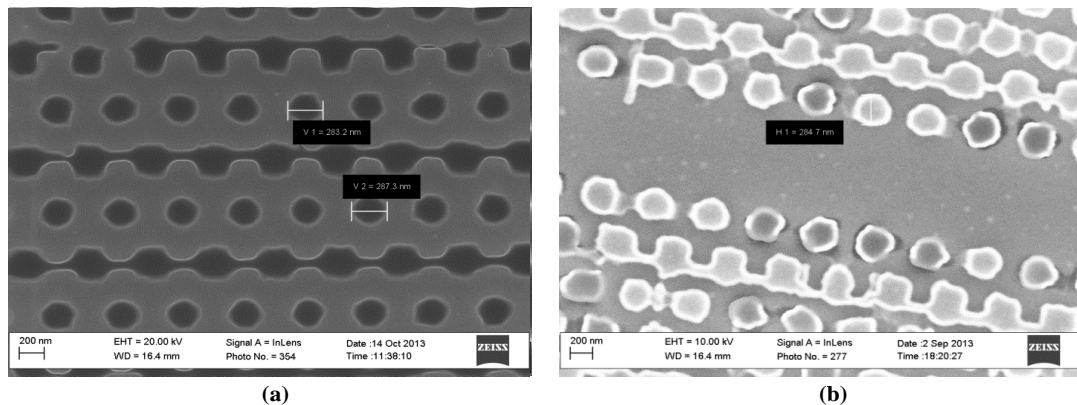


Figure 4.13: SEM image of PhC pattern on (a) PMMA with inverted mask and (b) After lift-off

Conclusion

As discussed earlier, for lift-off with positive resist, the mask has to be negative i.e. the circles should be unexposed and the surrounding region should be exposed to e-beam. However, on making inverted GDS mask file (detailed method is given in appendix) using CAD tools (cleWin, L-Edit, Raith layout editor) some lines were observed in the mask file and after EBL the same lines were transferred on the resist. These lines can be seen in the SEM image (shown in Fig.4.13). To solve this problem, the final mask was made in Raith layout editor by giving overlap between two unit cells and the detailed procedure to make the mask is given in Appendix B.

4.2.3 HSQ as Hard Mask

HSQ is a negative e-beam resist i.e. the exposed region will be hardened and the unexposed region will be dissolved in developer solution. The chemical composition of HSQ is $H_8Si_8O_{12}$. HSQ used in this work is manufactured by Dow Corning Corporation. HSQ has good dry etching resistance to Si etching recipes. So after optimizing fabrication parameters with silicon, same steps was used in SOI. The schematic of fabrication process flow to transfer PhC pattern on HSQ coated on SOI wafer is given in Fig.4.14. The corresponding fabrication details are given in following subsections.

EBL

1. HSQ coating :

Initial dose and development optimization's were done on silicon with ≈ 180 nm thick HSQ and the spinning parameters for the same are given in table 4.6. However, it was found that for ≈ 180 nm thickness of HSQ, the charging effect was more (which further aggravates on SOI substrate), giving rise to difficulty in imaging and the preliminary corrections like focus, stigmatism and wobble. In order to overcome this problem the thickness was reduced to ≈ 130 nm of HSQ. The charging effect for this thickness of HSQ was negligible. The thickness of HSQ was measured using ellipsometer. In order to get uniform thickness throughout the wafer, spinning was done in two steps.

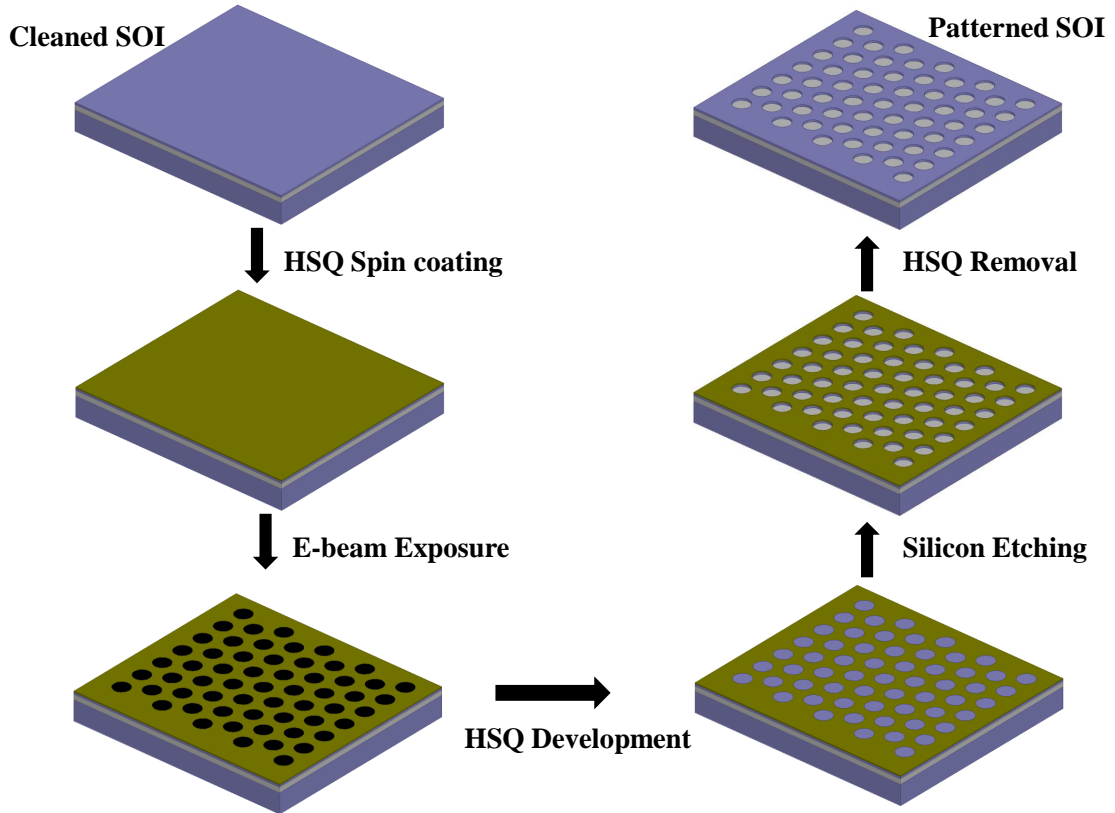


Figure 4.14: Fabrication process flow of PhC patterning using HSQ resist.

The optimized spinning parameters are given in table 4.7. HSQ was pre-baked on hot plate at 100 °C for 2 minute for hardening.

Table 4.6: Spin coating parameters for ≈ 180 nm thick HSQ.

| | |
|--------------|----------------|
| Speed | : 3000 rpm. |
| Acceleration | : 400 rpm/sec. |
| Time | : 60 sec. |

2. Mask Designing :

The inverted GDS mask file (as HSQ is negative resist as well as hard mask i.e. surrounding region to circular holes have to be exposed by e-beam) was created by Raith layout editor. The detailed procedure to make defect-free inverted mask file is discussed in Appendix B.

3. E-beam Exposure :

Table 4.7: Spin coating parameters for ≈ 130 nm thick HSQ.

| Step-1 | | |
|--------------|---|---------------|
| Speed | : | 100 rpm. |
| Acceleration | : | 1500 rpm/sec. |
| Time | : | 10 sec. |
| Step-2 | | |
| Speed | : | 3000 rpm. |
| Acceleration | : | 1500 rpm/sec. |
| Time | : | 40 sec. |

The EBL for the designed parameters with HSQ as resist was again optimized by doing dose experiments which include varying current, step size, write field size etc. For the larger aperture the current will be higher so the time required for writing patterns would be less. Initial optimization was carried out with larger aperture of $30 \mu\text{m}$ and finally it was done with lower aperture of $10 \mu\text{m}$. For ≈ 180 nm thick HSQ, optimized parameters were ; accelerating voltage : 20 KV, aperture : $30 \mu\text{m}$, working distance : 10 mm. The current value for this aperture was ≈ 222 pA. The step size used was 6 nm and the dose value was $150\text{-}160 \mu\text{C}/\text{cm}^2$. For ≈ 130 nm thick HSQ optimized parameters were turned out to be accelerating voltage : 20 KV, aperture : $10 \mu\text{m}$, working distance : 10 mm. The current value for this aperture was ≈ 40 pA and with 6 nm step size the dose value to get the desired PhC structure was $\sim 185\text{-}195 \mu\text{C}/\text{cm}^2$.

4. HSQ Development :

The development of exposed HSQ were carried out in two developer solutions: Tetramethylammonium hydroxide (TMAH) and MF-319. TMAH contains 25% TMAH in water while MF-319 contains 2.45% TMAH in water so with MF-319 the development will be slow. For TMAH the optimized development time was 30 second but it forms some particulates on the sample and also after development, the edges of PhCs were not smooth (SEM image is shown in Fig.4.15a). Development time optimization for sub-micron 2D PhC pillars in HSQ has been reported by (Hamza *et al.*, 2012) using MF CD-26 (MF CD-26 contains 2.4% TMAH in water) as 12 minutes. However,

for our designed PhCs the optimized development time using MF-319 was 8 minutes. It can be seen from the SEM image shown in Fig.4.15b that compared to the sample developed in TMAH, the roughness is very low and side walls are much better. The Optimized development parameters are given in table 4.8. In case of SOI, the sample

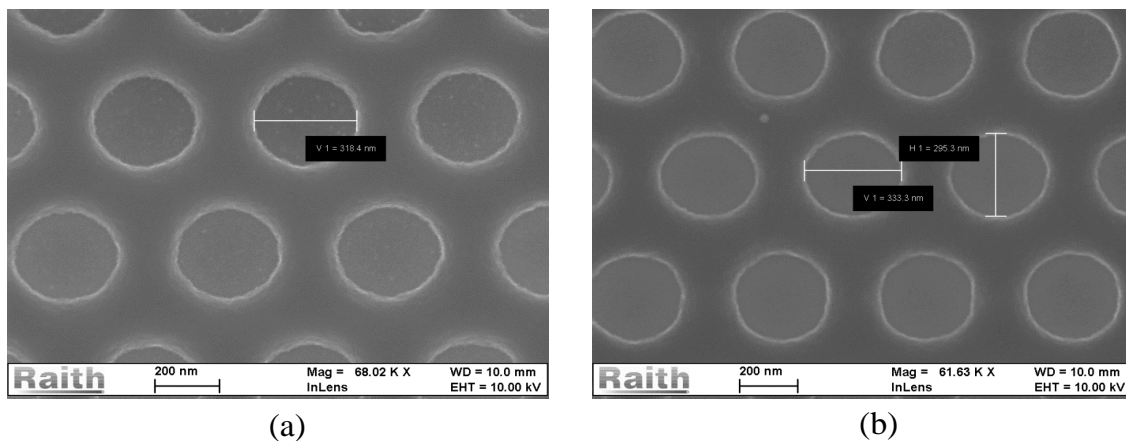


Figure 4.15: SEM image of developed silicon (a) with TMAH and (b) with MF-319.

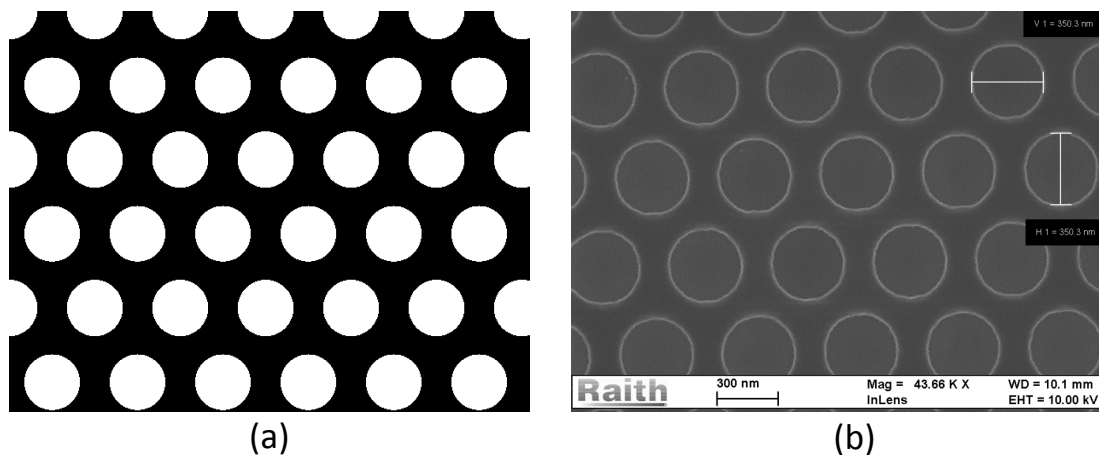


Figure 4.16: Figure shows (a) Screen shot of mask file and (b) SEM image of PhC after development with MF-319 on SOI.

was developed in MF-319 for 8 minute and the SEM image of the developed HSQ on SOI sample is shown in Fig.4.16b. After development and imaging the diameter of the circles was found to get enlarged from the desired value of 326 nm to \approx 350 nm and the period remained unchanged i.e. 500 nm. However, like PMMA after development the HSQ thickness in exposed region was reduced from 130 nm to \approx 90-100 nm. The possible reason for this reduction can be proximity effect.

Table 4.8: Optimized development parameters for HSQ.

| Developer solution | TMAH | MF-319 |
|------------------------------|---------|---------|
| Dipped in developer solution | 30 sec. | 8 min. |
| DI water rinse | 30 sec. | 30 sec. |
| IPA rinse | 15 sec. | 15 sec. |

Etching of Silicon

After patterning HSQ coated on silicon, Inductively Coupled Plasma Reactive Ion Etching (ICPRIE) was carried out with SF₆/Ar and Cl₂ plasma using HSQ as a mask. In case of SF₆/Ar recipe the etching was isotropic in nature and because of large undercut the holes started merging as shown in Fig.4.17a. This problem of under cut was overcome by using Cl₂ plasma. Anisotropic etching of silicon with Chlorine gas has been reported in the thesis (Askari, 2011). The etching parameters for Cl₂ plasma has been optimized by doing the silicon etching experiment for our lab environment. In case of Cl₂ plasma etching was anisotropic as can be seen from the SEM image shown in Fig.4.17b and the diameter of the etched circle was close to the designed value of 326 nm. The optimized SF₆/Ar and Cl₂ recipes are given in table 4.9.

The etch rate of HSQ with Cl₂ plasma was \approx 30 nm/min while the etch rate of silicon was \approx 125 nm/min. So, to increase etch resistance of HSQ, the sample was hard-baked at 300 °C for 5 minutes after development. Tilted SEM images of etched silicon sample is shown in Fig.4.18. The SEM image of etched SOI sample after hard-baking the HSQ is shown in Fig.4.19.

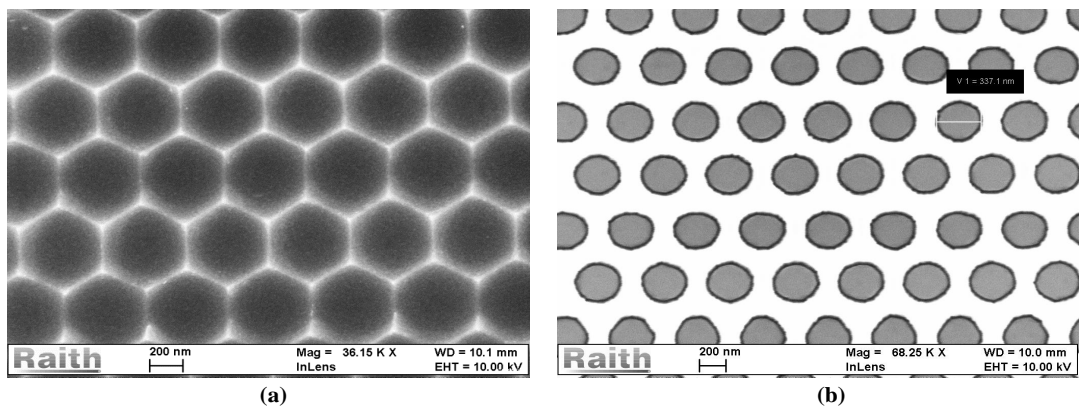


Figure 4.17: SEM image of etched silicon (a) with SF₆/Ar and (b) with Cl₂ plasma.

Table 4.9: Recipe used for ICPRIE to realize PhC on silicon.

| | | |
|---------------|------------------------------------|----------------------------|
| Gas flow rate | SF ₆ : Ar :: 20:20 sccm | Cl ₂ :: 10 sccm |
| Temperature | 25 °C | 25 °C |
| Pressure | 40 mTorr | 5 mTorr |
| ICP Power | 300 W | 100 W |
| RF Power | 50 W | 100 W |
| DC Bias | 175 V | 370 V |
| Etch rate | 230 nm/min | 125 nm/min |

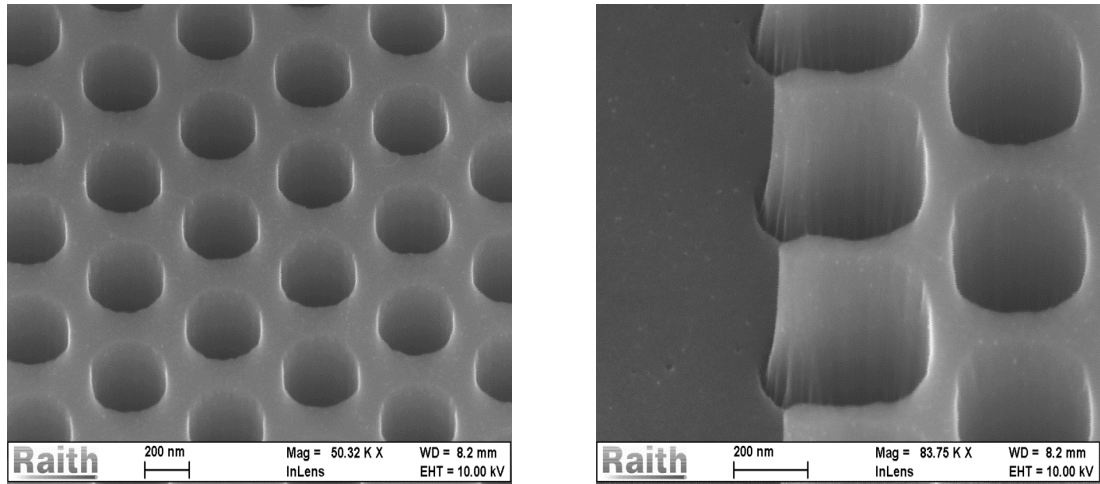


Figure 4.18: Tilted SEM images of etched silicon with Cl₂ plasma.

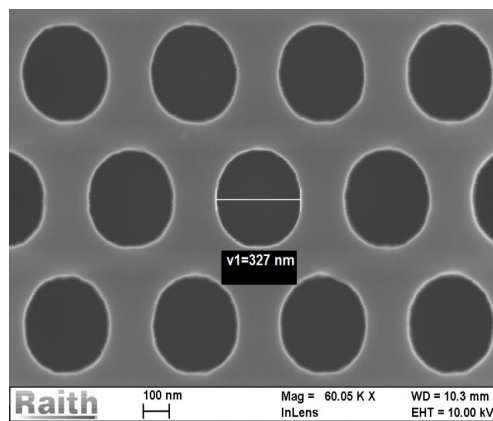


Figure 4.19: SEM image of PhC after etching on SOI with Cl₂ plasma.

Conclusion

HSQ has good contrast and dry etch resistance compared to PMMA, so using HSQ as a hard mask PhC patterns were successfully realized on SOI.

4.2.4 Photonic Wire Waveguide (PhW) Fabrication

As discussed in previous sections PhC patterns were successfully realized using HSQ as a hard mask. Hence, the same approach was used to fabricate PhW to couple light into PhCW. The process flow to fabricate PhW will be the same as given in Fig.4.14 except the mask file used was different. All the processes like wafer cleaning, resist coating, development, etching (with Cl_2 plasma) was same as given in section 4.2.3 for SOI wafer, except the dose value.

Optimized EBL parameters for PhW patterning are given as follows :

Resist thickness: 130 nm.

Accelerating voltage : 20 KV, aperture : 10 μm , working distance : 10 mm ($I \approx 40$ pA).

Dose value: 800 $\mu\text{C}/\text{cm}^2$.

Development: 8 minutes MF-319, 60 seconds rinse in DI water, 15 seconds IPA rinse.

SEM image of PhW after development and etching are shown in Fig.4.20 and Fig.4.21 respectively.

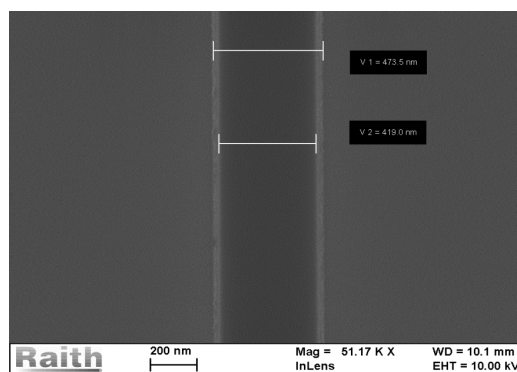


Figure 4.20: SEM image of PhW after development.

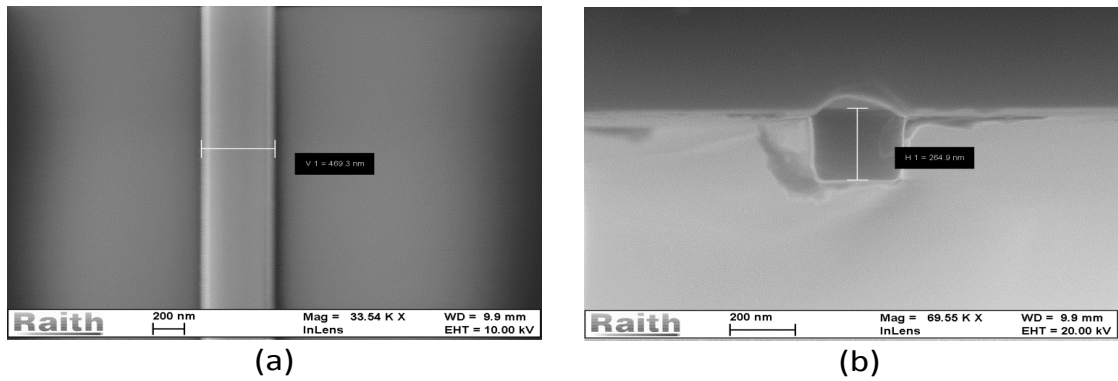


Figure 4.21: SEM image of PhW after etching : (a) Top view, (b) End facet.

4.3 Conclusions

Using UV photo lithography GaAs and Silicon etching optimization have been carried out with $\text{BCl}_3/\text{Cl}_2/\text{Ar}$ and SF_6/Ar plasma, respectively. To fabricate PhC on SOI, EBL have been optimized using resist PMMA and HSQ. Due to PMMA's poor dry etching resistance, it could not be used as a hard mask to etch silicon. Dry etching of silicon have been optimized with Cl_2 based plasma to fabricate PhC using HSQ as a hard mask. Finally, PhC and PhW have been fabricated on SOI with the optimized process steps.

CHAPTER 5

Conclusions

5.1 Summary

Design of single-mode 2D air bridge PhCW on GaAs/AlGaAs and SOI platforms and fabrication optimization for SOI PhC have been carried in this work.

First the design parameters of PhC were optimized to obtain sufficiently large PBG of the order of 500 nm centering at third generation optical communication window ($\lambda \sim 1550$ nm). In the optimized PhCs, a line defect was introduced to realize the waveguide. The optimized PhCW defect widths for single mode condition are 176 nm and 150 nm for GaAs and silicon, respectively. Design of SOI based PhCWs were further modified by introducing taper at both ends to improve coupling of light into PhCW from photonic wire waveguide. Using the designed taper, the throughput transmission has been improved from 14% to 33%. The extracted group velocity of a SOI based PhCW was found to be 3-10 times slower than that of a photonic wire waveguide operating at $\lambda \sim 1550$ nm. Such structures can be useful for slow-light and non linear applications.

Etching studies of GaAs were carried out with the present facilities in microelectronics lab. In order to make periodic circular patterns of diameter 4 μm and period 8 μm , photo lithography was carried on cleaned GaAs sample using positive photoresist. Chlorine based etch chemistries were used to etch the patterns on GaAs. It was found that $\text{BCl}_3/\text{Cl}_2/\text{Ar}/\text{N}_2$ recipe gives smoother surface and vertical sidewalls. Similarly etching studies of silicon was carried out for the periodic circles of diameter 4 μm and period 8 μm with fluorine plasma. It was found that SF_6/Ar recipe gives smoother sidewall with very good anisotropy. However, the recipe gives much larger undercut.

Photonic crystal structures were defined in SOI by electron beam lithography and subsequent inductively coupled plasma reactive ion etching. Negative tone resist HSQ was found to be better than positive tone resist PMMA for dry etching mask. Etching

of silicon was carried out using HSQ mask with SF₆/Ar and Cl₂ plasma, and it was found that SF₆/Ar was not suitable for etching of sub-micron dimensions because of its isotropic etching nature. Finally Cl₂ based recipe was used to realize the PhC patterns on SOI. With the optimized Cl₂ recipe, the etch rate of silicon was found to be 125 nm/min.

5.2 Scope for Future Work

PhCWs are promising devices in integrated optoelectronics and there are immense possibilities for them which can be further explored. Some of the possible improvements and further studies required are listed below.

- 1) The coupling efficiency for single mode PhCW can be increased by tuning the parameter of defect width and by increasing the designed taper length.
- 2) Integrated optical active/passive circuits like modulator, cavity resonator can be investigated.
- 3) Photonic crystal structures can be integrated with photonic wire structures for experimental studies.
- 4) Process parameters may need to be fine tuned after analyzing the experimental results.

APPENDIX A

Codes

A.1 Matlab Code to Calculate Band Structure using Theoretical Analysis

A.1.1 1D PhC : Normal Incidence

```
n1=1 %Refractive index of air
n2=3.38; % Refractive index of GaAs
x=1.5*1e-6; % wavelength used to calculate thickness of quarter wave stack layer
u=1e-6; % scaling factor
l=[.6688*u:.0001*u:1000*u];
a=x/(4*n1); % thickness of layer with refractive index n1
b=x/(4*n2); % thickness of layer with refractive index n2
c=3*1e8; % speed of light
n=a+b; % period of 1D structure
w=(2*3.14*c./l); % angular frequency variation with change in wavelength
k1=(n1*w/c); % wave number in medium n1
k2=(n2*w/c); % wave number in medium n2
y=(w.*n/(2*pi*c));
h= (.7*2*pi*c)/n;
m=(2*pi*c)/h;
% dispersion relation
k3=acos((cos(k1.*a).*cos(k2.*b))-((1/2)*((n2/n1)+(n1/n2)).*(sin(k1.*a).*sin(k2.*b))));
% plotting the real and imaginary bloch wavevector with normalized frequency
h1=figure(1)
plot(real((k3/(2*pi))),y,'-b','linewidth',2);
hold on;
plot(imag((-k3/(2*pi))),y,'-r','linewidth',2);
```

```

xlabel('kz [2pi/a]', 'fontsize', 20);
ylabel('f[a/c]', 'fontsize', 20);
set(gca, 'fontsize', 20)
print(h1, '-dpdf', 'normalize incidence dispersion ');

```

A.1.2 1D PhC : Angular Incidence

TE Polarization

```

clear all;
clc;
s=2.5;
n1=1; %(R.I. of air)
n2=3.38; %(R.I. of GaAs)
x=1.5*1e-6; %(free space wavelength)
u=1e-6;
p=1e6;
a=x/(4*n1);
b=x/(4*n2);
c=3*1e8;
n=a+b; %(period of the structure)
j=1;
for angle=0:.1:10
i=1 ;
for var =0:.1:10
l = 2*3.1416*n/var; %(.25um to 25.126um ) Wave length
thita=asin(angle*l/(2*3.14*n2*n));
w(i)=(2*3.14*c/l);
k4(j,i)=(w(i)*n2/c)*sin(thita);
k1(j,i)=sqrt(((n1*w(i)/c)^2)-(k4(j,i)^2));
k2(j,i)=sqrt(((n2*w(i)/c)^2)-(k4(j,i)^2));
y(i)=(w(i)*n/c);

```

```

k3(j,i) = cos(k1(j,i).*a).*cos(k2(j,i).*b)-0.5.*((k1(j,i)./k2(j,i))+(k2(j,i)./k1(j,i))).*sin(k1(j,i).*a).*sin(k2
disp(k3(j,i));
k5(j,i)=k4(j,i)*n;
if (abs(k3(j,i)) < 1)
plot(real(k5(j,i)),y(i),'g');
hold on;
else
plot(real(k5(j,i)),y(i),'r');
hold on;
end
i = i+1;
end
j=j+1;
hold on;
end

```

TM Polarization

The code used for plotting dispersion curve for TM polarization was same as of TE polarization code, the only difference was the dispersion relation. In TM polarization the dispersion relation used was :

$$k3(j,i) = \cos(k1(j,i).a) \cdot \cos(k2(j,i).b) - 0.5 \cdot \left(\frac{n_1^2}{n_2^2} \cdot \frac{k1(j,i)}{k2(j,i)} + \frac{n_2^2}{n_1^2} \cdot \frac{k2(j,i)}{k1(j,i)} \right) \cdot \sin(k1(j,i).a) \cdot \sin(k2(j,i).b)$$

A.1.3 2D PhC

```

clear all;
clc;
close all;
n=.250;
n1=sqrt(0.5);
n2=sqrt(8.2);
a=.8*n;

```

```

b=.2*n;
c=3*1e8;
l=0:.001:.6;
x=n./l;
β=-1000:1:1000;
for j=1:length(x)
w=(2*3.14*c)./x;
for i=1:length(β)
k1x=sqrt(((n1*w(j)/c)^2)-β(i));
k2x=sqrt(((n2*w(j)/c)^2)-β(i));
k1y=sqrt(((n1*w(j)/c)^2)+β(i));
k2y=sqrt(((n2*w(j)/c)^2)+β(i));
Ky=(1/n)*acos(cos(k1y*a)*cos(k2y*b)-(0.5*((k2y/k1y)+(k1y/k2y))*sin(k1y*a)*sin(k2y*b)));
Kx=(1/n)*acos(cos(k1x*a)*cos(k2x*b)-(0.5*((k2x/k1x)+(k1x/k2x))*sin(k1x*a)*sin(k2x*b)));
K1=(Kx*n)/pi;
K2=(Ky*n)/pi;
I1=imag(K1);
I2=imag(K2);
if ((I1==0) (I2==0))
s(i,j)=real(K1);
f(i,j)=real(K2);
K1 real=real(K1);
K2 real=real(K2);
var K1(j)=round(real(K1)*10);
var K2(j)=round(real(K2)*10);
if(var K2(j)==0)
gx(j)=K1 real;
y1(j)=n/x(j);
end
if (var K1(j)==9)
xm(j)=K2 real+1;
y2(j)=n/x(j);
end

```

```

K1 real1=round(real(K1)*10);
K2 real1=round(real(K2)*10);
if (K1 real1==K2 real1)
mg(j)=-sqrt(K1 real2+K2 real2)+2+sqrt(2);
y3(j)=n/x(j);
end
end
end
end
conc array x=[gx xm mg];
conc array y=[y1 y2 y3];
scatter(conc array x,conc array y);

```

A.2 Script for Band Structure Calculation Using LUMER-ICAL

A.2.1 Code for Band Structure Calculation of PhC

% This script combines the results from the Gamma-X-M-Gamma sweep and plots the frequency spectrum fs from the band structure object results over k, and the band structure. The band structure information is extracted using tolerance and num band specified by the user at the beginning of the script.

% Properties:

*% a: period used to normalize the frequency (f norm=f*a/c)*

% f band: Frequencies of bands in units of Hz

*% f band norm: Frequencies of bands in units of Hz * a / c*

% User Defined properties:

% tolerance = 1e-4; tolerance for finding peaks and accepting bands setting this too low will result in noisy data where sidelobes of peaks are interpreted as new bands setting it too high will mean that some bands are not found

num band =2 ; %number of bands to search for in the band structure

```

radius index=1; %radius
initial radius=217e-9;
increment=1e-9;
final radius=217e-9;
radius variation=initial radius:increment:final radius;
final matrix=matrix(length(initial radius:increment:final radius),7);
for(j=initial radius; j<=final radius; j=j+increment) {
?j;
setnamed("::model","radius",j);
run sweep; % run all three sweeps
% get a from model
a = getnamed("::model","ax");
period x=a;
% get fs data from the sweeps
sweepname="Gamma-M";
ky=getsweepdata(sweepname,"ky");
spectrum=getsweepresult(sweepname,"spectrum");
f=c/spectrum.lambda;
fs all=matrix(length(f),75); % initialize matrix to store fs data in
fs all(1:length(f),1:25)=spectrum.fs;
sweepname="M-K";
kx=getsweepdata(sweepname,"kx");
spectrum=getsweepresult(sweepname,"spectrum");
fs all(1:length(f),26:50)=spectrum.fs;
sweepname="K-Gamma";
k1=getsweepdata(sweepname,"kx");
k2=getsweepdata(sweepname,"ky");
kp=-sqrt(k1*k1+k2*k2);
spectrum=getsweepresult(sweepname,"spectrum");
fs all(1:length(f),51:75)=spectrum.fs;
%light line
f lightline G X = c*kx*(2*pi/period x)/(2*pi)/1*a/c;

```

```

f lightline X M = sqrt((c*ky*(2*pi/period x)/(2*pi)/1*a/c)^2+.5^2);
f lightline M G = c*kp*(2*pi/period x)/(2*pi)/1*a/c;
radius value="band structure@ "+num2str(j/1e-9)+"nm"+" logscale";
% simple imaging of fs vs k
image(1:75,f,transpose(fs all),"k (Gamma-J-M-Gamma)","f (Hz)",radius value,"logplot");
exportfigure(radius value);
radius value="band structure@ "+num2str(j/1e-9)+"nm"+" linearscale";
image(1:75,f,transpose(fs all),"k (Gamma-J-M-Gamma)","f (Hz)",radius value);
exportfigure(radius value);
setplot("colorbar min",0);
setplot("colorbar max",max(fs all)*1e-4);
% plot band structure
band structure=matrix(num band,75); % initialize matrix in which to store band frequency information
% loop over sweep results
for (i=1:75) {
%use findpeaks to find num band number of peaks
temp = findpeaks(fs all(1:length(f),i),num band);
%collect data for any peaks that are more than 'tolerance' of the maximum peak (to avoid minor peaks like sidelobes)
minvalue = fs all(temp(1),i)*tolerance;
f band=matrix(num band);
f band norm=matrix(num band);
for(bandcount = 1:num band) {
if( fs all(temp(bandcount),i) > minvalue) {
f band(bandcount) = f(temp(bandcount));
}
f band norm = f band*a/c; % normalize the frequency vector
band structure(1:num band,i)=f band norm;
}
}
band structure1=matrix(75,num band);
band structure1=transpose(band structure);

```

```

radius value="band structure@ "+num2str(j/1e-9)+"nm";
plot(1:75,band structure1,"k (Gamma-J-M-Gamma)","f (Hz*a/c)",radius value,"plot points");
exportfigure(radius value);
array 1=matrix(75,1);
array 2=matrix(75,1);
array 3=matrix(75,1);
array 1=band structure1(1:75,1);
array 2=band structure1(1:75,2);
array 3=band structure1(1:75,3);
%light line plot
radius value with light line="band structure@ "+num2str(j/1e-9)+"nm"+"light line";
plotxy(1:75,array 1,1:75,array 2,1:75,array 3,1:25,f lightline G X,26:50,f lightline X
M,51:75,-f lightline M G,"k (Gamma-X-M-Gamma)","f (Hz*a/c)",radius value,"light
line");
exportfigure(radius value with light line);
out max=max(array 1(50:50,1));
out min=min(array 2(24:26,1));
mid value=(out max+out min)/2;
wave length=500e-9/(mid value);
wl=1550e-9;
period=wl*mid value;
pbg=out min-out max;
final matrix(radius index,1)=radius variation(radius index);
final matrix(radius index,2)=out max;
final matrix(radius index,3)=out min;
final matrix(radius index,4)=mid value;
final matrix(radius index,5)=period;
final matrix(radius index,6)=wave length;
final matrix(radius index,7)=pbg;
radius index=radius index+1;
closeall;
}
str name="radius"+" "+out max"+" "+out min"+" "+mid value"+" "+period"+" "+wave

```

```
length"+" "+"pbg";
write("final matrix.txt",str name);
write("final matrix.txt",num2str(final matrix));
```

A.2.2 Code for Band Structure Calculation of PhCW

% This script combines the results from the Gamma-X-M-Gamma sweep and plots the frequency spectrum f_s from the band structure object results over k , and the band structure. The band structure information is extracted using tolerance and num band specified by the user at the beginning of the script.

% Properties:

% a: period used to normalize the frequency ($f_{norm}=f*a/c$)

% f band: Frequencies of bands in units of Hz

% f band norm: Frequencies of bands in units of $Hz * a / c$

% User Defined properties:

tolerance = 1e-4; %tolerance for finding peaks and accepting bands setting this too low will result in noisy data where sidelobes of peaks are interpreted as new bands setting it too high will mean that some bands are not found

num band =5 ; %number of bands to search for in the band structure

radius index=1; %radius

initial radius=163e-9;

increment=1e-9;

final radius=163e-9;

radius variation=initial radius:increment:final radius;

final matrix=matrix(length(initial radius:increment:final radius),7);

for(j=initial radius; j<=final radius; j=j+increment) {

?j;

setnamed("::model","radius",j);

runsweep; % run all three sweeps

% get a from model

a = getnamed("::model","ax");

period x=a;

```

% get fs data from the sweeps
sweepname="Gamma-J";
kx=getsweepdata(sweepname,"kx");
spectrum=getsweepresult(sweepname,"spectrum");
f=c/spectrum.lambda;
fs all=matrix(length(f),50); % initialize matrix to store fs data in
fs all(1:length(f),1:50)=spectrum.fs;
%light line
f lightline G X = c*kx*(2*pi/period x)/(2*pi)/1*a/c;
radius value="band structure@ "+num2str(j/1e-9)+"nm"+" logscale";
% simple imaging of fs vs k
image(1:50,f,transpose(fs all),"k (Gamma-J)","f (Hz)",radius value,"logplot");
exportfigure(radius value);
radius value="band structure@ "+num2str(j/1e-9)+"nm"+" linearscale";
image(1:50,f,transpose(fs all),"k (Gamma-J)","f (Hz)",radius value);
exportfigure(radius value);
setplot("colorbar min",0);
setplot("colorbar max",max(fs all)*1e-4);
% plot band structure
band structure=matrix(num band,50); % initialize matrix in which to store band fre-
quency information
% loop over sweep results
for (i=1:50) {
%use findpeaks to find num band number of peaks
temp = findpeaks(fs all(1:length(f),i),num band);
%collect data for any peaks that are more than 'tolerance' of the maximum peak (to
avoid minor peaks like sidelobes)
minvalue = fs all(temp(1),i)*tolerance;
f band=matrix(num band);
f band norm=matrix(num band);
for(bandcount = 1:num band) {
if( fs all(temp(bandcount),i) > minvalue) {
f band(bandcount) = f(temp(bandcount));

```

```

}
f band norm = f band*a/c; % normalize the frequency vector
band structure(1:num band,i)=f band norm;
}
}
band structure1=matrix(50,num band);
band structure1=transpose(band structure);
radius value="band structure@ "+num2str(j/1e-9)+"nm";
plot(1:50,band structure1,"k (Gamma-J)","f (Hz*a/c)", "plot points");
exportfigure(radius value);
radius index=radius index+1;
closeall;
}
str name="radius"+" "+"out max"+" "+"out min"+" "+"mid value"+" "+"period"+" "+"wave
length"+" "+"pbg";
write("final matrix.txt",str name);
write("final matrix.txt",num2str(final matrix));

```

APPENDIX B

Mask Generation

B.1 Mask File Design

For doing EBL, gds mask files are used for writing patterns in most of the EBL systems. Mask file for the desired patterns can be designed in any CAD tool like R-SOFT, CleWin, L-Edit, Raith Layout Editor and exported in gds format. For writing the PhC patterns on PMMA (positive resist), the mask patterns required are array of periodic circular holes, that could be easily generated from all the above mentioned CAD tools. The real problem faced by us was in making the inverted mask pattern to realize the same periodic circular holes in HSQ (negative resist). The screen shot of mask pattern required for making PhC structures with positive and negative (inverted mask) resist are shown in Fig.B.1a and Fig.B.1b respectively, here the dark region should be exposed to ebeam. To create the inverted mask for PhC patterns approach given in the Fig.B.2 should work, after subtracting the two patterns Fig.B.2a and Fig.B.2b, we should get the inverted patterns shown in Fig.B.2c. However, after doing subtraction of the two patterns, some lines connecting all circles were seen in the mask file as shown in Fig.B.3 and these line were also be seen after doing EBL, in the patterned e-beam resist. Another method was tried to make inverted mask using Raith Layout editor for triangular lattice PhC. A unit cell as shown in Fig.B.4a was made and then array of patterns were made using unit cell as a reference structure. In this mask though the lines were not seen as shown in Fig.B.4b, but after writing the pattern through EBL, lines were visible on the patterned resist at the boundary of unit cell in horizontal direction as shown in Fig.B.5. However, in vertical direction there were no lines, because some overlap was given between region 1 and region 2 as shown in Fig.B.4a in the unit cell. From here we got idea to give overlap in the horizontal direction also and we recreated our mask with 30 nm overlap in horizontal as well as vertical direction. With this mask file we could successfully transfer the circular patterns in e-beam resist.

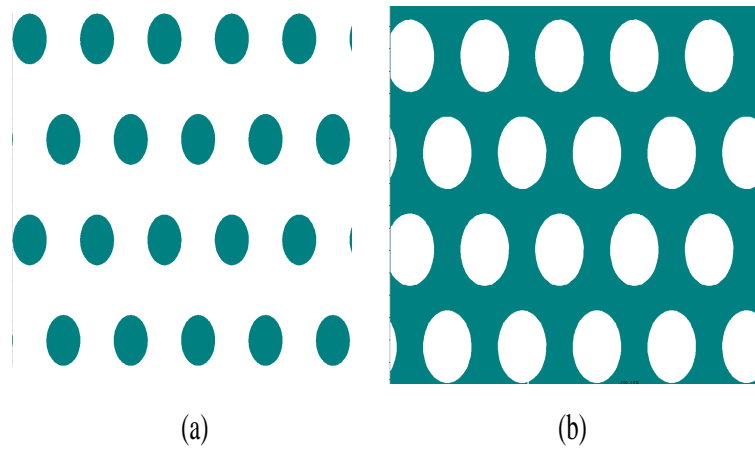


Figure B.1: Screen shot of mask files of PhCs (a) For positive resist. (b) For negative resist (Inverted mask)

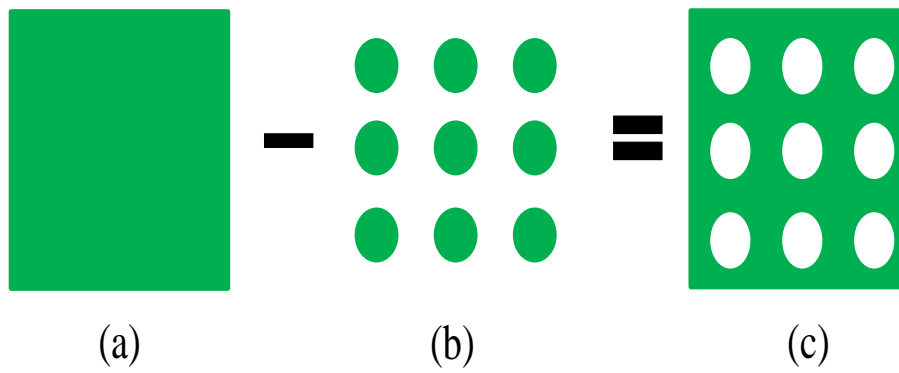


Figure B.2: By subtracting the a and b we should get c

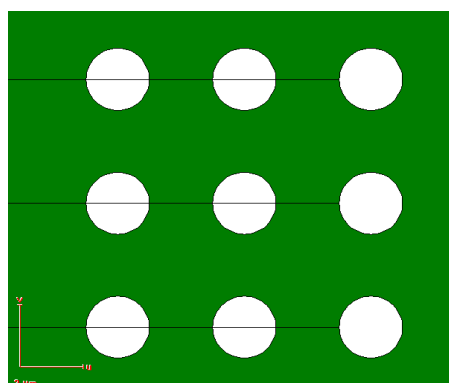


Figure B.3: Lines in the mask.

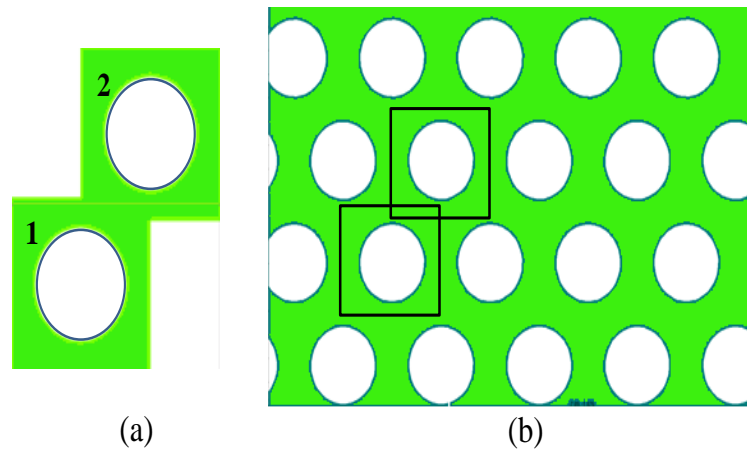


Figure B.4: (a) Unit cell. (b) Array of patterns made using the unit cell in raith layout editor.

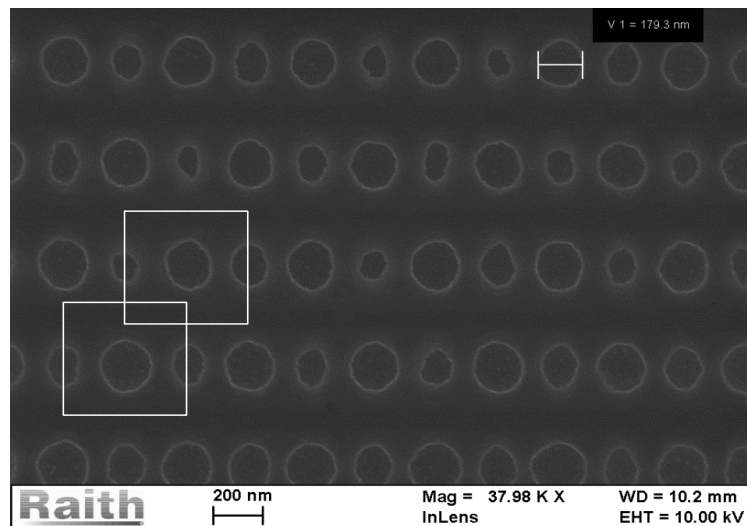


Figure B.5: SEM image of patterned HSQ using the mask file made in raith layout editor.

LIST OF PAPERS BASED ON THESIS

Conferences

1. **R. Joshi**, B. K. Das, N. DasGupta, "Design of 2D Photonic Crystals for Integrated Optical Slow-light Applications", IWPSD, Noida, India Dec. 2013.
2. I. Seethalakshmi, **R. Joshi**, B. K. Das, N. DasGupta, "Inductively Coupled Plasma Etching of GaAs with High Anisotropy for Photonics Applications", IWPSD, Noida, India Dec. 2013.

REFERENCES

1. **Akahane, Y., T. Asano, B. Song, and S. Noda** (2003). High-q photonic nanocavity in a two-dimensional photonic crystal. *Nature*, **425**(6961), 944–947.
2. **Askari, M.** (2011). High efficiency devices based on slow light in photonic crystals. *PhD thesis, Georgia Institute of Technology*.
3. **Baba, T., N. Fukaya, and J. Yonekura** (1999). Observation of light propagation in photonic crystal optical waveguides with bends. *Electronics letters*, **35**(8), 654–655.
4. **El-Kady, I., M. Sigalas, R. Biswas, and K. Ho** (1999). Dielectric waveguides in two-dimensional photonic bandgap materials. *Journal of lightwave technology*, **17**(11), 2042.
5. **Hamza, B., A. Kadiyala, L. Hornak, Y. Liu, and J. Dawson** (2012). Direct fabrication of two-dimensional photonic crystal structures in silicon using positive and negative hydrogen silsesquioxane (hsq) patterns. *Microelectronic Engineering*, **91**, 70–74.
6. **Haxha, S., I. Dayoub, F. AbdelMalek, W. Aroua, J. Trombi, H. Bouchriha, et al.** (2009). Light coupling between photonic crystal and standard photonic waveguides in a compact photonic integrated circuitry using 2d fddd. *Open Optics Journal*, **3**, 44–51.
7. **Jiang, W., L. Gu, X. Chen, and R. Chen** (2007). Photonic crystal waveguide modulators for silicon photonics: Device physics and some recent progress. *Solid-State Electronics*, **51**(10), 1278–1286.
8. **Jiang, Y., W. Jiang, L. Gu, X. Chen, and R. T. Chen** (2005). 80-micron interaction length silicon photonic crystal waveguide modulator. *Applied Physics Letters*, **87**(22), 221105.
9. **Joannopoulos, J. D., S. G. Johnson, J. N. Winn, and R. D. Meade**, *Photonic crystals: molding the flow of light*. Princeton university press, 2007.
10. **John, S.** (1987). Strong localization of photons in certain disordered dielectric superlattices. *Physical review letters*, **58**(23), 2486.
11. **Kuramochi, E., M. Notomi, S. Hughes, A. Shinya, T. Watanabe, and L. Ramunno** (2005). Disorder-induced scattering loss of line-defect waveguides in photonic crystal slabs. *Physical Review B*, **72**(16), 161318.
12. **Lin, C., X. Wang, S. Chakravarty, W. Lai, B. Lee, and R. Chen**, Group velocity independent coupling into slow light photonic crystal waveguide on silicon nanophotonic integrated circuits. *In SPIE OPTO*. International Society for Optics and Photonics, 2011.
13. **Lin, S., E. Chow, J. Bur, S. Johnson, and J. Joannopoulos** (2002). Low-loss, wide-angle y splitter at approximately $\sim 1.6\text{-}\mu\text{m}$ wavelengths built with a two-dimensional photonic crystal. *Optics letters*, **27**(16), 1400–1402.

14. **Loncar, M., T. Doll, J. Vuckovic, and A. Scherer** (2000). Design and fabrication of silicon photonic crystal optical waveguides. *Journal of Lightwave Technology*, **18**(10), 1402–1411.
15. **Martijn de Sterke, C., K. Dossou, T. White, L. Botten, and R. McPhedran** (2009). Efficient coupling into slow light photonic crystal waveguide without transition region: role of evanescent modes. *Optics express*, **17**(20), 17338–17343.
16. **Meade, R., A. Devenyi, J. Joannopoulos, O. Alerhand, D. Smith, and K. Kash** (1994). Novel applications of photonic band gap materials: Low-loss bends and high q cavities. *Journal of applied physics*, **75**(9), 4753–4755.
17. **Meier, M., A. Dodabalapur, J. Rogers, R. Slusher, A. Mekis, A. Timko, C. Murray, R. Ruel, and O. Nalamasu** (1999). Emission characteristics of two-dimensional organic photonic crystal lasers fabricated by replica molding. *Journal of applied physics*, **86**(7), 3502–3507.
18. **Mekis, A., J. Chen, I. Kurland, S. Fan, P. Villeneuve, and J. Joannopoulos** (1996). High transmission through sharp bends in photonic crystal waveguides. *Physical Review Letters*, **77**(18), 3787.
19. **Mittal, S. and J. Sabarinathan**, Optimization of coupling and transmission through finite height soi photonic crystal slab waveguides. *In Photonics North 2005*. International Society for Optics and Photonics, 2005.
20. **Ngo, Q., P. Nga, S. Kim, and H. Lim**, Novel tapers for slow-light coupling in photonic crystal waveguides. *In Photonics and Optoelectronics (SOPO), 2012 Symposium on*. IEEE, 2012.
21. **Noda, S., A. Chutinan, and M. Imada** (2000). Trapping and emission of photons by a single defect in a photonic bandgap structure. *Nature*, **407**(6804), 608–610.
22. **Noda, S., N. Yamamoto, M. Imada, H. Kobayashi, and M. Okano** (1999). Alignment and stacking of semiconductor photonic bandgaps by wafer-fusion. *Journal of lightwave technology*, **17**(11), 1948.
23. **Notomi, M.** (2010). Manipulating light with strongly modulated photonic crystals. *Reports on Progress in Physics*, **73**(9), 096501.
24. **Notomi, M., A. Shinya, S. Mitsugi, G. Kira, E. Kuramochi, and T. Tanabe** (2005). Optical bistable switching action of si high-q photonic-crystal nanocavities. *Optics Express*, **13**(7), 2678–2687.
25. **Notomi, M., K. Yamada, A. Shinya, J. Takahashi, C. Takahashi, and I. Yokohama** (2001). Extremely large group-velocity dispersion of line-defect waveguides in photonic crystal slabs. *Physical Review Letters*, **87**(25), 253902.
26. **Pottier, P., M. Gnan, and R. D. L. Rue** (2007). Efficient coupling into slow-light photonic crystal channel guides using photonic crystal tapers. *Optics express*, **15**(11), 6569–6575.
27. **Rayleigh, L.** (1887). Xvii. on the maintenance of vibrations by forces of double frequency, and on the propagation of waves through a medium endowed with a periodic structure. *The London, Edinburgh, and Dublin Philosophical Magazine and Journal of Science*, **24**(147), 145–159.

28. **Sanchis, P., J. Garcia, J. Marti, W. Bogaerts, P. Dumon, D. Taillaert, R. Baets, V. Wiaux, J. Wouters, and S. Beckx** (2004). Experimental demonstration of high coupling efficiency between wide ridge waveguides and single-mode photonic crystal waveguides. *Photonics Technology Letters, IEEE*, **16**(10), 2272–2274.
29. **Sugimoto, Y., N. Ikeda, N. Carlsson, K. Asakawa, N. Kawai, and K. Inoue** (2002). Fabrication and characterization of different types of two-dimensional algaas photonic crystal slabs. *Journal of applied physics*, **91**(3), 922–929.
30. **Volatier, M., D. Duchesne, R. Morandotti, R. Ares, and V. Aimez** (2010). Extremely high aspect ratio gaas and gaas/algaas nanowaveguides fabricated using chlorine icp etching with n2-promoted passivation. *Nanotechnology*, **21**(13), 134014.
31. **Yablonovitch, E.** (1987). Inhibited spontaneous emission in solid-state physics and electronics. *Physical review letters*, **58**(20), 2059.
32. **Yariv, A. and P. Yeh**, *Photonics: Optical Electronics in Modern Communications (The Oxford Series in Electrical and Computer Engineering)*. Oxford University Press, Inc., 2006.